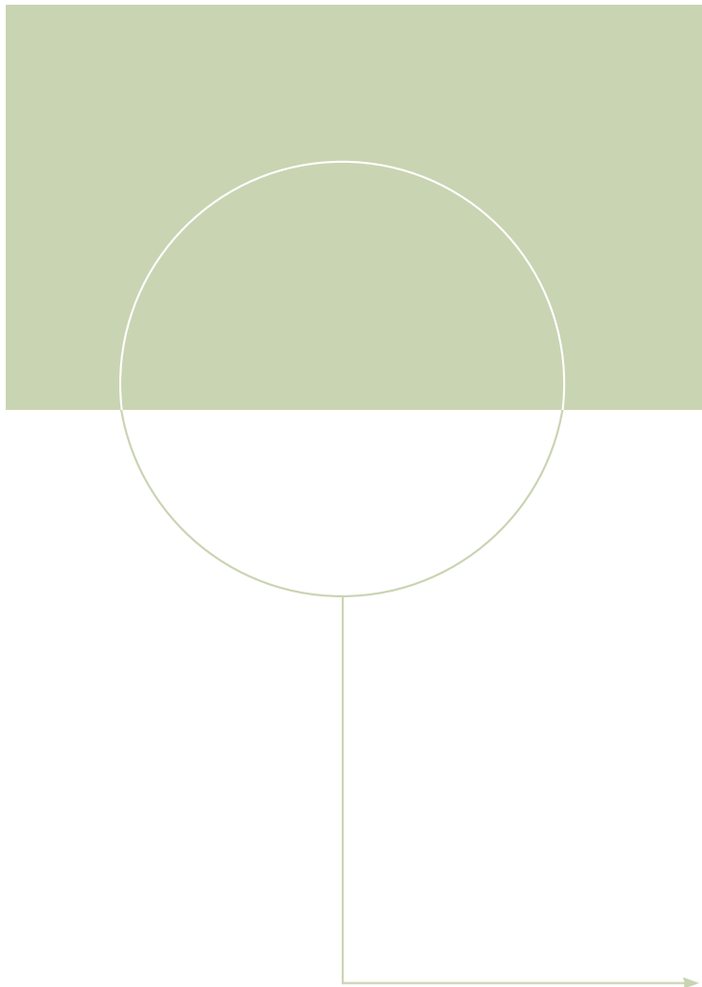

Master's thesis

2020

Sebastian Everard Nordby Price

NTNU
Norwegian University of
Science and Technology
Faculty of Natural Sciences
Department of Chemistry

Sebastian Everard Nordby Price

Improving the Perturbation Theory for Lennard-Jones Mixtures with Large Differences in Well-Depths

June 2020

NTNU
Norwegian University of
Science and Technology

NTNU
Norwegian University of
Science and Technology

NTNU
Norwegian University of
Science and Technology

Improving the Perturbation Theory for Lennard-Jones Mixtures with Large Differences in Well-Depths

Sebastian Everard Nordby Price

Chemical Engineering and Biotechnology
Submission date: June 2020
Supervisor: Anders Lervik
Co-supervisor: Øivind Wilhelmsen

Norwegian University of Science and Technology
Department of Chemistry

Acknowledgements

I would like to express my gratitude to my supervisor Øivind Wilhelmsen for all his valuable feedback and suggestions. I want to thank Morten Hammer and Ailo Aasen at Sintef Energi AS for giving me their Monte Carlo simulation program as well as lending me computer power for the simulations. I also want to thank them for all their good suggestions and help in my thesis.

In addition I want to thank Sintef Energy research and Øivind Wilhelmsen for funding my participation in the course ”Fundamentals and Computational Aspects of Thermodynamic Models” at the Technical University of Denmark at the beginning of the Autumn semester last year. The course has given me valuable knowledge as well as been helpful for several of the problems I have faced.

Lastly I want to thank Daniel Zhang and Lodin Ellingsen for interesting conversations and encouragement.

Abstract

The statistical associating fluid theory (SAFT) has been hugely successful in describing associating chain fluids. These SAFT like equations of state are usually written as a sum of the Helmholtz free energy, consisting of an ideal, a monomeric, a chain and an association contribution. Most of the work on these equations has been on the monomeric contribution, where the Barker-Henderson perturbation theory has shown promising results. Barker-Henderson perturbation theory is based on expanding the Helmholtz free energy from a well understood repulsive hard-sphere reference fluid into a perturbation series, where the perturbation adds on the attractive forces. Investigations of this method has shown promising results for pure fluids, but in a recent paper, Hammer et al. observed severe problems in describing the second and third order perturbation terms for mixtures with large differences in well-depth.

This thesis investigates the problem with the second order perturbation term in more detail and presents several approaches to solve the issue. Monte Carlo simulations has been performed for different reduced temperatures, reduced densities, mixture compositions and well-depth ratios in order to get a better understanding of how these parameters affect the second order perturbation term. In the paper by Hammer et al., they only studied the second order perturbation term using the macroscopic compressibility approximation (MCA), where they utilized the correction factor developed by Lafitte et al.. We have in this thesis tested the correction factor developed for Lennard-Jones fluids by van Westen and Gross. The results were slightly better, especially at the higher reduced temperature range.

Inspired by the work of Henderson we have also examined a numerical method in calculating the second order perturbation term for mixtures, without having to use the MCA. This method has been developed from two different reference fluids: a pure hard-sphere fluid and an additive binary hard-sphere fluid. They were both able to predict the general trend fairly well, but had a tendency to overestimate the slope at the higher reduced density range.

The Monte Carlo simulation data for the second order perturbation term can be divided into six different interaction terms when dealing with a binary mixture. We have shown how these can be estimated using the numerical method inspired by Henderson. Close comparisons between this method and Monte Carlo data of these terms has revealed that using an additive binary hard-sphere reference improves the prediction of the ”pure” interaction terms, compared to using a pure hard-sphere reference. The prediction of the cross-interaction terms appeared to be more unreliable.

For future development, either a better understanding of the 3- and 4-particle distribution functions used in the numerical method, is needed or a thorough extension to mixture of the MCA using a correction factor, should be conducted.

Norsk Sammendrag

Statistisk assosierende fluid teori (SAFT) har hatt stor suksess i å beskrive assosierende kjede fluider. Disse SAFT-type-tilstandsligningene er som regel skrevet som en sum av Helmholtz fri energi, bestående av et ideelt bidrag, et monomerisk bidrag, et kjede bidrag og et assosierende bidrag. Det meste av arbeidet på disse ligningene har vært på det monomeriske bidraget, hvor spesielt Barker-Henderson perturbasjonsteori har gitt lovende resultater. Barker-Henderson perturbasjonsteori er basert på å utvide Helmholtz fri energi fra det godt forståtte avstøtende hardsfære referanse fluidet til en perturbasjonsrekke, hvor perturbasjonen legger til de tiltrekkende kreftene. Man har i dag klart å utvikle gode modeller for de tre første perturbasjonsleddene for rene fluider, men det ble i artikkelen av Hammer et al. nylig observert store problemer i å beskrive det andre og tredje perturbasjonsleddet for blandinger med store forskjeller i brønndybde.

Denne oppgaven undersøker problemene med andreordens perturbasjonsleddet nærmere og presenterer flere mulige veier for å løse de. Det har blitt gjennomført Monte Carlo simuleringer ved ulike reduserte temperaturer, reduserte tettheter, blandingsforhold og brønndybder for å få en bedre forståelse av hvordan disse parameterne påvirker andreordens perturbasjonsleddet. I artikkelen av Hammer et al., så de kun på andreordens perturbasjonsleddet når man bruker den makroskopiske kompressibilitets approksimasjonen (MCA) med korreksjonsfaktoren utviklet av Lafitte et al.. Vi har i denne oppgaven testet korreksjonsfaktoren utviklet for Lennard-Jones fluider av van Westen og Gross. Den viste en liten forbedring, da spesielt i det høyere reduserte temperatur området.

Inspirert av arbeidet til Henderson, har vi også undersøkt en numerisk metode i å kalkulere andreordens perturbasjonsledd for blandinger uten å bruke MCA. Denne metoden har blitt utviklet for to ulike referansefluider: et rent hardsfære fluid og et additivt binært hardsfære fluid. Begge viste seg å følge den generelle trenden relativt godt, men hadde en tendens til å overestimere senkningen ved høyere reduserte tettheter.

Det er mulig å dele opp Monte Carlo simuleringsdataen for andreordens perturbasjonsleddet i seks ulike interaksjonsledd, når man har en binærblanding. Vi har vist hvordan man kan estimere disse ved bruk av den numeriske metoden inspirert av Henderson. Omfattende sammenligner mellom denne numeriske metoden og Monte Carlo data viser at bruk av en binær additiv hardsfære referanse forbedrer prediksjonen av de ”rene” interaksjonsleddene over å bruke en ren hardsfære referanse. Sammenligningene har også vist at den numeriske metoden er noe upålitelig i predikering av krysstermer.

For framtidig arbeid, vil man enten trenge en bedre forståelse av 3- og 4-partikkel distribusjonsfunksjoner som brukes i den numeriske metoden, eller en skikkelig utvidelse av den makroskopiske kompressibilitets approksimasjonen med korreksjonsfaktor, for blandinger.

Table of Contents

List of Figures

List of Symbols

A	Helmholtz free energy
A^{id}	Helmholtz free energy for ideal gas
A^{res}	Residual Helmholtz free energy, which is the Helmholtz free energy subtracted by the ideal Helmholtz free energy
A_0^{res}	Residual Helmholtz free energy of the reference system
A_1^{res}	First order perturbation residual Helmholtz free energy
A_d^{hs}	Residual Helmholtz free energy for a hard-sphere fluid
$\bar{A}$	Helmholtz free energy per particle A/N
$\hat{A}$	First term in the approximation of y_d^{hs}
$\tilde{A}_0$	Constant used in the work on g^{py} by Trokhymchuk et al.
$\mathcal{A}$	Intrinsic Helmholtz free energy
$\mathcal{A}^{\text{id}}$	Intrinsic Helmholtz free energy for ideal gas
$\mathcal{A}^{\text{res}}$	Intrinsic residual Helmholtz free energy, which is the intrinsic Helmholtz free energy subtracted by the intrinsic ideal Helmholtz free energy
a^{ad}	Term accounting for non-additivity to the Helmholtz free energy
a^{chain}	The reduced chain contribution to the Helmholtz free energy
a^{mono}	The reduced association contribution to the Helmholtz free energy
a^{id}	The reduced Helmholtz free energy for ideal system
a^{mono}	The reduced monomeric contribution to the Helmholtz free energy
a^{res}	The reduced residual Helmholtz free energy
a_0	The reduced Helmholtz free energy of the reference system.
a_i	The reduced ith perturbation term of the Helmholtz free energy.
a_d^{hs}	The reduced Helmholtz free energy of hard-sphere.
$a_{d,\text{mix}}^{\text{hs}}$	The reduced Helmholtz free energy of a mixture of hard-spheres.
$\hat{B}$	The second term in the approximation of y_d^{hs}
$B(\eta; l)$	$12\eta\epsilon \left(\frac{1-\eta/2}{(1-\eta)^3} \hat{I}_l(x_0) - \frac{9\eta(1+\eta)}{2(1-\eta)^3} \hat{J}_l(x_0) \right)$
$B_{\text{num}}(\eta; l)$	$12\epsilon\eta \int_{x_0}^1 y_d^{\text{hs}}(\eta; x) x^{2-l} \mathrm{d}x$
$\tilde{B}_0$	Constant used in the work on g^{py} by Trokhymchuk et al.
$\hat{b}_i(T^*)$	Function used for the van Westen and Gross χ-factor
$\hat{C}$	The third term in the approximation of y_d^{hs}
$\tilde{C}_0$	Constant used in the work on g^{py} by Trokhymchuk et al.

$\mathcal{C}$	$\frac{l_r}{l_r-l_a}\left(\frac{l_r}{l_a}\right)^{\frac{l_a}{l_r-l_a}}$
$c^{(n)}(\mathbf{r}^n)$	n-particle direct correlation function
$\hat{c}_i(l)$	The ith function in estimating η_{eff}
D_l	The lth Legendre polynomial integral with h_d^{hs} used for calculating J_5
d	Hard-sphere diameter
E_l	The lth Legendre polynomial integral with wg_d^{hs} used for calculating J_5
e_0	Boltzmann factor of the reference system exp$(-\beta u_0(r))$
e_d^{hs}	Boltzmann factor of a hard-sphere potential exp$(-\beta u_d^{\text{hs}}(r))$
F^c	Fitted function used in the work of Henderson
$\mathcal{F}^{[N]}$	Phase-space probability density for N particles
$\mathcal{F}_0^{[N]}$	Equilibrium probability density for N particles
$\mathcal{F}_M^{[n]}$	n-particle Maxwell distribution of momenta
f	A general function
$f_{\text{M}}(r)$	Mayer function $e(r)-1$
G^{py}	Laplace transformed Percus-Yevick approximation of the radial distribution function
g_0	Radial distribution function of the reference system
g_d^{hs}	Radial distribution function for a hard-sphere fluid with diameter d
$g_{d,ij,c}^{\text{hs}}$	Radial distribution function for a hard-sphere fluid mixture at its contact value
$g_n^{[N]}$	n-particle distribution function
g^{py}	Percus-Yevick approximation of the radial distribution function
H	Heaviside function
$\mathcal{H}$	Hamiltonian for the system
h	Planck's constant
$h(r)$	$g(r)-1$
$h_0(r)$	$g_0(r)-1$
h_d^{hs}	$g_d^{\text{hs}}(r)$-1
I_{1A}	The first integral in a_1: $2\pi\rho\int_d^\infty w(r)g_0(r)r^2\mathrm{d}r$
I_{1B}	The second integral in a_1: $-2\pi\rho\int_d^\sigma w(r)g_0(r)r^2\mathrm{d}r$
$I_1^S(\eta,l)$	Correlation integral over a hard-core Sutherland potential of exponent l
I_m	$\int_0^\infty\left(\frac{r}{d}-1\right)^m\Delta e(r)\mathrm{d}(r/d)$
$\hat{I}_l(x_0)$	$-\frac{x_0^{3-l}-1}{l-3}$

J_i	Integrals used for the superposition approximation, with i being in the range from 1-5.
J_i^*	Integrals used for the superposition approximation divided by epsilon, with i being in the range from 1-5.
$\hat{J}_3$	Combined integrals used in the work of Henderson
$\hat{J}_l(x_0)$	$-\frac{x_0^{4-l}(l-3)-x_0^{3-l}(l-4)-1}{(l-3)(l-4)}$
K^{hs}	$k_BT(\partial\rho/\partial P)_T$
K_N	Kinetic energy for an N-particle system
k	General constant
k_B	Boltzmann constant
$\hat{k}_i$	Correlation constant
$L(\tau)$	$12\eta[(1+\frac{1}{2}\eta)\tau+(1+2\eta)]$
l	Exponent value used for Sutherland potentials. If denoted by r it means it is the repulsive part and if denoted by a it is the attractive part
m	Mass
N	Number of particles
N_{blk}	Number of Monte Carlo blocks
n	Subset of particles
$\mathcal{O}$	Higher order terms
P	Pressure
$\mathcal{P}_l$	The lth Legendre polynomial
$p(N)$	Probability that at equilibrium the system will contain exactly N particles irrespective of their coordinates and momenta
$\mathbf{p}_i$	Three dimensional momentum of a particle i
$\mathbf{p}^N$	$3N$ dimensional momentum's of N particles
Q_N	Canonical partition function for N particles
Q_N^{id}	Canonical partition function for N ideal gas particles
r	Radial distance from the particle in question
r_{ij}	The distance between particle i and j
$\mathbf{r}_i$	Three dimensional coordinate of a particle i
$\mathbf{r}_{ij}$	$\mathbf{r}_j-\mathbf{r}_i$
$\mathbf{r}^N$	$3N$ dimensional coordinates of N particles
$\mathbb{R}$	Real numbers
$\mathcal{R}$	Allowed cube region in Monte Carlo
$S(\tau)$	$(1+\eta)^2\tau^3+6\eta(1-\eta)\tau^2+18\eta^2\tau-12\eta(1+2\eta)$
$\mathcal{S}$	Entropy

s	Standard error
T	Temperature
T^*	Reduced temperature k_BT/ϵ (k_BT/ϵ_{11} for mixtures)
t	Time
U_N	Inter-particular potential energy for an N-particle system
$U_{N,0}$	Inter-particular potential energy for an N-particle reference system
$\mathcal{U}$	Internal energy
u	Pair potential
u_0	Pair potential for the reference system
u_d^{hs}	Pair potential for a hard-sphere fluid
u^{lj}	Pair potential for a Lennard-Jones fluid
u^{mie}	Pair potential for the Mie fluid
V	Volume
$v_i(\alpha)$	Closed functional form used for the Lafitte et al. χ-factor
W_N	Inter-particular perturbation potential energy for an N-particle system
$W_{ij,\text{lrc}}$	Long range correction for the inter-particular potential energy between particle type i and j
w	Perturbation pair potential
w^*	Perturbation pair potential divided by epsilon
x	r/d
x_0	σ/d
x_i	Fraction of component i
y	Cavity-correlation function
y_0	Cavity-correlation function for a reference system
y_d^{hs}	Cavity-correlation function for hard-sphere fluid
Z_N	Configurational integral for N particles
Z_N^{id}	Configurational integral for N ideal gas particles
z	Activity ($\frac{\exp(\beta\mu)}{\Lambda^3}$)
α	Dimensionless van der Waals-like attractive constant
α_0	Constant used in the work on g^{py} by Trokhymchuk et al.
$\mathbb{\alpha}$	Symmetrical stochastic matrix
β	$1/k_BT$
β_0	Constant used in the work on g^{py} by Trokhymchuk et al.
χ	Zhang correction factor for the MCA
χ_T	Isothermal compressibility factor
δ_0	Constant used in the work on g^{py} by Trokhymchuk et al.

ϵ	Depth of the potential
η	Packing fraction $\frac{\pi}{6}\rho d^3$
η_{eff}	Effective packing fraction that satisfies the work of Lafitte et al. [23].
$\gamma(x)$	Inner integrals used in the J_i terms
$\gamma^*(x)$	Inner integrals divided by epsilon used in the J_i^* terms
γ_0	Constant used in the work on g^{py} by Trokhymchuk et al.
κ_0	Constant used in the work on g^{py} by Trokhymchuk et al.
g_n^{residue}	Residue of $G^{\text{py}}(\tau)$ at the roots of the denominator $L(\tau) + S(\tau)e^{\tau}$.
Λ	Broglie thermal wavelength
λ	Coupling parameter for switching on a perturbation
μ	Chemical potential
μ^{res}	Residual chemical potential
μ_0	Constant used in the work on g^{py} by Trokhymchuk et al.
ν	Effective hard-sphere diameter
Ω	Grand potential
$\omega_{i,n}$	Correlated coefficients used in the Lafitte et al. χ-factor
ω_0	Constant used in the work on g^{py} by Trokhymchuk et al.
Φ_N	Potential energy from interaction between the N particles with some spatially varying external field
ϕ	Potential energy from interaction between a particle with some spatially varying external field
φ	Reduced free energy density $-\beta A^{\text{res}}/V$
φ_0	Reduced free energy density of a reference system
φ_d^{hs}	Reduced free energy density of a hard-sphere liquid
Π	An $N \times N$ transition matrix for an irreducible Markov chain
ψ	Intrinsic chemical potential
ρ	Number density
$\rho_N^{[n]}$	Equilibrium n-particle density
ρ^*	Reduced density $\rho\sigma^3$ ($\frac{N_1^2\sigma_{11}^3+2N_1N_2\sigma_{12}^3+N_2^2\sigma_{22}^3}{NV}$ for mixtures)
$\boldsymbol{\rho}$	Probability vector
σ	Collision diameter
ς	Mean value theorem value
τ	Laplace transform variable
θ	Angle between two vectors
Ξ	Grand partition function
ξ	Softness parameter

ζ_m	$\frac{\pi\rho}{6}\left(\sum_i x_i d_{ii}\right)$
$\bar{\zeta}_x$	$\frac{\pi\rho}{6}\sum_i \sum_j x_i x_j \sigma_{ij}^3$

Chapter 1

Introduction

For a long time it has been desirable to describe the volumetric properties of particles such as the pressure (P), volume (V) and temperature (T) relations. They have usually been described using an equation of state (EOS), a mathematical equation which relates thermodynamic state variables [33]. The well-known ideal gas law of Boyle is one of the early attempts in an EOS, with the major assumptions being volume-less particles, perfectly elastic collisions and no inter-particular interactions. It was not until van der Waals published the van der Waals EOS in 1873, that a systematic approach in explaining a real gas was made. This equation considers both the volume and the inter-particular interactions. Since then, several equations of states has been made and today they serve many purposes. They can describe the PVT properties for interpolation and data smoothing, be used for differentiation and integration for obtaining thermodynamic properties, predict the gas phase properties of both pure fluids and their mixtures from just a small set of experimental data as well as predict the vapour-liquid equilibria of mixtures [47]. Just to mention a few of their many purposes.

There are numerous ways of developing more realistic equations of states. One common starting point is to describe the interaction between the particles through a mathematical pair potential with repulsive and/or attractive regions. Some of the more well known potentials being the hard-sphere, Mie and Lennard-Jones pair potentials. Taking into account the pair potential when deriving an equation of state increases the difficulty however. Even the very simple hard-sphere potential which only has a contact repulsion cannot be described exactly analytically [18]. Approximate methods have therefore been essential.

In 1954, Zwanzig developed a perturbation method were the thermodynamic properties of one system can be related over to a slightly different system and to the difference in the inter-particular potentials of the two. This makes it possible to use a repulsive hard-sphere fluid as a reference system, with the attractive forces added on as a perturbation [58]. One of the difficulties with this theory is its sensitivity to the choice of hard-sphere diameter and the perturbing potential. Based on the work of Zwanzig, Barker and Henderson were able to develop a successful perturbation theory, where they among other things used a temperature dependent hard-sphere diameter [5].

In recent years, perturbation theory has regained an interest due to the success of the Statistical Associating Fluid Theory (SAFT) originally developed by Chapman et al. [11] in 1989 by applying previous work of Wertheim [50, 51, 52, 53]. There has been written many articles on SAFT-like expressions since then. Two of the more famous ones are

SAFT-VR by Gil-Villegas et al. [13] and PC-SAFT by Gross and Sadowski [14]. The SAFT-like equations of state are usually written as a sum of the reduced Helmholtz free energy:

$$a = a^{\text{id}} + a^{\text{mono}} + a^{\text{chain}} + a^{\text{assoc}} \tag{1.1}$$

were the subscripts id, mono, chain and assoc refer to the ideal, monomeric, chain and association contributions to the reduced Helmholtz free energy respectively. Most of the later SAFT-like equations of states have tried to improve the monomeric term of the original SAFT equation. This is where the perturbation theory of Barker and Henderson [5] comes in, as this theory has shown promising results in the context of SAFT theory.

Most of the research on perturbation theory and SAFT equation of states has been focused on single component fluids and little on mixtures. The highly successful SAFT-VR-Mie by Lafitte et al. [23] works well for single component fluids, but struggles in describing mixtures, especially the second order perturbation term as shown in the paper of Hammer et al. [16]. Recently, the SAFT approach has also been developed for Feynman-Hibbs corrected Mie Fluids by Aasen et al. [1, 2] in order to describe novel quantum mixtures between helium and neon that can be used to improve the hydrogen liquefaction process for large-scale export of liquid hydrogen produced from renewable energy. The challenge with neon and helium mixtures however, is that helium has a much smaller well-depth than neon [2] which makes it very difficult to describe. Figure 1.1 illustrates the well-depth of a Lennard-Jones potential. The focus of this paper will therefore be on binary mixtures of Lennard-Jones particles with large differences in well-depths.

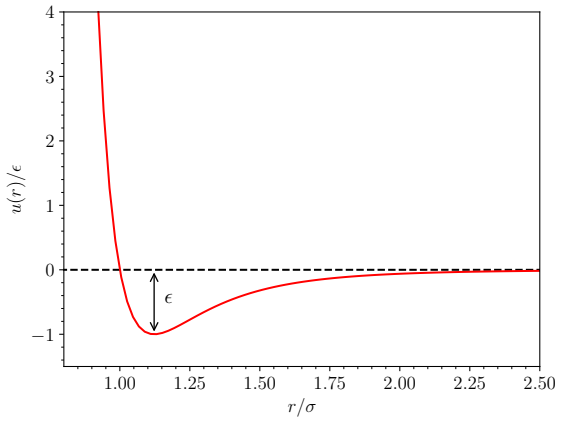

Figure 1.1: The reduced Lennard-Jones potential (u/ϵ) as a function of r/σ. Where r is the distance between two particles, σ is the distance in which the potential is zero and ϵ is the well-depth.

As mentioned previously, the second order term in the work of Lafitte et al. [23] fails for mixtures, but the work of van Westen and Gross [54] has yet to be extended to mixtures, which we will do in this paper. Both Lafitte et al. [23] and van Westen and Gross [54] have used the macroscopic compressibility approximation (MCA) with a correction factor for the second order term, this could be partly the reason for the failure of mixtures. We will therefore also be going back to the older papers and see if a second order term developed, not using the MCA could yield better results. Leonard et al. [26] laid much of the foundation for mixtures in a seminal paper. They derived the perturbation theory for three references: pure component, additive and non-additive. We will only focus on the two first theories. Here the paper by Smith et al. [41] is of particular interest.

All the models will be implemented in Python and compared to Monte Carlo data. The paper is structured in the following way:

- The theoretical foundation behind the perturbation theory will be described in section 2.
- An explanation on how the Monte Carlo data was obtained will be given in section 4.2.
- The results will be compared and discussed in section 5.
- Some suggestions on further work will be given in section 7.

Chapter 2

Theory

The theory section will first go through some general theory and relations from elementary statistical mechanics that will be used to derive the remaining theory, followed by a presentation of the three very well known pair potentials Hard-Sphere, Lennard-Jones and Mie potentials. Then the general perturbation theory will be presented by use of the λ-expansion and the "blip function" procedure for soft core reference systems. This is followed by the specific perturbation procedure of Barker and Henderson.

2.1 Statistical Mechanics

The first part of this section will explain how to start from the general Hamiltonian and end up with the Helmholtz free energy and the equilibrium density for the canonical ensemble. It will also present the configurational integral and the distribution function. The last part of this section will present the grand canonical ensemble and some useful relations there.

Consider a macroscopic, isolated system containing N identical spherical shaped particles of mass m in a volume V. $3N$ coordinates $\mathbf{r}^N \equiv \mathbf{r}_1, ..., \mathbf{r}_N$ and $3N$ momenta $\mathbf{p}^N \equiv \mathbf{p}_1, ..., \mathbf{p}_N$ of the particles completely specifies the dynamical state of a classical mechanical system. The $6N$ variables define a phase point in the $6N$ dimensional phase space. The Hamiltonian ($\mathcal{H}$) of the system can be written in the general form as

$$\mathcal{H}(\mathbf{r}^N, \mathbf{p}^N) = K_N(\mathbf{p}^N) + U_N(\mathbf{r}^N) + \Phi_N(\mathbf{r}^N) \tag{2.1}$$

where K_N is the kinetic energy

$$K_N = \sum_{i=1}^{N} \frac{|\mathbf{p}_i|^2}{2m} \tag{2.2}$$

U_N is the inter-particular potential energy and Φ_N is the potential energy from the interaction between the particles and some spatially varying, external field [18]. Separating the energy in this way is only possible if the potential energy is not dependent upon the velocities. For almost all potential energy functions that are in use this is a safe assumption [24]. The phase-space probability density $\mathcal{F}^{[N]}(\mathbf{r}^N, \mathbf{p}^N; t)$ is introduced, where the quantity $\mathcal{F}^{[N]}\mathrm{d}\mathbf{r}^N\mathrm{d}\mathbf{p}^N$ is the probability that at time t the physical system state can be

represented by a phase point lying in the $6N$-dimensional phase-space element $\mathrm{d}\mathbf{r}^N\mathrm{d}\mathbf{p}^N$. This implies that the integral of $\mathcal{F}^{[N]}$ over all phase space is

$$\int\int \mathcal{F}^{[N]}(\mathbf{r}^N, \mathbf{p}^N; t)\mathrm{d}\mathbf{r}^N\mathrm{d}\mathbf{p}^N = 1 \tag{2.3}$$

for all t. The description of the system that the full phase-space probability density provides is usually more detailed than what is needed. Usually one is more interested in a subset of particles of size n. Thus a reduced phase-space distribution function $\mathcal{F}^{(n)}(\mathbf{r}^n, \mathbf{p}^n; t)$ is defined as:

$$\mathcal{F}^{(n)}(\mathbf{r}^n, \mathbf{p}^n; t) = \frac{N!}{(N-n)!}\int\int \mathcal{F}^{[N]}(\mathbf{r}^N, \mathbf{p}^N; t)\mathrm{d}\mathbf{r}^{(N-n)}\mathrm{d}\mathbf{p}^{(N-n)}. \tag{2.4}$$

Since the redundant information can be eliminated by integrating $\mathcal{F}^{[N]}$ over the coordinates and the momenta of the other $(N-n)$ particles. The combinatorial factor $\frac{N!}{(N-n)!}$ is the number of ways of choosing a subset of size n. The quantity $\mathcal{F}^{[n]}\mathrm{d}\mathbf{r}^n\mathrm{d}\mathbf{p}^n$ gives the probability of a subset n lying in the reduced phase-space element $\mathrm{d}\mathbf{r}^n\mathrm{d}\mathbf{p}^n$ at time t, irrespective of the coordinates and the momenta of the other $N-n$ particles [18].

2.1.1 The canonical Ensemble

Some thermodynamic properties of a physical system can be written as averages of particle coordinate and momenta dependent functions. The so called mechanical properties. At thermal equilibrium state, these averages has to be independent of time. One procedure in obtaining these is to average over a constructed ensemble. A statistical-mechanical ensemble is an arbitrarily large collection of fictional systems, where each of them is a replica of the physical system in interest. They are characterized by the same macroscopic parameters and differ from each other in the assignment of coordinates and momenta of each particle. We will be using the canonical NVT ensemble which is characterized by the same values of N, V and T. The constant T is justified by assuming that the systems of the ensemble are initially brought into thermal equilibrium with each other by submerging them in a heat bath at temperature T. This ensemble has the equilibrium probability density function ($\mathcal{F}_0^{[N]}(\mathbf{r}^N, \mathbf{p}^N)$) for a system of identical spherical particles

$$\mathcal{F}_0^{[N]}(\mathbf{r}^N, \mathbf{p}^N) = \frac{1}{h^{3N}N!}\frac{\exp(-\beta\mathcal{H})}{Q_N} \tag{2.5}$$

where h is the Planck's constant and Q_N is the canonical partition function

$$Q_N = \frac{1}{h^{3N}N!}\int\int \exp(-\beta\mathcal{H})\mathrm{d}\mathbf{r}^N\mathrm{d}\mathbf{p}^N \tag{2.6}$$

while β is $1/k_BT$, where k_B is the Boltzmann constant. Connecting statistical mechanics with thermodynamics is beneficial, thus the Helmholtz free energy A is introduced, which is an appropriate thermodynamical potential for an NVT ensemble, defined as

$$A = \mathcal{U} - T\mathcal{S} \tag{2.7}$$

where T is the temperature, $\mathcal{U}$ is the internal energy and $\mathcal{S}$ is the entropy. The link between statistical mechanics and thermodynamics is through the relation between the thermodynamic potential and the partition function, which for Helmholtz free energy is:

$$A = -k_BT\ln Q_N \tag{2.8}$$

It will be convenient to separate the Helmholtz free energy into an ideal part containing the contribution from a uniform ideal gas which is readily calculable and into a residual part containing the contributions arising from interactions between particles. This can be obtained by rewriting the canonical partition function. First the Hamiltonian is separated in the same way as equation 2.1 and it is assumed no external force. The momenta for the canonical partition function can be integrated analytically and thus the canonical partition function is rewritten as:

$$\begin{aligned} Q_N &= \frac{1}{h^{3N}N!}\int\int \exp(-\beta(K_N(\mathbf{p}^N)+U_N(\mathbf{r}^N)))\mathrm{d}\mathbf{r}^N\mathrm{d}\mathbf{p}^N \\ &= \frac{1}{h^{3N}N!}\int \exp(-\beta U_N(\mathbf{r}^N))\mathrm{d}\mathbf{r}^N \int \exp(-\beta K_N(\mathbf{p}^N))\mathrm{d}\mathbf{p}^N \\ &= \frac{1}{h^{3N}N!}\int \exp(-\beta U_N(\mathbf{r}^N))\mathrm{d}\mathbf{r}^N \int \exp\left(-\beta\sum_{i=1}^{N}\frac{|\mathbf{p}_i|^2}{2m}\right)\mathrm{d}\mathbf{p}^N \end{aligned} \tag{2.9}$$

Since all the particles are equal and their momenta are independent of each other, then each integral over the momenta will also be equal to each other, independent of the momentum label

$$\begin{aligned} Q_N &= \frac{1}{h^{3N}N!}\int \exp(-\beta U_N(\mathbf{r}^N))\mathrm{d}\mathbf{r}^N \left[\int_{-\infty}^{\infty}\exp(-\beta\frac{\mathrm{p}^2}{2m})\mathrm{dp}\right]^{3N} \\ &= \frac{1}{h^{3N}N!}\int \exp(-\beta U_N(\mathbf{r}^N))\mathrm{d}\mathbf{r}^N \left(\frac{2\pi m}{\beta}\right)^{3N/2} \end{aligned} \tag{2.10}$$

Inserting the Broglie thermal wavelength Λ

$$\Lambda = \left(\frac{\beta h^2}{2\pi m}\right)^{1/2} \tag{2.11}$$

into the equation, the following form for the canonical partition function is obtained

$$Q_N = \frac{1}{N!}\frac{Z_N}{\Lambda^{3N}} \tag{2.12}$$

where Z_N is the configurational integral

$$Z_N = \int \exp(-\beta U_N(\mathbf{r}^N))\mathrm{d}\mathbf{r}^N. \tag{2.13}$$

By assuming there are no interactions between the particles $U_N = 0$, the configurational integral for ideal gas is obtained:

$$Z_N^{\mathrm{id}} = \int \exp(-\beta\cdot 0)\mathrm{d}\mathbf{r}^N = \int\cdots\int \mathrm{d}\mathbf{r}_1\cdots\mathrm{d}\mathbf{r}_N = V^N \tag{2.14}$$

where V is the volume. The partition function of an ideal gas will then be

$$Q_N^{\mathrm{id}} = \frac{1}{N!}\frac{V^N}{\Lambda^{3N}} \tag{2.15}$$

The partition function of a system with interacting particles can conveniently be written as

$$Q_N = Q_N^{\mathrm{id}}\frac{Z_N}{V^N} \tag{2.16}$$

and thus the desired form of Helmholtz free energy is obtained:

$$A = -k_B T \ln(Q_N^{\text{id}} \frac{Z_N}{V^N}) = -k_B T \ln Q_N^{\text{id}} - k_B T \ln \frac{Z_N}{V^N} = A^{\text{id}} + A^{\text{res}} \tag{2.17}$$

Returning back onto the equilibrium probability equation 2.5, it would be convenient to obtain an equilibrium particle density, as the work in this thesis will mostly be dealing with position dependent inter-particular potentials. To obtain such a density, a reduced form of the equilibrium probability density function must first be obtained, by inserting equation 2.5 into equation 2.4

$$\begin{aligned}
\mathcal{F}_0^{(n)}(\mathbf{r}^n, \mathbf{p}^n) &= \frac{N!}{(N-n)!} \int\int \mathcal{F}_0^{[N]}(\mathbf{r}^N, \mathbf{p}^N) \mathrm{d}\mathbf{r}^{(N-n)} \mathrm{d}\mathbf{p}^{(N-n)} \\
&= \frac{N!}{(N-n)!} \int\int \frac{1}{h^{3N} N!} \frac{\exp(-\beta \mathcal{H})}{Q_N} \mathrm{d}\mathbf{r}^{(N-n)} \mathrm{d}\mathbf{p}^{(N-n)} \\
&= \frac{N!}{(N-n)!} \frac{1}{h^{3N} N! Q_N} \int \exp(-\beta U_N) \mathrm{d}\mathbf{r}^{(N-n)} \int \exp\left(-\beta \sum_{i=1}^{N} \frac{|\mathbf{p}_i|^2}{2m}\right) \mathrm{d}\mathbf{p}^{(N-n)}
\end{aligned} \tag{2.18}$$

As shown previously in equation 2.10 integration over a component of momentum yields $(2\pi m/\beta)^{1/2}$, so equation 2.18 can be rewritten as

$$\begin{aligned}
\mathcal{F}_0^{(n)}(\mathbf{r}^n, \mathbf{p}^n) =& \frac{N!}{(N-n)!} \frac{1}{h^{3N} N! Q_N} \int \exp(-\beta U_N) \mathrm{d}\mathbf{r}^{(N-n)} \int \exp\left(-\beta \sum_{i=1}^{N} \frac{|\mathbf{p}_i|^2}{2m}\right) \mathrm{d}\mathbf{p}^N \\
&\cdot \frac{1}{(2\pi m/\beta)^{3n/2}} \exp\left(-\beta \sum_{i=1}^{n} \frac{|\mathbf{p}_i|^2}{2m}\right) \\
=& \frac{N!}{(N-n)!} \frac{1}{h^{3N} N! Q_N} \int\int \exp(-\beta \mathcal{H}) \mathrm{d}\mathbf{r}^{(N-n)} \mathrm{d}\mathbf{p}^N \\
&\cdot \frac{1}{(2\pi m/\beta)^{3n/2}} \exp\left(-\beta \sum_{i=1}^{n} \frac{|\mathbf{p}_i|^2}{2m}\right) \\
=& \rho_N^{(n)}(\mathbf{r}^n) f_M^{(n)}(\mathbf{p}^n)
\end{aligned} \tag{2.19}$$

where $\mathcal{F}_M^{(n)}(\mathbf{p}^n)$ is the n-particle Maxwell distribution of momenta

$$\mathcal{F}_M^{(n)}(\mathbf{p}^n) = \frac{1}{(2\pi m/\beta)^{3n/2}} \exp\left(-\beta \sum_{i=1}^{n} \frac{|\mathbf{p}_i|^2}{2m}\right) \tag{2.20}$$

and $\rho_N^{(n)}(\mathbf{r}^n)$ is the desired equilibrium n-particle density

$$\begin{aligned}
\rho_N^{(n)}(\mathbf{r}^n) &= \frac{N!}{(N-n)!}\frac{1}{h^{3N}N!Q_N}\int\int \exp(-\beta\mathcal{H})\mathrm{d}\mathbf{r}^{(N-n)}\mathrm{d}\mathbf{p}^N \\
&= \frac{N!}{(N-n)!}\frac{1}{h^{3N}N!Q_N}\int \exp(-\beta U_N)\mathrm{d}\mathbf{r}^{(N-n)}\int \exp\left(-\beta\sum_{i=1}^{N}\frac{|\mathbf{p}_i|^2}{2m}\right)\mathrm{d}\mathbf{p}^N \\
&= \frac{N!}{(N-n)!}\frac{N!\Lambda^{3N}}{h^{3N}N!Z_N}\int \exp(-\beta U_N)\mathrm{d}\mathbf{r}^{(N-n)}\left(\frac{2\pi m}{\beta}\right)^{3N/2} \\
&= \frac{N!}{(N-n)!}\frac{\Lambda^{3N}}{Z_N}\int \exp(-\beta U_N)\mathrm{d}\mathbf{r}^{(N-n)}\frac{1}{\Lambda^{3N}} \\
&= \frac{N!}{(N-n)!}\frac{1}{Z_N}\int \exp(-\beta U_N)\mathrm{d}\mathbf{r}^{(N-n)}
\end{aligned} \tag{2.21}$$

Finally the n-particle distribution function $g_N^{(n)}(\mathbf{r}^n)$ is introduced, defined as

$$g_N^{(n)}(\mathbf{r}^n) = \frac{\rho_N^{(n)}(\mathbf{r}^n)}{\Pi_{i=1}^{n}\rho_N^{(1)}(\mathbf{r}_i)}. \tag{2.22}$$

which measures how much the structure of a fluid deviates from complete randomness. This thesis will be dealing with homogeneous systems, which simplifies the equation to

$$\rho_N^{(n)}(\mathbf{r}^n) = \rho^n g_N^{(n)}(\mathbf{r}^n) \tag{2.23}$$

where ρ is the particle density N/V [18]. The two relations from equation 2.21 and equation 2.23 will be important in the perturbation theory section.

2.1.2 The Grand Canonical Ensemble

The previous section was for a homogeneous system with constant number of particles (closed). This section will discuss a homogeneous open system. The thermodynamic state is then defined by specifying the values of μ, V and T, where μ is the chemical potential. The corresponding thermodynamic potential is the grand potential Ω, defined as

$$\Omega = A - \langle N\rangle\mu \tag{2.24}$$

where $\langle N\rangle$ is the average number of particles [18]. It is assumed that there is no external field and that the system is homogeneous, thus the internal energy can be written as

$$\mathcal{U} = T\mathcal{S} - PV + \mu\langle N\rangle \tag{2.25}$$

which reduces the grand potential to

$$\Omega = -PV \tag{2.26}$$

while the differential form of equation 2.24 is

$$\mathrm{d}\Omega = -\mathcal{S}\mathrm{d}T - P\mathrm{d}V - \langle N\rangle\mathrm{d}\mu \tag{2.27}$$

From the derivatives of Ω the following properties can be obtained

$$\mathcal{S} = -\left(\frac{\partial\Omega}{\partial T}\right)_{V,\mu} \tag{2.28}$$

$$P = -\left(\frac{\partial \Omega}{\partial V}\right)_{T,\mu} \tag{2.29}$$

$$\langle N \rangle = -\left(\frac{\partial \Omega}{\partial \mu}\right)_{T,V} \tag{2.30}$$

The grand canonical ensemble is the ensemble for systems that have constant μ, V and T values. This is ensured by assuming that all the systems of the ensemble are allowed to come to equilibrium with a reservoir, where they can exchange both heat and matter. The normalised probability density function is now

$$\mathcal{F}_0(\mathbf{r}^N, \mathbf{p}^N; N) = \frac{\exp(-\beta(\mathcal{H} - N\mu))}{\Xi} \tag{2.31}$$

where Ξ is the grand partition function given as

$$\Xi = \sum_{N=0}^{\infty} \frac{\exp(N\beta\mu)}{h^{3N} N!} \int\int \exp(-\beta\mathcal{H}) \mathrm{d}\mathbf{r}^N \mathrm{d}\mathbf{p}^N = \sum_{N=0}^{\infty} \frac{z^N}{N!} Z_N \tag{2.32}$$

and z is the activity given as

$$z = \frac{\exp(\beta\mu)}{\Lambda^3} \tag{2.33}$$

The link with thermodynamics is obtained by the relation

$$\Omega = -k_B T \ln \Xi \tag{2.34}$$

The probability, $p(N)$ that at equilibrium this system will contain exactly N particles irrespective of their coordinates and momenta is

$$p(N) = \frac{1}{h^{3N} N!} \int\int \mathcal{F}_0 \mathrm{d}\mathbf{r}^N \mathrm{d}\mathbf{p}^N = \frac{1}{\Xi} \frac{z^N}{N!} Z_N \tag{2.35}$$

the average number of particles $\langle N \rangle$ is then

$$\langle N \rangle = \sum_{N=0}^{\infty} N p(N) = \frac{1}{\Xi} \sum_{N=0}^{\infty} N \frac{z^N}{N!} Z_N = \frac{\partial \ln \Xi}{\partial \ln z} \tag{2.36}$$

A measure of fluctuation in number of particles about its average value can be obtained by the mean-square deviation, which can be obtained by differentiating $\langle N \rangle$ with respect to $\ln z$:

$$\begin{aligned} \frac{\partial \langle N \rangle}{\partial \ln z} &= z \frac{\partial}{\partial z} \left(\frac{1}{\Xi} \sum_{N=0}^{\infty} N \frac{z^N}{N!} Z_N \right) \\ &= \frac{1}{\Xi} \sum_{N=0}^{\infty} N^2 \frac{z^N}{N!} Z_N - \left(\frac{1}{\Xi} \sum_{N=0}^{\infty} N \frac{z^N}{N!} Z_N \right)^2 \\ &= \langle N^2 \rangle - \langle N \rangle^2 \equiv \langle (\Delta N)^2 \rangle \end{aligned} \tag{2.37}$$

Which can be rewritten as

$$\frac{\langle (\Delta N)^2 \rangle}{\langle N \rangle} = \frac{1}{\langle N \rangle} \frac{\partial \langle N \rangle}{\partial \mu} \frac{\partial \mu}{\partial \ln z} = \frac{k_B T}{\langle N \rangle} \frac{\partial \langle N \rangle}{\partial \mu}. \tag{2.38}$$

The right hand side is an intensive quantity, which means that the left hand side also has to be intensive. Therefore when $\langle N\rangle \to \infty$, $\langle(\Delta N)^2\rangle^{1/2}/\langle N\rangle \to 0$. in other words, in the thermodynamic limit $\langle N\rangle \to \infty$, $V \to \infty$, with $\rho = \langle N\rangle/V$ held constant, the number of particles in the system can be found from the grand canonical average $\langle N\rangle$. The thermodynamic properties calculated from other ensembles will become identical in the thermodynamic limit. We introduce the isothermal compressibility χ_T, defined as

$$\chi_T = -\frac{1}{V}\left(\frac{\partial V}{\partial P}\right)_T. \tag{2.39}$$

We want to relate this to the intensive ratio (equation 2.38). In order to do this we note that the Helmholtz free energy is an extensive property and therefore must be expressible as

$$A = N\bar{A}(\rho, T) \tag{2.40}$$

where $\bar{A}$ is the free energy per particle. Using the following relation for the Helmholtz free energy

$$\mu = \left(\frac{\partial A}{\partial N}\right)_{T,V} \tag{2.41}$$

the following relations can be obtained for the free energy per particle

$$\mu = \bar{A} + \rho\left(\frac{\partial \bar{A}}{\partial \rho}\right)_T \tag{2.42}$$

$$\left(\frac{\partial \mu}{\partial \rho}\right)_T = 2\left(\frac{\partial \bar{A}}{\partial \rho}\right)_T + \rho\left(\frac{\partial^2 \bar{A}}{\partial \rho^2}\right)_T \tag{2.43}$$

We also have the following relation for the Helmholtz free energy

$$P = -\left(\frac{\partial A}{\partial V}\right)_{T,N} = -\frac{\partial A}{\partial \rho}\frac{\partial \rho}{\partial V} = \rho^2\left(\frac{\partial \bar{A}}{\partial V}\right)_T \tag{2.44}$$

Taking the derivative of this relation gives us

$$\left(\frac{\partial P}{\partial \rho}\right)_T = 2\rho\left(\frac{\partial \bar{A}}{\partial \rho}\right)_T + \rho^2\left(\frac{\partial^2 \bar{A}}{\partial \rho^2}\right)_T = \rho\left(\frac{\partial \mu}{\partial \rho}\right)_T \tag{2.45}$$

combining this with

$$\left(\frac{\partial P}{\partial \rho}\right)_T = -\frac{V^2}{N}\left(\frac{\partial P}{\partial V}\right)_{N,T} = \frac{1}{\rho\chi_T} \tag{2.46}$$

and

$$\left(\frac{\partial \mu}{\partial \rho}\right)_T = V\left(\frac{\partial \mu}{\partial N}\right)_{V,T} \tag{2.47}$$

gives the relation

$$\begin{aligned} \frac{1}{\rho\chi_T} &= \rho V\left(\frac{\partial \mu}{\partial N}\right)_{V,T} \\ N\left(\frac{\partial \mu}{\partial N}\right)_{V,T} &= \frac{1}{\rho\chi_T} \end{aligned} \tag{2.48}$$

combining this with equation 2.38 at the thermodynamic limit gives the useful relation

$$\frac{\langle(\Delta N)^2\rangle}{\langle N\rangle} = \rho k_B T \chi_T \tag{2.49}$$

which will be an important relation for the macroscopic compressibility approximation explained in section 2.4 [18].

2.2 Hard-Sphere Potential

The repulsion between molecules or atoms at short range that have their origin from the overlap of the outer electron shell, is very important for the calculation of pair potentials. The attractive force however, although acting on long ranges, vary much more smoothly and has a minor impact on the liquid structure. The simplest model for a fluid reflecting these observations is the hard-sphere model, that ignores the attractive force all together. The pair potential $u(r)$ is written as

$$u_d^{\text{hs}}(r) = \begin{cases} \infty & r < d \\ 0 & r > d \end{cases} \tag{2.50}$$

where d is the hard-sphere diameter. This model works well for studies where the hard-core of the potential is dominant. The understanding one have of the model today, is mostly from computer simulations and have had no significant difference from more complicated inter particular potential models, especially at conditions close to crystallization [18].

2.3 Lennard-Jones and Mie Potential

A more realistic potential for neutral atoms than the hard-sphere potential can be obtained from quantum mechanical calculations. When the separation between the particles is large, the dominant contribution to the potential comes from dispersion forces such as dipole-dipole interaction, dipole-quadrupole interaction and London dispersion. All these terms represent attractive contributions to the potential, the leading term however is the dipole-dipole interaction varying with r^{-6}. The other terms are generally small compared to the leading term and are thus neglected. The short range interaction however is harder to calculate, thus for mathematical convenience, it is common to represent the short range contribution with an inverse-power law on the form of r^{-l}. For closed-shell atoms l will be between 9 and 15. $u(r)$ in the limiting cases of $r \to \infty$ and $r \to 0$ can be described as

$$u^{\text{lj}}(r) = 4\epsilon \left[\left(\frac{\sigma}{r}\right)^{12} - \left(\frac{\sigma}{r}\right)^{6} \right] \tag{2.51}$$

which is the 12-6 Lennard-Jones potential originally proposed by Jones [20], where σ is the collision diameter, which is the separation of particles ($u(r) = 0$). ϵ is the depth of the potential well at the minimum potential in $u(r)$, which is at $r_{\text{min}} = 2^{1/6}\sigma$ [18]. The alternative to the Lennard-Jones potential is the Mie potential by Mie [30]. This potential allows for a more flexible description of the repulsive and the attractive terms:

$$u^{\text{mie}}(r) = \mathcal{C}\epsilon \left[\left(\frac{\sigma}{r}\right)^{l_r} - \left(\frac{\sigma}{r}\right)^{l_a} \right] \tag{2.52}$$

where

$$\mathcal{C} = \frac{l_r}{l_r - l_a}\left(\frac{l_r}{l_a}\right)^{\frac{l_a}{l_r - l_a}}. \tag{2.53}$$

The variable $\mathcal{C}$ is described as it is to ensure that the minimum of the potential remains $-\epsilon$ regardless of what the repulsive l_r and the attractive l_a parameters are. The repulsive parameter l_r will always have to be larger than the attractive parameter l_a. By letting $l_r = 12$ and $l_a = 6$ the Lennard-Jones potential is recovered. Figure 2.1 shows the Mie potential for different repulsive and attractive parameters.

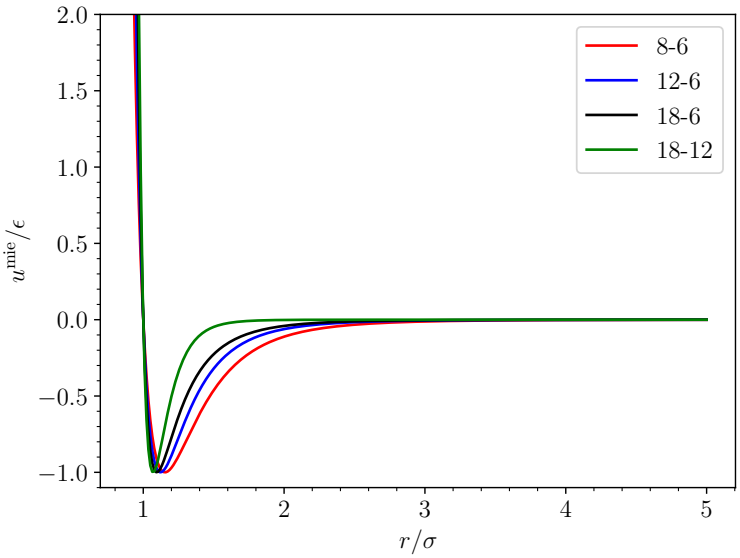

Figure 2.1: The reduced 8-6, 12-6, 18-6 and 18-12 Mie potential as a function of r/σ.

This project will be focusing on the Lennard-Jones potential.

2.4 Perturbation Theory

This section will explain the general perturbation theory. It is assumed a homogeneous system and that the interactions between particles are spherically symmetric and pairwise additive. The basis of the perturbation theory that is discussed is the division of the pair potential

$$u(r_{ij}) = u_0(r_{ij}) + w(r_{ij}) \tag{2.54}$$

where $u_0(r_{ij})$ is the pair potential of the reference system, while $w(r_{ij})$ is the perturbation. The perturbation calculation usually proceed in two stages, where the first step is to calculate the effects of the perturbation on the thermodynamic properties and pair distribution function of the reference system. This will be done systematically through an expansion in powers of the inverse temperature up to the second order term, the λ-expansion. We will also present two other different approaches in calculating the second order term. The second step is then to relate the properties of the soft-core reference system over to those of a hard-sphere fluid, as the hard-sphere system is much more well understood and thus easier to perform the perturbation on.

2.4.1 The λ-Expansion

This section will present the λ-expansion.
We start by considering the following pair potential

$$u_\lambda(r_{ij}) = u_{\lambda_0}(r_{ij}) + w_\lambda(r_{ij}) \tag{2.55}$$

where λ is a coupling parameter that gradually switches the perturbation w_λ on from the reference system u_0. We let $U_N(\mathbf{r}^N;\lambda)$ be the total potential energy of the system due to particle interaction

$$U_N(\mathbf{r}^N;\lambda) = \sum_{i=1}^{N}\sum_{j>i}^{N} u_\lambda(r_{ij}) \tag{2.56}$$

Recall that the Helmholtz energy can be written on the form $A = A^{\text{id}} + A^{\text{res}}$. Since the decomposition is on the inter-particular potential, it has no effect on the kinetic part of the Helmholtz free energy and thus the attention is on the residual Helmholtz free energy. Taking the derivative of the residual Helmholtz free energy

$$\begin{aligned}
\frac{\partial A^{\text{res}}(\lambda)}{\partial\lambda} &= -\frac{\partial\left(k_BT\ln\frac{Z_N(\lambda)}{V^N}\right)}{\partial\lambda} \\
&= -\frac{1}{\beta Z_N(\lambda)}\frac{\partial Z_N(\lambda)}{\partial\lambda} \\
&= \frac{1}{\beta Z_N(\lambda)}\int \exp(-\beta U_N(\mathbf{r}^N;\lambda))\beta\frac{\partial U_N(\mathbf{r}^N;\lambda)}{\partial\lambda}\mathrm{d}\mathbf{r}^N \\
&= \langle U_N'(\mathbf{r}^N;\lambda)\rangle_\lambda
\end{aligned} \tag{2.57}$$

The angular brackets denotes a canonical ensemble average for a system of N particles

$$\langle f\rangle = \frac{\int f\exp(-\beta U_N)\mathrm{d}\mathbf{r}^N}{Z_N} \tag{2.58}$$

By integrating equation 2.57 an equation for the perturbed residual Helmholtz free energy is obtained

$$A^{\text{res}}(\lambda_1) = A_0^{\text{res}} + \int_{\lambda_0}^{\lambda_1}\langle U_N'(\mathbf{r}^N;\lambda)\rangle_\lambda\mathrm{d}\lambda \tag{2.59}$$

where A_0^{res} is the residual Helmholtz free energy of the reference system. We expand the ensemble average in a series expansion about $\lambda = \lambda_0$

$$\langle U_N'(\mathbf{r}^N;\lambda)\rangle_\lambda = \langle U_N'(\mathbf{r}^N;\lambda)\rangle_{\lambda_0} + (\lambda-\lambda_0)\frac{\partial}{\partial\lambda}\langle U_N'(\mathbf{r}^N;\lambda)\rangle_\lambda\bigg|_{\lambda=\lambda_0} + \mathcal{O}(\lambda-\lambda_0)^2 \tag{2.60}$$

The first derivative of $\langle U'_N(\lambda)\rangle_\lambda$ with respect to λ is

$$\begin{aligned}
\frac{\partial\langle U'_N(\mathbf{r}^N;\lambda)\rangle_\lambda}{\partial\lambda} =& \frac{Z_N(\lambda)\int(-\beta\exp(-\beta U_N(\mathbf{r}^N;\lambda))U'_N(\mathbf{r}^N;\lambda)U'_N(\mathbf{r}^N;\lambda))\mathrm{d}\mathbf{r}^N}{Z_N(\lambda)^2} \\
&+ \frac{Z_N(\lambda)\int(\exp(-\beta U_N(\mathbf{r}^N;\lambda))U''_N(\mathbf{r}^N;\lambda)\mathrm{d}\mathbf{r}^N}{Z_N(\lambda)^2} \\
&- \frac{Z'_N(\lambda)\int(\exp(-\beta U_N(\mathbf{r}^N;\lambda))U'_N(\lambda)\mathrm{d}\mathbf{r}^N}{Z_N(\lambda)^2} \\
=& -\frac{\beta\int\exp(-\beta U_N(\mathbf{r}^N;\lambda))U'_N(\lambda)^2\mathrm{d}\mathbf{r}^N}{Z_N(\lambda)} \\
&+ \frac{\int(\exp(-\beta U_N(\mathbf{r}^N;\lambda))U''_N(\mathbf{r}^N;\lambda)\mathrm{d}\mathbf{r}^N}{Z_N(\lambda)} \\
&- \frac{Z'_N(\lambda)\int\exp(-\beta U_N(\mathbf{r}^N;\lambda))U'_N(\mathbf{r}^N;\lambda)\mathrm{d}\mathbf{r}^N}{Z_N(\lambda)^2} \\
=&\langle U''_N(\mathbf{r}^N;\lambda)\rangle_\lambda - \beta\langle U'_N(\mathbf{r}^N;\lambda)^2\rangle_\lambda - \\
&\frac{1}{Z_N(\lambda)^2}\left[-\beta\int\exp(-\beta U_N(\mathbf{r}^N;\lambda))U'_N(\mathbf{r}^N;\lambda)\mathrm{d}\mathbf{r}^N\right. \\
&\left.\cdot\int\exp(-\beta U_N(\mathbf{r}^N;\lambda))U'_N(\mathbf{r}^N;\lambda)\mathrm{d}\mathbf{r}^N\right] \\
=&\langle U''_N(\mathbf{r}^N;\lambda)\rangle_\lambda - \beta\langle U'_N(\mathbf{r}^N;\lambda)^2\rangle_\lambda + \beta\langle U'_N(\mathbf{r}^N;\lambda)\rangle^2_\lambda
\end{aligned} \tag{2.61}$$

Inserting the derivative into equation 2.60 and equation 2.59 gives

$$\begin{aligned}
A^{\mathrm{res}}(\lambda_1) =& A_0^{\mathrm{res}} + \int_{\lambda_0}^{\lambda_1}(\langle U'_N(\mathbf{r}^N;\lambda_0)\rangle_{\lambda_0} + (\lambda-\lambda_0)\left[\langle U''_N(\mathbf{r}^N;\lambda_0)\rangle_{\lambda_0}\right. \\
&\left.-\beta\langle U'_N(\mathbf{r}^N;\lambda_0)^2\rangle_{\lambda_0} + \beta\langle U'_N(\mathbf{r}^N;\lambda_0)\rangle^2_{\lambda_0}\right])\mathrm{d}\lambda + \int_{\lambda_0}^{\lambda_1}\mathcal{O}(\lambda-\lambda_0)^2\mathrm{d}\lambda \\
=& A_0^{\mathrm{res}} + \left[\lambda\langle U'_N(\mathbf{r}^N;\lambda_0)\rangle_{\lambda_0} + \left(\frac{1}{2}\lambda^2 - \lambda\lambda_0\right)\left[\langle U''_N(\mathbf{r}^N;\lambda_0)\rangle_{\lambda_0}\right.\right. \\
&\left.\left.-\beta\langle U'_N(\mathbf{r}^N;\lambda_0)^2\rangle_{\lambda_0} + \beta\langle U'_N(\mathbf{r}^N;\lambda_0)\rangle^2_{\lambda_0}\right]\right]_{\lambda_0}^{\lambda_1} + \mathcal{O}(\lambda-\lambda_0)^3 \\
=& A_0^{\mathrm{res}} + (\lambda_1-\lambda_0)\langle U'_N(\mathbf{r}^N;\lambda_0)\rangle_{\lambda_0} + \left(\frac{1}{2}\lambda_1^2 - \frac{1}{2}\lambda_0^2 - \lambda_1\lambda_0 + \lambda_0^2\right) \\
&\cdot\left[\langle U''_N(\mathbf{r}^N;\lambda_0)\rangle_{\lambda_0} - \beta\langle U'_N(\lambda_0)^2\rangle_{\lambda_0} + \beta\langle U'_N(\mathbf{r}^N;\lambda_0)\rangle^2_{\lambda_0}\right] + \mathcal{O}(\lambda-\lambda_0)^3 \\
=& A_0^{\mathrm{res}} + (\lambda_1-\lambda_0)\langle U'_N(\mathbf{r}^N;\lambda_0)\rangle_{\lambda_0} + \frac{1}{2}(\lambda_1-\lambda_0)^2\left[\langle U''_N(\mathbf{r}^N;\lambda_0)\rangle_{\lambda_0}\right. \\
&\left.-\beta[\langle U'_N(\mathbf{r}^N;\lambda_0)^2\rangle_{\lambda_0} - \langle U'_N(\mathbf{r}^N;\lambda_0)\rangle^2_{\lambda_0}]\right] + \mathcal{O}(\lambda-\lambda_0)^3
\end{aligned} \tag{2.62}$$

For small attractive perturbations, a linear scaling on the coupling parameter can simplify the expressions. Thus the pair potential is written as

$$u_\lambda(r_{ij}) = u_0(r_{ij}) + \lambda w(r_{ij}) \tag{2.63}$$

with $\lambda_0 = 0$ and $\lambda_1 = 1$. We choose to define the total perturbation energy for $\lambda = 1$ as

$$W_N(\mathbf{r}^N) = \sum_{i=1}^{N} \sum_{j>i}^{N} w(r_{ij}). \tag{2.64}$$

Then $U'_N(\mathbf{r}^N) = W_N(\mathbf{r}^N)$ and $U''_N(\mathbf{r}^N) = 0$ [18]. Equation 2.62 then simplifies to

$$A^{\text{res}} = A_0^{\text{res}} + \langle W_N(\mathbf{r}^N)\rangle_0 - \frac{1}{2}\beta[\langle W_N(\mathbf{r}^N)^2\rangle_0 - \langle W_N(\mathbf{r}^N)\rangle_0^2] + \mathcal{O}(\beta^2) \tag{2.65}$$

This is the same equation that was originally derived by Zwanzig [58]. The dimensionless Helmholtz energy per particle $a^{\text{res}} = \beta A^{\text{res}}/N$ is introduced and the perturbation is written as

$$a^{\text{res}} = \sum_{i=0}^{\infty} a_i \beta^i \tag{2.66}$$

[23] with

$$a_1 = \frac{1}{N}\langle W_N(\mathbf{r}^N)\rangle_0 \tag{2.67}$$

$$a_2 = -\frac{1}{2N}[\langle W_N(\mathbf{r}^N)^2\rangle_0 - \langle W_N(\mathbf{r}^N)\rangle_0^2] \tag{2.68}$$

By noticing that the double sum in equation 2.64 yields $N(N-1)/2$ terms, each of which gives the same result after integration, the a_1 term can be further simplified to

$$a_1 = \frac{1}{N}\frac{N(N-1)}{2}\int\int w(r_{12})\left(\frac{1}{Z_N}\int\cdots\int \exp(-\beta U_{N,0}(\mathbf{r}^N))\mathrm{d}\mathbf{r}_3\cdots\mathrm{d}\mathbf{r}_N\right)\mathrm{d}\mathbf{r}_1\mathrm{d}\mathbf{r}_2 \tag{2.69}$$

where $U_{N,0}$ is the reference system potential. We recognize the inner integration's as the n-particle density equation 2.21 and insert this into the equation

$$\begin{aligned} a_1 &= \frac{1}{N}\frac{N(N-1)}{2}\int\int w(r_{12})\frac{(N-2)!}{N!}\rho^{(2)}_{N,0}(\mathbf{r}_1,\mathbf{r}_2)\mathrm{d}\mathbf{r}_1\mathrm{d}\mathbf{r}_2 \\ &= \frac{1}{N}\frac{N(N-1)}{2}\int\int w(r_{12})\frac{1}{N(N-1)}\rho^{(2)}_{N,0}(\mathbf{r}_1,\mathbf{r}_2)\mathrm{d}\mathbf{r}_1\mathrm{d}\mathbf{r}_2 \\ &= \frac{1}{N}\frac{1}{2}\int\int w(r_{12})\rho^{(2)}_{N,0}(\mathbf{r}_1,\mathbf{r}_2)\mathrm{d}\mathbf{r}_1\mathrm{d}\mathbf{r}_2 \end{aligned} \tag{2.70}$$

The n-particle distribution function 2.23 is inserted:

$$a_1 = \frac{1}{N}\frac{\rho^2}{2}\int\int w(r_{12})g^{(2)}_{N,0}(\mathbf{r}_1,\mathbf{r}_2)\mathrm{d}\mathbf{r}_1\mathrm{d}\mathbf{r}_2. \tag{2.71}$$

Let the position of particle 1 be the origin of the coordinates and set $\mathbf{r}_{12} = \mathbf{r}_2 - \mathbf{r}_1$. Utilizing that d$\mathbf{r}_{12}$=d$\mathbf{r}_2$ and integrating over coordinate $\mathbf{r}_1$ we obtain

$$\begin{aligned} a_1 &= \frac{1}{N}\frac{\rho^2}{2}\int\int w(r_{12})g_0(r_{12})\mathrm{d}\mathbf{r}_1\mathrm{d}\mathbf{r}_{12} \\ &= \frac{1}{N}\frac{\rho^2 V}{2}\int w(r)g_0(r)\mathrm{d}\mathbf{r} \end{aligned} \tag{2.72}$$

Here it is assumed that the system is isotropic thus $g_0(\mathbf{r}_{12}) = g_0(r_{12})$. The integration yields the volume as both $w(r_{12})$ and $g_0(r_{12})$ are independent of $\mathbf{r}_1$ as the position of particle 1 is the origin. Finally the three dimensional $\mathrm{d}\mathbf{r}$ is substituted with $4\pi r^2 \mathrm{d}r$

$$\begin{aligned} a_1 &= \frac{1}{N} 2\pi\rho^2 V \int_0^\infty w(r) g_0(r) r^2 \mathrm{d}r \\ &= 2\pi\rho \int_0^\infty w(r) g_0(r) r^2 \mathrm{d}r \end{aligned} \tag{2.73}$$

The radial distribution function $g(r)$ is important in the physics of monoatomic liquids. First of all, it is measurable by radiation-scattering experiments. Secondly, the form of the function gives insight into what the structure of liquid means, as the definition of $g(r)$ implies that on average the number of particles between r and $r + \mathrm{d}r$ from a reference particle will be $4\pi r^2 \rho g(r) \mathrm{d}r$ [18]. The physical interpretation of the first order perturbation term is that it is the average particle interaction potential calculated using the structure of the reference system [13].

The results obtained by Zwanzig [58] as seen in equation 2.65 is unfortunately not as useful for the second order term, as it has been obtained in the canonical ensemble and is therefor only valid for a finite system. To obtain a more useful expression, one can take the thermodynamic limit ($N \to \infty$, N/V fixed). However this involves the asymptotic behaviour of the four-body distribution function, when two of the particles involved are remote from the other two. A way to avoid this is to derive the necessary results in the grand canonical ensemble, where there is no problems with the asymptotic behaviour of the distribution functions. These can then be used for the canonical ensemble through suitable transformations. We expand the free energy in powers of λ into the following perturbation series

$$A = A_0 + \lambda \left(\frac{\partial A}{\partial \lambda} \right)_{\lambda=0} + \frac{1}{2}\lambda^2 \left(\frac{\partial^2 A}{\partial \lambda^2} \right)_{\lambda=0} + \mathcal{O}(\lambda^3) \tag{2.74}$$

The first step now is to find the first and second derivative of the logarithm of the grand partition function 2.32 with respect to λ. The first derivative is

$$\begin{aligned} \frac{\partial \ln(\Xi(\lambda))}{\partial \lambda} &= \frac{\partial \ln\left(\sum_{N=0}^\infty \frac{z^N}{N!} Z_N(\lambda) \right)}{\partial \lambda} \\ &= -\frac{\beta}{\Xi(\lambda)} \sum_{N=0}^\infty \frac{z^N}{N!} \int \exp(-\beta U_N(\mathbf{r}^N; \lambda)) \frac{\partial U_N(\mathbf{r}^N; \lambda)}{\partial \lambda} \mathrm{d}\mathbf{r}^N \end{aligned} \tag{2.75}$$

Once again, only pair interactions are considered for $U_N(\mathbf{r}^N; \lambda)$ and $u_\lambda(r_{ij})$ is on the form of equation 2.63. Since the system is assumed to be homogeneous, the double sum will yield $N(N-1)/2$ terms with all giving the same result after integration and hence the term is simplified to

$$\frac{\partial \ln(\Xi)}{\partial \lambda} = -\frac{\beta}{2\Xi} \sum_{N=0}^\infty \frac{z^N}{N!} N(N-1) \int\int w(r_{12}) \left(\int \cdots \int \exp(-\beta U_{N,0}(\mathbf{r}^N)) \mathrm{d}\mathbf{r}^{N-2} \right) \mathrm{d}\mathbf{r}_1 \mathrm{d}\mathbf{r}_2 \tag{2.76}$$

In the grand canonical ensemble, the probability of there being particles in the element $\mathrm{d}\mathbf{r}_1 \cdots \mathrm{d}\mathbf{r}_n$ is

$$\rho^{(n)}(\mathbf{r}^n) = \frac{1}{\Xi} \sum_{N=n}^\infty \frac{z^N}{(N-n)!} \int \exp(-\beta U_N) \mathrm{d}\mathbf{r}^{N-n} \tag{2.77}$$

Inserting this into equation 2.76 and realising that the two first terms in the sum ($N = 0$ and $N = 1$) will be zero, the following expression is obtained

$$\frac{\partial \ln\Xi}{\partial \lambda} = -\frac{\beta}{2}\int\int \rho_0^{(2)}(\mathbf{r}_1,\mathbf{r}_2)w(r_{12})\mathrm{d}\mathbf{r}_1\mathrm{d}\mathbf{r}_2 \tag{2.78}$$

The second derivative becomes

$$\begin{aligned}
\frac{\partial^2 \ln\Xi}{\partial \lambda^2} =& -\frac{\beta}{2}\int\int \rho_0^{(2)}(\mathbf{r}_1,\mathbf{r}_2)\frac{\partial w(r_{12})}{\partial\lambda}\mathrm{d}\mathbf{r}_1\mathrm{d}\mathbf{r}_2 - \frac{\beta}{2}\int\int \frac{\partial \rho_0^{(2)}(\mathbf{r}_1,\mathbf{r}_2)}{\partial\lambda}w(r_{12})\mathrm{d}\mathbf{r}_1\mathrm{d}\mathbf{r}_2 \\
=&\frac{\beta}{2}\int\int \frac{1}{\Xi^2}\left(\sum_{N=2}^{\infty}\frac{z^N}{(N-2)!}\int\cdots\int \exp(-\beta U_N)\mathrm{d}\mathbf{r}^{N-2}\right)w(r_{12})\frac{\partial\Xi}{\partial\lambda}\mathrm{d}\mathbf{r}_1\mathrm{d}\mathbf{r}_2 \\
&+\frac{\beta^2}{2}\left(\sum_{N=2}^{\infty}\frac{1}{\Xi}\frac{z^N}{N!}\frac{1}{2}\sum_{i\neq j}\sum_{k\neq l}\int w(r_{ij})w(r_{kl})\exp(-\beta U_N)\mathrm{d}\mathbf{r}^N\right) \\
=&-\frac{\beta}{4}\int\int\int\int \rho_0^{(2)}(\mathbf{r}_1,\mathbf{r}_2)\rho_0^{(2)}(\mathbf{r}_3,\mathbf{r}_4)w(r_{12})w(r_{34})\mathrm{d}\mathbf{r}_1\mathrm{d}\mathbf{r}_2\mathrm{d}\mathbf{r}_3\mathrm{d}\mathbf{r}_4 + \\
&\frac{\beta^2}{4}\sum_{N=2}^{\infty}\frac{z^N}{\Xi N!}\frac{N!}{(N-4)!}\int\int\int\int w(r_{12})w(r_{34})\left(\int\cdots\int \exp(-\beta U_N)\mathrm{d}\mathbf{r}^{N-4}\right)\mathrm{d}\mathbf{r}_1\mathrm{d}\mathbf{r}_2\mathrm{d}\mathbf{r}_3\mathrm{d}\mathbf{r}_4 \\
&+\frac{\beta^2}{4}\sum_{N=2}^{\infty}\frac{z^N}{\Xi N!}\frac{N!}{(N-3)!}4\int\int\int w(r_{12})w(r_{23})\left(\int\cdot\int \exp(-\beta U_N)\mathrm{d}\mathbf{r}^{N-3}\right)\mathrm{d}\mathbf{r}_1\mathrm{d}\mathbf{r}_2\mathrm{d}\mathbf{r}_3 \\
&+\frac{\beta^2}{4}\sum_{N=2}^{\infty}\frac{z^N}{\Xi N!}\frac{N!}{(N-2)!}\int\int w(r_{12})^2\left(\int\cdot\int \exp(-\beta U_N)\mathrm{d}\mathbf{r}^{N-2}\right)\mathrm{d}\mathbf{r}_1\mathrm{d}\mathbf{r}_2 \\
=&\frac{\beta^2}{2}\int\int \rho_0^{(2)}(\mathbf{r}_1,\mathbf{r}_2)w(r_{12})^2\mathrm{d}\mathbf{r}_1\mathrm{d}\mathbf{r}_2 + \beta^2\int\int\int \rho_0^{(3)}(\mathbf{r}_1,\mathbf{r}_2,\mathbf{r}_3)w(r_{12})w(r_{23})\mathrm{d}\mathbf{r}_1\mathrm{d}\mathbf{r}_2\mathrm{d}\mathbf{r}_3 \\
&\frac{\beta^2}{4}\int\int\int\int \left(\rho_0^{(4)}(\mathbf{r}_1,\mathbf{r}_2,\mathbf{r}_3,\mathbf{r}_4) - \rho_0^{(2)}(\mathbf{r}_1,\mathbf{r}_2)\rho_0^{(2)}(\mathbf{r}_3,\mathbf{r}_4)\right)w(r_{12})w(r_{34})\mathrm{d}\mathbf{r}_1\mathrm{d}\mathbf{r}_2\mathrm{d}\mathbf{r}_3\mathrm{d}\mathbf{r}_4
\end{aligned} \tag{2.79}$$

The derivatives of Helmholtz free energy can now be obtained through thermodynamic arguments. From equation 2.24, 2.26 and 2.34 one have that

$$A = \langle N\rangle\mu - PV = \langle N\rangle\mu - k_BT\ln\Xi \tag{2.80}$$

While from equation 2.30 one can obtain the relation

$$\langle N\rangle = k_BT[\partial(\ln\Xi)/\partial\mu]_{\lambda,T,V} \tag{2.81}$$

therefore

$$\begin{aligned}
\left(\frac{\partial A}{\partial\lambda}\right)_\rho =&\langle N\rangle\left(\frac{\partial\mu}{\partial\lambda}\right)_\rho - k_BT\left(\frac{\partial(\ln\Xi)}{\partial\lambda}\right)_\rho \\
=&\langle N\rangle\left(\frac{\partial\mu}{\partial\lambda}\right)_\rho - k_BT\left(\frac{\partial(\ln\Xi)}{\partial\lambda}\right)_\mu - k_BT\left(\frac{\partial(\ln\Xi)}{\partial\mu}\right)_\lambda\left(\frac{\partial\mu}{\partial\lambda}\right)_\rho \\
=&-k_BT\left(\frac{\partial(\ln\Xi)}{\partial\lambda}\right)_\mu
\end{aligned} \tag{2.82}$$

inserting equation 2.76 and equation 2.23 as well as integrating in the same way as explained in the previous section gives

$$\left(\frac{\partial A}{\partial\lambda}\right)_{\lambda=0} = \frac{1}{2}N\rho\int g_0(r_{12})w(r_{12})\mathrm{d}\mathbf{r}_2 \tag{2.83}$$

which is the same result as the one obtained in the canonical ensemble. The second derivative gives

$$\left(\frac{\partial^2 A}{\partial\lambda^2}\right) = -k_BT\left(\frac{\partial^2(\ln\Xi)}{\partial\lambda^2}\right)_\mu - k_BT\left(\frac{\partial^2(\ln\Xi)}{\partial\lambda\partial\mu}\right)\left(\frac{\partial\mu}{\partial\lambda}\right)_\rho \tag{2.84}$$

Differentiating equation 2.81 gives

$$\mathrm{d}\langle N\rangle = k_B T \left(\frac{\partial^2(\ln\Xi)}{\partial\mu^2}\right)_{T,V} \mathrm{d}\mu + k_B T \left(\frac{\partial^2(\ln\Xi)}{\partial\lambda\partial\mu}\right)_{T,V} \mathrm{d}\lambda \tag{2.85}$$

and hence from the cyclic relation

$$\left(\frac{\partial\mu}{\partial\lambda}\right)_{\rho} = \frac{\partial^2(\ln\Xi)}{\partial\lambda\partial\mu} \Big/ \frac{\partial^2(\ln\Xi)}{\partial\mu^2} \tag{2.86}$$

Inserting this into equation 2.84 gives

$$\left(\frac{\partial^2 A}{\partial\lambda^2}\right) = -k_B T \left(\frac{\partial^2(\ln\Xi)}{\partial\lambda^2}\right)_{\mu} + \frac{k_B T[\partial^2(\ln\Xi)/\partial\lambda\partial\mu]^2}{\partial^2(\ln\Xi)/\partial\mu^2} \tag{2.87}$$

Since

$$k_B T \frac{\partial^2(\ln\Xi)}{\partial\lambda\partial\mu} = -\frac{\partial}{\partial\mu}\left(\frac{1}{2}N\rho\int g_0(r_{12})w(r_{12})\mathrm{d}\mathbf{r}_2\right) \tag{2.88}$$

and

$$k_B T \left(\frac{\partial^2(\ln\Xi)}{\partial\mu^2}\right)_{T,V} = \left(\frac{\partial\langle N\rangle}{\partial\mu}\right)_{T,V} \tag{2.89}$$

the second derivative becomes

$$\left(\frac{\partial^2 A}{\partial\lambda^2}\right) = -k_B T \left(\frac{\partial^2(\ln\Xi)}{\partial\lambda^2}\right)_{\mu} + \frac{(1/k_B T)(\frac{\partial}{\partial\mu}\frac{1}{2}N\rho\int g_0(r_{12})w(r_{12})\mathrm{d}\mathbf{r}_2)^2}{(1/k_B T)\partial\langle N\rangle/\partial\mu} \tag{2.90}$$

Then by using the relation as seen in equation 2.44

$$\left(\frac{\partial}{\partial\mu}\right)_T = \left(\frac{\partial\rho}{\partial\mu}\right)_T \frac{\partial}{\partial\rho} = \rho\left(\frac{\partial\rho}{\partial P}\right)_T \frac{\partial}{\partial\rho} \tag{2.91}$$

it becomes

$$\left(\frac{\partial^2 A}{\partial\lambda^2}\right) = -k_B T \left(\frac{\partial^2(\ln\Xi)}{\partial\lambda^2}\right)_{\mu} + N\left(\frac{\partial\rho}{\partial P}\right)_0 \left[\frac{\partial}{\partial\rho}\left(\frac{1}{2}\rho^2\int g_0(r_{12})w(r_{12})\mathrm{d}\mathbf{r}_2\right)\right]^2 \tag{2.92}$$

and finally by inserting equation 2.79 and equation 2.23 as well as integrate once the following form is obtained

$$\begin{aligned}\left(\frac{\partial^2 A}{\partial\lambda^2}\right) = &-\frac{\beta N\rho}{2}\int g_0(\mathbf{r}_1,\mathbf{r}_2)w(r_{12})^2\mathrm{d}\mathbf{r}_2 - \beta N\rho^2\int\int g_0(\mathbf{r}_1,\mathbf{r}_2,\mathbf{r}_3)w(r_{12})w(r_{23})\mathrm{d}\mathbf{r}_2\mathrm{d}\mathbf{r}_3 \\ &-\frac{\beta N\rho^3}{4}\int\int\int \left(g_0(\mathbf{r}_1,\mathbf{r}_2,\mathbf{r}_3,\mathbf{r}_4) - g_0(\mathbf{r}_1,\mathbf{r}_2)g_0(\mathbf{r}_3,\mathbf{r}_4)\right)w(r_{12})w(r_{34})\mathrm{d}\mathbf{r}_2\mathrm{d}\mathbf{r}_3\mathrm{d}\mathbf{r}_4 \\ &+N\left(\frac{\partial\rho}{\partial P}\right)_0\left[\frac{\partial}{\partial\rho}\left(\frac{1}{2}\rho^2\int g_0(r_{12})w(r_{12})\mathrm{d}\mathbf{r}_2\right)\right]^2\end{aligned} \tag{2.93}$$

[12]. We can from this write the second order perturbation term a_2 as

$$\begin{aligned}a_2 = &-\frac{\rho}{4}\int g_0(\mathbf{r}_1,\mathbf{r}_2)w(r_{12})^2\mathrm{d}\mathbf{r}_2 - \frac{\rho^2}{2}\int\int g_0(\mathbf{r}_1,\mathbf{r}_2,\mathbf{r}_3)w(r_{12})w(r_{23})\mathrm{d}\mathbf{r}_2\mathrm{d}\mathbf{r}_3 \\ &-\frac{\rho^3}{8}\int\int\int \left(g_0(\mathbf{r}_1,\mathbf{r}_2,\mathbf{r}_3,\mathbf{r}_4) - g_0(\mathbf{r}_1,\mathbf{r}_2)g_0(\mathbf{r}_3,\mathbf{r}_4)\right)w(r_{12})w(r_{34})\mathrm{d}\mathbf{r}_2\mathrm{d}\mathbf{r}_3\mathrm{d}\mathbf{r}_4 \\ &+\frac{k_B T}{8}\left(\frac{\partial\rho}{\partial P}\right)_0\left[\frac{\partial}{\partial\rho}\left(\frac{1}{2}\rho^2\int g_0(r_{12})w(r_{12})\mathrm{d}\mathbf{r}_2\right)\right]^2\end{aligned} \tag{2.94}$$

The physical interpretation of the second order term is that it describes the fluctuation of the attractive energy due to the compression of the particles from the action of the attractive perturbation. The problem with the expression we just presented is that it requires knowledge about the three and four particle distribution functions of the reference system. There are currently no exact analytical form for these. The situation gets further difficult for the higher order terms. In order to solve this, Barker and Henderson came with the discrete representation in 1967 [5]. The argument here is based on a semi-macroscopic one. The range of interparticle distances can be divided into intervals with equal length, where r_m to r_{m+1} would be Δr, with $m = 0, 1, 2, ...$ They further imagined two concentric spheres of radius r_m and r_{m+1} drawn around each particle of the reference system. The number of neighbours in the spherical shells between two successive spheres would on average be

$$\langle N_m \rangle_0 = 2\pi N \rho \int_{r_m}^{r_{m+1}} g_0(r) r^2 \mathrm{d}r \tag{2.95}$$

They then assumed Δr to be sufficiently small such that the perturbation $w(r)$ would essentially have the same value w_m at all points within the shell. Inserting this relation into equation 2.65 would give

$$A^{\text{res}} = A_0^{\text{res}} + \sum_m \langle N_m \rangle_0 w_m - \frac{1}{2}\beta \sum_m \sum_n [\langle N_m N_n \rangle_0 - \langle N_m \rangle_0 \langle N_n \rangle_0] w_m w_n + \mathcal{O}(\beta^2) \tag{2.96}$$

If the shells are of macroscopic volume, there will be no correlation between the number of particles in different shells, thus $\langle N_m N_n \rangle_0 = \langle N_m \rangle_0 \langle N_n \rangle_0$ for the cases where $m \neq n$. The second order term then becomes

$$A_2 = -\frac{1}{2} \sum_m \langle \Delta N_m^2 \rangle_0 w_m^2 \tag{2.97}$$

where $\langle \Delta N_m^2 \rangle_0 \equiv \langle N_m^2 \rangle_0 - \langle N_m \rangle_0^2$. Additionally the fluctuation in number of particles in a shell will be related to the compressibility of the reference system through the macroscopic expression 2.49

$$\langle \Delta N_m^2 \rangle_0 = \langle N_m \rangle_0 k_B T \rho \chi_T^0 = \langle N_m \rangle_0 k_B T \left(\frac{\partial \rho}{\partial P} \right)_0 \tag{2.98}$$

inserting this into the expression for A_2, replacing the sum with an integral gives

$$\frac{A_2}{N} = a_2 = -\pi \rho k_B T \int_0^\infty w(r)^2 \left(\frac{\partial \rho}{\partial P} \right)_0 g_0(r) r^2 \mathrm{d}r \tag{2.99}$$

This is known as the macroscopic compressibility approximation (MCA) and has shown to give quite poor results [41]. To improve this description, Zhang [57] proposed multiplying it with a correction factor $(1 + \chi)$ to account for the particle correlation between the neighbouring coordination shells:

$$a_2 = -\pi \rho k_B T \left(\frac{\partial \rho}{\partial P} \right)_0 (1 + \chi) \int_0^\infty g_0(r) w(r)^2 r^2 \mathrm{d}r \tag{2.100}$$

Many different functional dependencies of the correction parameter have been proposed, where some of them will be further investigated in section 3.2. Figure 2.2 shows a comparison between MCA with and without the χ-factor to Monte Carlo simulation data.

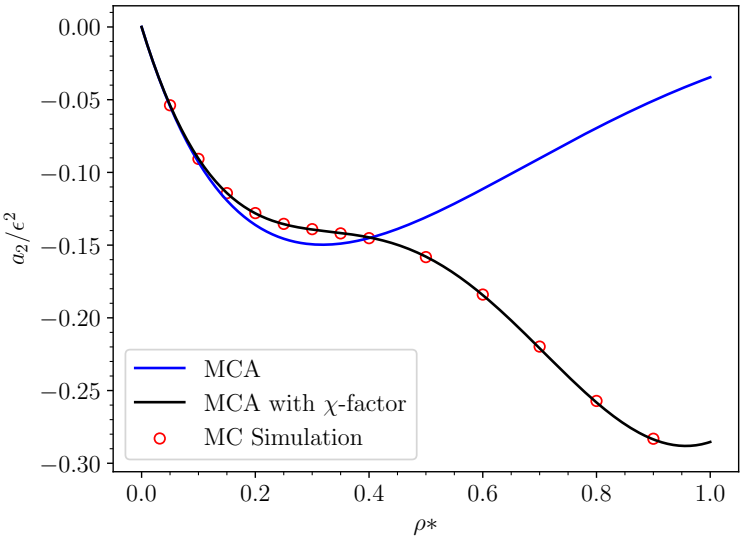

Figure 2.2: The second order perturbation term for the Barker and Henderson theory at the reduced temperature $T^* = k_B T/\epsilon = 1$ as a function of the reduced density $\rho^* = N\sigma^3/V$. The figure compares the macroscopic compressibility approximation with and without the χ-factor as given by van Westen and Gross [54] to Monte Carlo simulation data from this thesis.

2.4.2 Soft-Core Reference Systems

For perturbation theory to be useful, a well-understood reference system is needed. Hard-sphere systems are usually chosen due to their simplicity. Realistic inter-particular potentials do not have an infinitely steep repulsive core, thus it will be better to use a harshly repulsive, but continuous potential for the reference system [18]. This section will establish a relation between the reference system and the system of hard-spheres through the "blip-function" method of Hans C. Andersen and Chandler [17]. For a harshly repulsive reference system, the Boltzmann factor $e_0(r) = \exp[-\beta u_0(r)]$ will typically be very similar to the Boltzmann factor of a hard-sphere potential $e_d^{\text{hs}}(r)$. For a well chosen hard-sphere diameter d, $\Delta e(r)$

$$\Delta e(r) = e_0(r) - e_d^{\text{hs}}(r) \tag{2.101}$$

will be effectively non-zero only over a small range of r. Let this range be $d\xi$. ξ will then be a dimensionless parameter, which works as a measure of the softness of the potential. Figure 2.3 is an illustration of the "blip-function" and shows what is meant by the dimensionless parameter ξ.

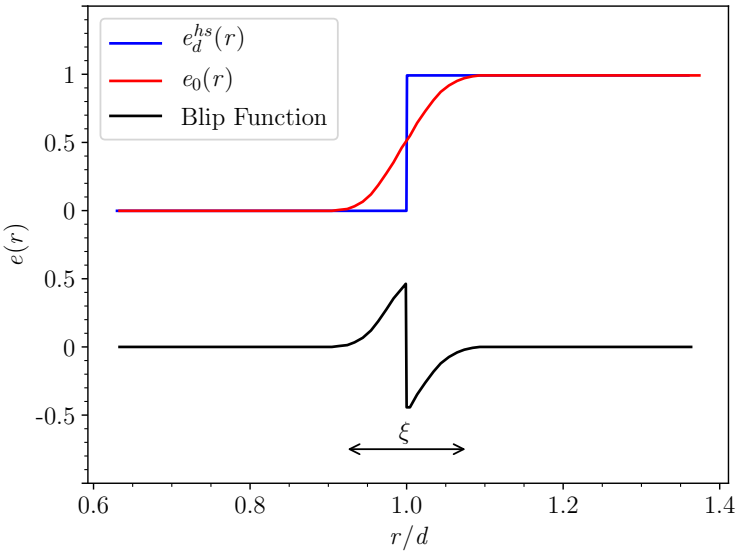

Figure 2.3: The blip function. The blue plot is the Boltzmann factor for the hard-sphere potential $e_d^{\text{hs}}(r)$ and the red plot is the Boltzmann factor for the reference potential $e_0(r)$. Beneath these two plots, the "blip-function" $\Delta e(r) = e_0(r) - e_d^{\text{hs}}(r)$ is plotted. The dimensionless ξ is here the range for which the "blip-function" is non-zero.

Using a small value for ξ, an expansion for the properties of the reference system about those of a hard-sphere system in powers of ξ can be obtained. This is done through a functional Taylor expansion of the reduced free energy density $\varphi = -\beta A^{\text{res}}/V$ in powers of $\Delta e(r)$ with the hard sphere system as the reference system φ_d^{hs}

$$\varphi_0 = \varphi_d^{\text{hs}} + \int \frac{\delta\varphi}{\delta e(\mathbf{r})}\bigg|_{e=e_d^{\text{hs}}} \Delta e(\mathbf{r})\mathrm{d}\mathbf{r} + \frac{1}{2!}\int\int \frac{\delta^2\varphi}{\delta e(\mathbf{r})\delta e(\mathbf{r}')}\bigg|_{e=e_d^{\text{hs}}} \Delta e(\mathbf{r})\Delta e(\mathbf{r}')\mathrm{d}\mathbf{r}\mathrm{d}\mathbf{r}' + \ldots \tag{2.102}$$

Evaluating the first functional derivative gives

$$\begin{aligned}
\frac{\delta\varphi}{\delta e(\mathbf{r})} &= \frac{\delta(-\beta A^{\text{res}}/V)}{\delta e(\mathbf{r})} \\
&= \frac{1}{V}\frac{\delta(-\beta(-\frac{1}{\beta}\ln\frac{Z_N}{V^N}))}{\delta e(\mathbf{r})} \\
&= \frac{1}{VZ_N}\frac{\delta Z_N}{\delta e(\mathbf{r})} \\
&= \frac{1}{VZ_N}\frac{\delta(\int e(\mathbf{r}^N)\mathrm{d}\mathbf{r}^N)}{\delta e(\mathbf{r})}
\end{aligned} \tag{2.103}$$

where $e(\mathbf{r}^N)$ is $\exp[-\beta U(\mathbf{r}^N)]$ and

$$U(\mathbf{r}^N) = \sum_{i=1}^{N}\sum_{j>i}^{N} u(r_{ij}) \tag{2.104}$$

Inserting this relation and using the definition for functional differentiation, we end up

with the following expression

$$\begin{aligned}\delta\varphi =& \frac{1}{VZ_N}\Bigg(\int\cdots\int \delta e(\mathbf{r}_{12})e(\mathbf{r}_{13})e(\mathbf{r}_{14})\cdots e(\mathbf{r}_{N-1,N})\mathrm{d}\mathbf{r}_1\cdots\mathrm{d}\mathbf{r}_N. \\ &+ \int\cdots\int e(\mathbf{r}_{12})\delta e(\mathbf{r}_{13})e(\mathbf{r}_{14})\cdots e(\mathbf{r}_{N-1,N})\mathrm{d}\mathbf{r}_1\cdots\mathrm{d}\mathbf{r}_N \\ &+ (\ N(N\text{-}1)\text{-}2 \text{ other terms})\Bigg)\end{aligned} \tag{2.105}$$

It is once again assumed a mono-particle system, thus each of the terms in the double sum will yield the same integral result, which can further simplify the equation to

$$\delta\varphi = \frac{1}{VZ_N}\frac{N(N-1)}{2}\int\int \delta e(\mathbf{r}_{12})\left[\int\cdots\int e(\mathbf{r}_{13})e(\mathbf{r}_{14})\cdots e(\mathbf{r}_{N-1,N})\mathrm{d}\mathbf{r}_3\cdots\mathrm{d}\mathbf{r}_N\right]\mathrm{d}\mathbf{r}_1\mathrm{d}\mathbf{r}_2 \tag{2.106}$$

Let the position of particle 1 be the origin and integrate over coordinate $\mathbf{r}_1$.

$$\begin{aligned}\delta\varphi &= \frac{1}{VZ_N}\frac{N(N-1)}{2}\int\int \delta e(\mathbf{r}_{12})\left[\int\cdots\int e(\mathbf{r}_{13})e(\mathbf{r}_{14})\cdots e(\mathbf{r}_{N-1,N})\mathrm{d}\mathbf{r}_{13}\cdots\mathrm{d}\mathbf{r}_{1N}\right]\mathrm{d}\mathbf{r}_1\mathrm{d}\mathbf{r}_{12} \\ &= \frac{V}{VZ_N}\frac{N(N-1)}{2}\int \delta e(\mathbf{r}_{12})\left[\int\cdots\int e(\mathbf{r}_{13})e(\mathbf{r}_{14})\cdots e(\mathbf{r}_{N-1,N})\mathrm{d}\mathbf{r}_{13}\cdots\mathrm{d}\mathbf{r}_{1N}\right]\mathrm{d}\mathbf{r}_{12}\end{aligned} \tag{2.107}$$

Using the definition of functional differentiation to obtain

$$\frac{\delta\varphi}{\delta e(\mathbf{r})} = \frac{N(N-1)}{2}\frac{\int\cdots\int e(\mathbf{r}_{13})e(\mathbf{r}_{14})\cdots e(\mathbf{r}_{N-1,N})\mathrm{d}\mathbf{r}_{13}\cdots\mathrm{d}\mathbf{r}_{1N}}{Z_N} \tag{2.108}$$

Inserting the equation for the equilibrium n-particle density (equation 2.21) gives

$$\begin{aligned}\frac{\delta\varphi}{\delta e(\mathbf{r})} &= \frac{N(N-1)}{2}\frac{(N-2)!}{N!}\exp(\beta u(\mathbf{r}_{12}))\rho_N^{(2)}(\mathbf{r}_1\mathbf{r}_2) \\ &= \frac{1}{2}\exp(\beta u(\mathbf{r}_{12}))\rho_N^{(2)}(\mathbf{r}_1\mathbf{r}_2)\end{aligned} \tag{2.109}$$

Recalling that the system is homogenous. The n-particle distribution function for homogenous systems (equation 2.23) is inserted. By defining the cavity-correlation function $y(\mathbf{r}) = \exp(\beta u(\mathbf{r}))g(\mathbf{r})$ this gives the following form

$$\begin{aligned}\frac{\delta\varphi}{\delta e(\mathbf{r})} &= \frac{1}{2}\rho^2\exp(\beta u(\mathbf{r}))g(\mathbf{r}) \\ &= \frac{1}{2}\rho^2 y(\mathbf{r})\end{aligned} \tag{2.110}$$

Inserting this relation to the functional Taylor expansion gives

$$\varphi_0 = \varphi_d^{\text{hs}} + \frac{1}{2}\rho^2\int y_d^{\text{hs}}(\mathbf{r})\Delta e(\mathbf{r})\mathrm{d}\mathbf{r} + \frac{1}{2!}\int\int \left.\frac{\delta^2\varphi}{\delta e(\mathbf{r})\delta e(\mathbf{r}')}\right|_{e=e_d}\Delta e(\mathbf{r})\Delta e(\mathbf{r}')\mathrm{d}\mathbf{r}\mathrm{d}\mathbf{r}' + ... \tag{2.111}$$

The system is isotropic thus $y_d^{\text{hs}}(\mathbf{r})$ will be the same as $y_d^{\text{hs}}(r)$, same goes for $\Delta e(\mathbf{r})$. A natural choice for d will be one that causes the first order term to vanish, thus d is found implicit by

$$\begin{aligned}\frac{1}{2}\rho^2\int y_d^{\text{hs}}(r)\Delta e(r)\mathrm{d}\mathbf{r} &= 0 \\ 2\pi\rho^2\int y_d^{\text{hs}}(r)\Delta e(r)r^2\mathrm{d}r &= 0\end{aligned} \tag{2.112}$$

[18]. With this choice for d, the second order term, that originally was of order ξ^2, become of order ξ^4 as was shown by Hans C. Andersen and Chandler [17] and the subsequent terms becomes of order ξ^4 or higher. Equation 2.112 represents the Weeks, Chandler and Andersen method of calculating the hard sphere diameter which is one of many methods. The method that Barker and Henderson used can also be recovered as will be shown here. Since $\Delta e(r)$ is only none-zero in a narrow range of r, we can expand ry_d^{hs} in a Taylor series about $r = d$.

$$r^2 y_d^{\text{hs}}(r) = r^2 y_d^{\text{hs}}(r)\big|_{r=d} + d\frac{\mathrm{d}}{\mathrm{d}r} r^2 y_d^{\text{hs}}(r)\left(\frac{r}{d}-1\right)\bigg|_{r=d} + d^2\frac{\mathrm{d}^2}{\mathrm{d}r^2} r^2 y_d^{\text{hs}}(r)\left(\frac{r}{d}-1\right)^2\bigg|_{r=d} + \cdots \tag{2.113}$$

Inserting this into equation 2.112 we get

$$\sum_{m=0}^{\infty} \frac{d^m}{m!}\frac{\mathrm{d}^m}{\mathrm{d}r^m} y_d^{\text{hs}}(r)\bigg|_{r=d} I_m = 0 \tag{2.114}$$

where

$$\begin{aligned} I_m &= \int_0^\infty \left(\frac{r}{d}-1\right)^m \Delta e(r)\mathrm{d}(r/d) \\ &= -\frac{1}{m+1}\int_0^\infty \left(\frac{r}{d}-1\right)^{m+1} \frac{\mathrm{d}}{\mathrm{d}r}\exp[-\beta u_0(r)]\mathrm{d}r \end{aligned} \tag{2.115}$$

$u_0(r)$ will vary rapidly with r, thus the derivative in the equation will approximately be a $\delta-$function at $r = d$ and the series is therefore quickly convergent. By only keeping the first term we get

$$\begin{aligned} 0 =& -\int_0^\infty \left(\frac{r}{d}-1\right)\delta(r-d)\mathrm{d}r \\ =& 1 - \int_0^\infty \frac{r}{d}\delta(r-d)\mathrm{d}r \end{aligned} \tag{2.116}$$

We can then use the following relation

$$\int_0^\infty r\delta(r-d)\mathrm{d}r = d = \int_0^\infty (1 - H(r-d))\,\mathrm{d}r \tag{2.117}$$

where $H(r-d)$ is a heaviside function. Inserting this relation and utilizing that $\int \delta(r-d)\mathrm{d}r = H(r-d) = \exp[-\beta u_0(r)]$ we can rewrite equation 2.116 as

$$d = \int_0^\infty (1 - \exp[-\beta u_0(r)])\mathrm{d}r \tag{2.118}$$

This is the same equation as Barker and Henderson [5] derived differently.
Using all the derived relations we can see that the reduced Helmholtz free energy density of the reference system is related to the hard-sphere fluid by

$$\varphi_0 = \varphi_d^{\text{hs}} + \mathcal{O}(\xi^4) \tag{2.119}$$

Multiplying each term with $-V/N$ gives the useful relation

$$a_0 = a_d^{\text{hs}} + \mathcal{O}(\xi^4) \tag{2.120}$$

2.5 Barker-Henderson Perturbation Theory

Recall from the perturbation theory that the inter-particular potential is divided into a repulsive reference part and an attractive perturbation part (see equation 2.63) leading to the following expression

$$u(r) = u_0(r) = \lambda w(r). \tag{2.121}$$

What remains now is to define the reference and the perturbation part [18]. For this we will be following the work of Barker and Henderson [5] (BH). There are many other perturbation theories that could be used as well, such as the well known Weeks-Chandler-Andersen (WCA) perturbation theory, but as BH is one of the most used ones, as well as being relative simple and performing well [54], it will be the one we will be using for this thesis.

We choose to use the Mie potential to define the reference and the perturbation part as the Lennard-Jones potential can easily be recovered by letting $l_r = 12$ and $l_a = 6$:

$$u_0(r) = \begin{cases} u^{\text{mie}}(r) & r \leq \sigma \\ 0 & r > \sigma \end{cases} \tag{2.122}$$

$$w(r) = \begin{cases} 0 & r \leq \sigma \\ u^{\text{mie}}(r) & r > \sigma \end{cases} \tag{2.123}$$

Figure 2.4 shows a plot of the reference potential and the perturbation

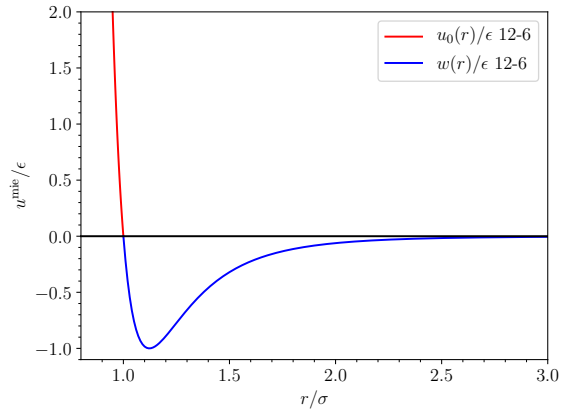

Figure 2.4: The BH potential. The red line shows the reference potential while the blue line shows the perturbation. Here we have used the Mie 12-6 potential (Lennard-Jones).

This choice for the repulsive reference fluid is softly repulsive and thus the Helmholtz energy will not directly follow from a system of hard-spheres. However using the theory established in section 2.4.2 one can map the properties of the softly repulsive reference fluid onto a system of hard-spheres [54]. Further, the equation 2.120 as seen in the section 2.4.2, can be approximated as

$$a_0 \approx a_d^{\text{hs}} \tag{2.124}$$

by choosing the effective hard-sphere diameter such that it satisfies equation 2.116 and neglecting the higher order terms. Barker and Henderson [5] lastly assumed that $g_0(r)$ could be approximated from the hard-sphere radial distribution function:

$$g_0(r) \approx g_d^{\text{hs}}(r) \tag{2.125}$$

The only part left now is to fully specify the Helmholtz free energy of the reference fluid, which is usually done by using the equation of Carnahan and Starling [10].

$$A_d^{\text{hs}} = Nk_BT\frac{4\eta - 3\eta^2}{(1-\eta)^2} \tag{2.126}$$

where η is the ratio of the volume occupied by the spheres to the total volume:

$$\eta = \frac{\pi}{6}\rho d^3 \tag{2.127}$$

The Carnahan-Starling equation of state has shown to behave very well at low densities as well as well as the metastable region and does not diverge until it reaches a packing fraction of one. Since most of the previous work on perturbation theory has been on spherical particles, hence the packing fraction will never exceed $(\pi/6)2^{1/2} = 0.7405$ and combined with it being a very simple model, Carnahan-Starling has usually been the choice for describing the hard-sphere fluid [31, 56].

Combining everything from the Barker-Henderson perturbation theory we end up with the following equation for the reduced Helmholtz free energy

$$a = a^{\text{id}} + a_d^{\text{hs}} + \sum_{i=1}^{\infty} a_i \beta^i \tag{2.128}$$

where our attention will be on the second order term in the infinite sum.

Chapter 3

Implementation of the First and Second Order Perturbation Terms

This section will first present how the hard-sphere diameter d was calculated, then how analytical expressions for the first and the second order perturbation terms can be obtained for pure fluids using the MCA with a correction factor for the second order term. We will then explain the basis for mixtures, before we extend the analytical forms to mixtures. Finally we will present an alternative numerical approach that does not utilize the MCA inspired by the work of Smith et al. [41] and Henderson [19].

3.1 Analytical Implementation of the Pure First Order Perturbation Term

The hard-sphere diameter was calculated numerically using the following temperature dependent formula by Barker and Henderson [5]

$$d = \int_0^\sigma [1 - \exp(-\beta u^{\text{mie}}(r))]\mathrm{d}r. \tag{3.1}$$

For the numerical calculation, a 16 point Gauss-Legendre Quadrature was used, which is described more in detail in section 4.1.

In order to find the first order perturbation term, equation 2.73 is rewritten utilizing the equation 2.123 for $w(r)$

$$\begin{aligned} a_1 &= 2\pi\rho \int_\sigma^\infty w(r) g_0(r) r^2 \mathrm{d}r \\ &= 2\pi\rho \int_d^\infty u^{\text{mie}}(r) g_0(r) r^2 \mathrm{d}r - 2\pi\rho \int_d^\sigma u^{\text{mie}}(r) g_0(r) r^2 \mathrm{d}r \\ &= I_{1A} + I_{1B} \end{aligned} \tag{3.2}$$

[23, 54]. To simplify further the BH approximation $g_0(r) \approx g_d^{\text{hs}}(r)$ is used.

$$a_1 = 2\pi\rho \int_d^\infty u^{\text{mie}}(r) g_d^{\text{hs}}(r) r^2 \mathrm{d}r - 2\pi\rho \int_d^\sigma u^{\text{mie}}(r) g_d^{\text{hs}}(r) r^2 \mathrm{d}r = I_{1A} + I_{1B} \tag{3.3}$$

The attention is now put onto the first integral I_{1A}

$$\begin{aligned} I_{1A} &= 2\pi\rho \int_d^\infty g_d^{\text{hs}}(r)\mathcal{C}\epsilon \left[\left(\frac{\sigma}{r}\right)^{l_r} - \left(\frac{\sigma}{r}\right)^{l_a} \right] r^2 \mathrm{d}r \\ &= 2\pi\rho\mathcal{C}\epsilon d^3 \left[x_0^{l_r} \int_1^\infty x^{-l_r} g_d^{\text{hs}}(xd) x^2 \mathrm{d}x - x_0^{l_a} \int_1^\infty x^{-l_a} g_d^{\text{hs}}(xd) x^2 \mathrm{d}x \right] \end{aligned} \tag{3.4}$$

where the last relation is once again from the substitution of $x = r/d$, by using that $\mathrm{d}r = d\mathrm{d}x$ and $x_0 = \sigma/d$. Rewriting the equation in the form of correlation integrals over a hard-core Sutherland potential [44] of exponent l, which is defined as

$$\begin{aligned} I_1^S(\eta, l) &= -2\pi\rho\epsilon d^3 \int_1^\infty g_d^{\text{hs}}(xd) \left(\frac{1}{x}\right)^l x^2 \mathrm{d}x \\ &= -12\epsilon\eta \int_1^\infty g_d^{\text{hs}}(xd) \left(\frac{1}{x}\right)^l x^2 \mathrm{d}x \end{aligned} \tag{3.5}$$

gives the following form for I_{1A}

$$I_{1A} = \mathcal{C}\left[x_0^{l_a} I_1^S(\eta; l_a) - x_0^{l_r} I_1^S(\eta; l_r) \right] \tag{3.6}$$

[23]. Gil-Villegas et al. [13], proposed solving these hard-core Sutherland potential terms with the use of the mean-value theorem (MVT). MVT states that if $f_1 : [a, b] \to \mathbb{R}$ is continuous and f_2 is an integrable function that does not change sign on the interval $[a, b]$, then there exists a $\varsigma \in [a, b]$ value such that

$$\int_a^b f_1(x) f_2(x) \mathrm{d}x = f_1(\varsigma) \int_a^b f_2(x) \mathrm{d}x \tag{3.7}$$

where $\mathbb{R}$ are all real numbers [59]. They let $f_1(x) = g_d^{\text{hs}}(xd)$ and $f_2(x) = \left(\frac{1}{x}\right)^l x^2$ and got the following relation

$$\int_1^\infty g_d^{\text{hs}}(xd) \left(\frac{1}{x}\right)^l x^2 \mathrm{d}x = g_d^{\text{hs}}(\varsigma) \int_1^\infty \left(\frac{1}{x}\right)^l x^2 \mathrm{d}x \tag{3.8}$$

The radial distribution function g_d^{hs} is also affected by the packing fraction η, thus for convenience sake one wants to represent the full function $g_d^{\text{hs}}(\varsigma; \eta)$ by its contact value, but evaluated at an effective packing fraction η_{eff} such that

$$g_d^{\text{hs}}(\varsigma; \eta) = g_d^{\text{hs}}(1; \eta_{\text{eff}}) \tag{3.9}$$

This is possible, as the value at $x = 1$ for the radial distribution function g_d^{hs} will decrease as the packing fraction η decreases, see figure 3.1 for an illustration.

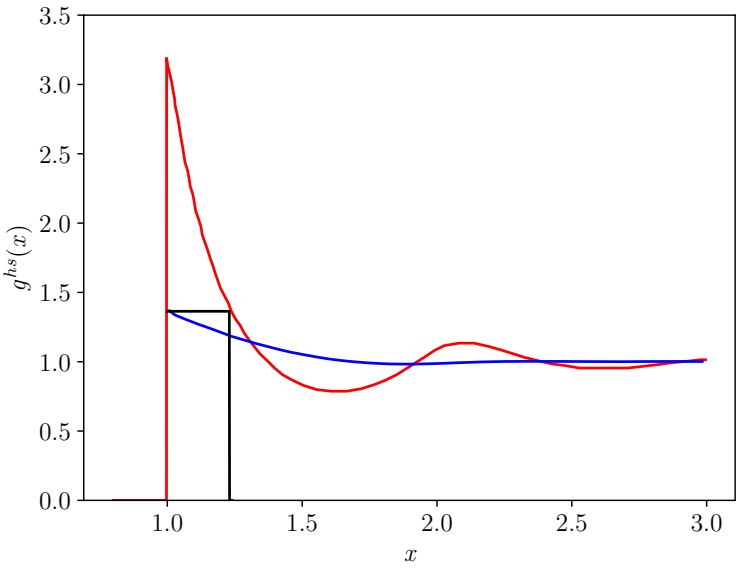

Figure 3.1: The relationship between $g_d^{\text{hs}}(\varsigma;\eta)$ and $g_d^{\text{hs}}(1;\eta_{\text{eff}})$. Data for the hard-sphere radial distribution function $g_d^{\text{HS}}(x)$ extracted from the work of Gil-Villegas et al. [13] for $\eta = 0.36$ is shown as the red curve. The value of $g_d^{\text{hs}}(\varsigma;\eta = 0.36)$ with $\varsigma = 1.24$, here illustrated as the point where the vertical black line meets the red plot corresponds to the contact value $g_d^{\text{hs}}(1;\eta_{\text{eff}})$ where $\eta_{\text{eff}} = 0.11$ here shown as the blue plot. This radial distribution was also extracted from the work of Gil-Villegas et al. [13].

From the Carnahan and Starling equation of state, the following form for the radial distribution function at the contact value is obtained

$$g_d^{\text{hs}}(1;\eta_{\text{eff}}) = \frac{1-\eta_{\text{eff}}/2}{(1-\eta_{\text{eff}})^3} \tag{3.10}$$

By inserting this into equation 3.8, multiplying by $-12\epsilon\eta$ and integrating they obtained the following analytical form for the integral

$$I_1^S(\eta;l) = -12\epsilon\eta\left(\frac{1}{l-3}\right)\frac{1-\eta_{\text{eff}}(\eta;l)/2}{(1-\eta_{\text{eff}}(\eta;l))^3} \tag{3.11}$$

[13]. The next step is to find the dependence of η_{eff} on the actual value of η and on the potential range. One way to do this, would be to use exact values of a_1 obtained from computer simulations. A second way is to integrate the a_1 integral using an exact representation for $g_d^{\text{hs}}(r)$. Both the work of Gil-Villegas et al. [13] and Lafitte et al. [23] used the latter method by solving the Ornstein-Zernike equation (see appendix section 7.2) with the Malijevsky and Labik formula for the hard-sphere bridge function [27]. The original Gil-Villegas et al. [13] parametrization was derived for exponents of the Sutherland potential in the range of $3 < l \leq 12$, but in this project, the work of Lafitte et al. [23] which created the model for a much broader range of $5 < l \leq 100$ will be used:

$$\eta_{\text{eff}}(\eta;l) = \hat{c}_1(l)\eta + \hat{c}_2(l)\eta^2 + \hat{c}_3(l)\eta^3 + \hat{c}_4(l)\eta^4 \tag{3.12}$$

with

$$\begin{bmatrix}\hat{c}_1\\ \hat{c}_2\\ \hat{c}_3\\ \hat{c}_4\end{bmatrix} = \begin{bmatrix}0.81096 & 1.7888 & -37.578 & 92.248\\ 1.0205 & -19.341 & 151.26 & -463.50\\ -1.9057 & 22.845 & -228.14 & 973.92\\ 1.0885 & -6.1962 & 106.98 & -677.64\end{bmatrix}\begin{bmatrix}1\\ 1/l\\ 1/l^2\\ 1/l^3\end{bmatrix} \tag{3.13}$$

For the second integral I_{1B}, Lafitte et al. [23] approximated $g_d^{\text{hs}}(r)$ with a Taylor expansion of the contact value of $g_d^{\text{hs}}(r)$ with respect to the separation r.

$$g_d^{\text{hs}}(xd) \approx g_d^{\text{hs}}(d) + (x-1)\left(\frac{\mathrm{d}g_d^{\text{hs}}(xd)}{\mathrm{d}x}\right)_{x=1} \tag{3.14}$$

Using this approximation, I_{1B} can be written as

$$I_{1B} \approx -2\pi\rho d^3(g_d^{\text{hs}}(d)\int_1^{x_0} u^{\text{mie}}(xd)x^2\mathrm{d}x + \left(\frac{\mathrm{d}g_d^{\text{hs}}(xd)}{\mathrm{d}x}\right)_{x=1}\int_1^{x_0} u^{\text{mie}}(xd)x^2(x-1)\mathrm{d}x) \tag{3.15}$$

For simplicity the following integrals are defined:

$$\hat{I}_l(x_0) = \int_1^{x_0}\frac{x^2}{x^l}\mathrm{d}x = -\frac{x_0^{3-l}-1}{l-3} \tag{3.16}$$

$$\hat{J}_l(x_0) = \int_1^{x_0}\frac{(x^3-x^2)}{x^l}\mathrm{d}x = -\frac{x_0^{4-l}(l-3)-x_0^{3-l}(l-4)-1}{(l-3)(l-4)} \tag{3.17}$$

They then used the Carnahan-Starling expression for $g_d^{\text{hs}}(d)$ at the contact value from equation 3.10 and the Percus-Yevick approximation for the derivative

$$g_d^{\text{hs}}(d) = \frac{1-\eta/2}{(1-\eta)^3} \tag{3.18}$$

$$\left(\frac{\mathrm{d}g_d^{\text{hs}}(xd)}{\mathrm{d}x}\right) = -\frac{9\eta(1+\eta)}{2(1-\eta)^3} \tag{3.19}$$

Using these simplifications the second integral I_{1B} can be written as

$$I_{1B} = 4(x_0^6 B(\eta; l_a) - x_0^{12} B(\eta; l_r)) \tag{3.20}$$

where

$$B(\eta; l) = 12\eta\epsilon\left(\frac{1-\eta/2}{(1-\eta)^3}\hat{I}_l(x_0) - \frac{9\eta(1+\eta)}{2(1-\eta)^3}\hat{J}_l(x_0)\right) \tag{3.21}$$

From this, the first order term a_1 can be written as

$$a_1 = \mathcal{C}\left[x_0^{l_a}(I_1^S(\eta; l_a) + B(\eta; l_a)) - x_0^{l_r}(I_1^S(\eta; l_r) + B(\eta; l_r))\right] \tag{3.22}$$

3.2 Analytical Implementation of the Pure Second Order Perturbation Term

Using the MCA approximation (see equation 2.100) as basis and the same procedure as shown in the previous section 3.1 both Lafitte et al. [23] and van Westen and Gross [54] ended up with the expression

$$\begin{aligned} a_2 =& -\pi\rho K^{\text{hs}}(1+\chi)\int_\sigma^\infty g_d^{\text{hs}}(r)(u^{\text{mie}}(r))^2 r^2\mathrm{d}r \\ =& -\pi\rho K^{\text{hs}}(1+\chi)\int_d^\infty g_d^{\text{hs}}(r)(u^{\text{mie}}(r))^2 r^2\mathrm{d}r + \pi\rho K^{\text{hs}}(1+\chi)\int_d^\sigma g_d^{\text{hs}}(r)(u^{\text{mie}}(r))^2 r^2\mathrm{d}r \end{aligned} \tag{3.23}$$

where $K^{\text{hs}} = k_B T(\partial\rho/\partial P)_T$, which from using the Carnahan Starling EOS was calculated to be

$$K^{\text{hs}} = \frac{(1-\eta)^4}{1+4\eta+4\eta^2-4\eta^3+\eta^4}. \tag{3.24}$$

To calculate the integrals in equation 3.23 they both used the first-order perturbation terms I_1^S for the first integral, while for the second integral Lafitte et al. [23] used the B terms, while van Westen and Gross [54] numerically integrated these. We will be presenting both methods here starting with the work of Lafitte we get the following expression for a_2:

$$\begin{aligned} a_2 =& \frac{1}{2}K^{\text{hs}}\mathcal{C}^2\Big[x_0^{2l_a}(I_1^S(\eta;2l_a)+B(\eta;2l_a)) - 2x_0^{l_r+l_a}(I_1^S(\eta;l_r+l_a)+B(\eta;l_r+l_a)) \\ &+x_0^{2l_r}(I_1^S(\eta;2l_r)+B(\eta;2l_r))\Big] \end{aligned} \tag{3.25}$$

van Westen and Gross on the other hand integrated the second term in equation 3.23 numerically using the approximation of y_d^{hs} from de Souza and Ben-Amotz [43], developed for $x = r/d < 1.5$ which has the following form

$$\begin{aligned} y_d^{\text{hs}}(\eta;x) &= \exp(\hat{A}+\hat{B}x+\hat{C}x^3) \\ \hat{A} &= \frac{3-\eta}{(1-\eta)^3} - 3 \\ \hat{B} &= \frac{-3\eta(2-\eta)}{(1-\eta)^3} \\ \hat{C} &= \ln\left[\frac{2-\eta}{2(1-\eta)^3}\right] - \frac{\eta(2-6\eta+3\eta^2)}{(1-\eta)^3} \end{aligned} \tag{3.26}$$

Recall that $y_d^{\text{hs}} = g_d^{\text{hs}}$ for $r > d$. By defining $B_{\text{num}}(\eta;l)$ as:

$$B_{\text{num}}(\eta;l) = 12\epsilon\eta\int_{x_0}^{1} y_d^{\text{hs}}(\eta;x)x^{2-l}\mathrm{d}x \tag{3.27}$$

we get the following expression for a_2

$$\begin{aligned} a_2 =& \frac{1}{2}K^{\text{hs}}\mathcal{C}^2\Big[x_0^{2l_a}(I_1^S(\eta;2l_a)+B_{\text{num}}(\eta;2l_a)) - 2x_0^{l_r+l_a}(I_1^S(\eta;l_r+l_a) \\ &+ B_{\text{num}}(\eta;l_r+l_a)) +x_0^{2l_r}(I_1^S(\eta;2l_r)+B_{\text{num}}(\eta;2l_r))\Big] \end{aligned} \tag{3.28}$$

where all instances of B_{num} are integrated numerically using a 16 point Gauss-Legendre quadrature procedure. For the correction factor χ, Lafitte et al. [23] and van Westen and Gross [54] also here had different approaches, both of these will be investigated in this thesis. Lafitte et al. wrote the χ factor on the following form

$$\chi = v_1(\alpha)\eta x_0^3 + v_2(\alpha)(\eta x_0^3)^5 + v_3(\alpha)(\eta x_0^3)^8 \tag{3.29}$$

where α is a dimensionless van der Waals-like attractive constant, defined as

$$\alpha = \frac{1}{\epsilon\sigma^3}\int_{\sigma}^{\infty} u^{\text{mie}}(r)\mathrm{d}r = \mathcal{C}\left(\frac{1}{l_a-3}-\frac{1}{l_r-3}\right) \tag{3.30}$$

while $v_i (i = 1,2,3)$ is a function with the following closed functional form

$$v_i(\alpha) = \left(\sum_{n=0}^{n=3}\omega_{i,n}\alpha^n\right) / \left(1+\sum_{n=4}^{n=6}\omega_{i,n}\alpha^{n-3}\right) \;\; i = 1,...,6 \tag{3.31}$$

The coefficients $\omega_{i,n}$ were determined by Lafitte et al. in two steps. First $\omega_{i,n}$ $(i = 1, ..., 3)$ were obtained by correlating them to the exact a_2 values from Monte Carlo data for a fixed reduced temperature $T^* = 1$ and the literature vapor-liquid equilibrium (VLE) data. Then the remaining $\omega_{i,n}$ $(i = 4, ..., 6)$ coefficients were estimated from VLE data including critical temperatures and critical densities. The coefficient values can be found in the paper of Lafitte et al. [23].

van Westen and Gross [54] on the other hand wrote the χ factor on the following form

$$\chi(\rho^*, T^*) = \sum_i^5 \hat{b}_i(T^*)\rho^{*i} \tag{3.32}$$

where

$$\hat{b}_i(T^*) = \hat{b}_{i0} + \hat{b}_{i1}/\sqrt{T^*} + \hat{b}_{i2}/T^* + \hat{b}_{i3}/T^{*2} \tag{3.33}$$

The constants were obtained from correlating them to Monte Carlo simulation data for a_2. Their values can be found in the paper of van Westen and Gross [54]. The major difference between the χ factor of Lafitte et al. and van Westen and Gross is that the one from Lafitte et al. was made for Mie potentials and depends on the reduced density and the dimensionless van der Waals-like attractive constant, while the one of van Westen and Gross was made for the Lennard-Jones potential and is both reduced density and reduced temperature dependent.

3.3 Extension to Mixtures

In this section, we will extend the perturbation theory over to mixtures, with a special attention on the second order perturbation term.

Before we begin the mixture extension it is important to define the reference to develop the perturbation theory for mixtures from. Leonard et al. [26] derived in a seminal paper a perturbation theory for mixtures from three different references. They were the following: a pure component hard-sphere fluid, an additive hard-sphere fluid and a non-additive hard-sphere fluid. We will only be looking at the two first. For a review of the non-additive hard-sphere fluid we direct the interested reader to the paper of Hammer et al. [16].

When using a pure hard-sphere fluid as the reference, Leonard et al. [26] said that the following hard-sphere diameter should be used:

$$d = \sum_i \sum_j x_i x_j \nu_{ij} \tag{3.34}$$

where x_i is the fraction of component i and ν_{ij} is the effective hard-sphere diameter:

$$\nu_{ij} = \int_0^{\sigma_{ij}} [1 - \exp(-\beta u_{0,ij}(r))]\mathrm{d}r \tag{3.35}$$

Using this as the foundation, the reduced Helmholtz free energy can be described from

$$a^{\text{res}} = a_d^{\text{hs}} + 2\pi\rho\beta \sum_i \sum_j x_i x_j \int_{\sigma_{ij}}^{\infty} g_d^{\text{hs}}(r) w_{ij}(r) r^2 \mathrm{d}r + \mathcal{O}(\beta^2) \tag{3.36}$$

When using the additive hard-sphere fluid as the reference the following hard sphere diameters are used

$$d_{ii} = \nu_{ii} \tag{3.37}$$

$$d_{ij} = 0.5(d_{ii} + d_{jj}) \tag{3.38}$$

thus, there are individual hard-sphere diameters where the cross specie interactions are explained by taking the average of the two diameters. Using this as the foundation, the reduced Helmholtz free energy can be described from

$$a^{\text{res}} = a^{\text{hs}}_{d,\text{mix}} + a^{\text{ad}} + 2\pi\rho\beta \sum_i \sum_j x_i x_j \int_{\sigma_{ij}}^{\infty} g^{\text{hs}}_{d,ij}(r) w_{ij}(r) r^2 \mathrm{d}r + \mathcal{O}(\beta^2) \tag{3.39}$$

where $a^{\text{hs}}_{d,\text{mix}}$ is the hard sphere contribution to the residual Helmholtz free energy and a^{ad} is a term accounting for the non-additivity of the system that is usually very small and written as

$$a^{\text{ad}} = -2\rho\pi \sum_i \sum_j x_i x_j d_{ij}^2 g^{\text{hs}}_{d,ij,c}(d_{ij} - \nu_{ij}) \tag{3.40}$$

where $g^{\text{hs}}_{d,ij,c}$ is the radial distribution function at its contact value. Now that the foundation for two different perturbation mixture theories using different references has been explained, we will define our mixing rules.

The interaction between species i and j will be described using the following Mie potential

$$u^{\text{mie}}_{ij} = \mathcal{C}_{ij}\epsilon_{ij} \left(\left(\frac{\sigma_{ij}}{r_{ij}} \right)^{l_{r,ij}} - \left(\frac{\sigma_{ij}}{r_{ij}} \right)^{l_{a,ij}} \right) \tag{3.41}$$

where

$$\mathcal{C}_{ij} = \frac{l_{r,ij}}{l_{r,ij} - l_{a,ij}} \left(\frac{l_{r,ij}}{l_{a,ij}} \right)^{\frac{l_{a,ij}}{l_{r,ij} - l_{a,ij}}} \tag{3.42}$$

For l_{ij} and σ_{ij} the commonly used mixing rules for classical Mie fluids will be used:

$$l_{k,ij} = \sqrt{(l_{k,ii} - 3)(l_{k,jj} - 3)} + 3, k = a, r \tag{3.43}$$

$$\sigma_{ij} = \frac{\sigma_{ii} + \sigma_{jj}}{2} \tag{3.44}$$

while for ϵ_{ij} the geometrical combining rule will be used

$$\epsilon_{ij} = \sqrt{\epsilon_{ii}\epsilon_{jj}} \tag{3.45}$$

We are now ready to present the various models that we have tested in this thesis. We will start with explaining the one by Lafitte et al. [23].

3.3.1 Lafitte et al. Analytical Second Order Perturbation Term for Mixtures

Lafitte et al. [23] used an additive hard-sphere fluid as a reference. For the hard-sphere contribution to the residual Helmholtz free energy, the expression of Boublík [9] and Mansoori et al. [28] was used

$$a^{\text{hs}}_{d,\text{mix}} = \frac{1}{\zeta_0} \left[\frac{3\zeta_1\zeta_2}{1 - \zeta_3} + \frac{\zeta_2^3}{\zeta_3(1 - \zeta_3)^2} + \left(\frac{\zeta_2^3}{\zeta_3^2} - \zeta_0 \right) \ln(1 - \zeta_3) \right] \tag{3.46}$$

where

$$\zeta_m = \frac{\pi\rho}{6} \left(\sum_i x_i d_{ii} \right), m = 0, 1, 2, 3. \tag{3.47}$$

The first order perturbation term was written as

$$a_1 = \sum_{i=1}^{n}\sum_{j=1}^{n} x_i x_j a_{1,ij} \tag{3.48}$$

where following the work of Lafitte et al. [23]

$$\begin{aligned} a_{1,ij} =& \mathcal{C}_{ij}\eta_{ij}\left[x_{0,ij}^{l_{a,ij}}(I_{1,ij}^{S}(\eta_{ij};l_{a,ij}) + B_{ij}(\eta_{ij};l_{a,ij})) - x_{0,ij}^{l_{r,ij}}(I_{1}^{S}(\eta_{ij};l_{r,ij})\right. \\ &\left. + B_{ij}(\eta_{ij};l_{r,ij}))\right] \end{aligned} \tag{3.49}$$

where $x_{0,ij} = \sigma_{ij}/d_{ij}$, $\eta_{ij} = \pi\rho d_{ij}^3/6$ while $I_{1,ij}^{S}$ is

$$I_{1,ij}^{S}(\eta_{ij};l_{ij}) = -12\left(\frac{1}{l_{ij}-3}\right)\frac{1-\eta_{\text{eff}}(\zeta_3;l_{ij})/2}{(1-\eta_{\text{eff}}(\zeta_3;l_{ij}))^3} \tag{3.50}$$

and

$$B_{ij}(\eta_{ij};l_{ij}) = 12\left(\frac{1-\zeta_3/2}{(1-\zeta_3)^3}\hat{I}_{l_{ij}}(x_{0,ij}) - \frac{9\zeta_3(1+\zeta_3)}{2(1-\zeta_3)^3}\hat{J}_{l_{ij}}(x_{0,ij})\right) \tag{3.51}$$

For the second order term the following form was suggested by Lafitte et al. [23]

$$a_2 = \sum_{i=1}^{n}\sum_{j=1}^{n} x_i x_j a_{2,ij} \tag{3.52}$$

where

$$\begin{aligned} a_{2,ij} =& \frac{1}{2}K^{\text{hs}}(1+\chi_{ij})\mathcal{C}_{ij}^2\epsilon_{ij}^2\eta_{ij}\left[x_{0,ij}^{2l_{a,ij}}(I_{1,ij}^{S}(\eta_{ij};2l_{a,ij}) + B_{ij}(\eta_{ij};2l_{a,ij}))\right. \\ &- 2x_{0,ij}^{l_{a,ij}+l_{r,ij}}(I_{1,ij}^{S}(\eta_{ij};l_{a,ij}+l_{r,ij}) + B_{ij}(\eta_{ij};l_{a,ij}+l_{r,ij})) \\ &\left.+ x_{0,ij}^{2l_{r,ij}}(I_{1,ij}^{S}(\eta_{ij};2l_{r,ij}) + B_{ij}(\eta_{ij};2l_{r,ij}))\right] \end{aligned} \tag{3.53}$$

Here K^{hs} is

$$K^{\text{hs}} = \frac{(1-\zeta_3)^4}{1+4\zeta_3+4\zeta_3^2-4\zeta_3^3+\zeta_3^4}. \tag{3.54}$$

while

$$\chi_{ij} = v_1(\alpha_{ij})\bar{\zeta}_x + v_2(\alpha_{ij})\bar{\zeta}_x^5 + v_3(\alpha_{ij})\bar{\zeta}_x^8 \tag{3.55}$$

where

$$\bar{\zeta}_x = \frac{\pi\rho}{6}\sum_i\sum_j x_i x_j \sigma_{ij}^3 \tag{3.56}$$

and α_{ij} is the dimensionless van der Waals energy of the i-j interaction

$$\alpha_{ij} = \mathcal{C}_{ij}\left(\frac{1}{l_{a,ij}-3} - \frac{1}{l_{r,ij}-3}\right). \tag{3.57}$$

3.3.2 van Westen and Gross Analytical Second Order Perturbation Term for Mixtures

We have extended the work of van Westen and Gross originally created for pure Lennard-Jones fluids, to Lennard-Jones mixtures. We did this by following the work of Lafitte et al. [23] for mixtures, but instead using the χ-factor as seen in equation 3.32 with the reduced temperature and the reduced density defined as

$$T^* = \frac{k_B T}{\epsilon_{11}} \tag{3.58}$$

$$\rho^* = \frac{N_1^2\sigma_{11}^3 + 2N_1N_2\sigma_{12}^3 + N_2^2\sigma_{22}^3}{NV} \tag{3.59}$$

We also changed the B term, with B_{num} from equation 3.27, but extended to mixtures in the following way

$$B_{\text{num},ij}(\eta_{ij}; l_{ij}) = 12\int_{x_{0,ij}}^{1} y_d^{\text{hs}}(\zeta_3; x)x^{2-l_{ij}}\,\mathrm{d}x \tag{3.60}$$

This gives us the following form for a_{ij} to use in equation 3.52

$$\begin{aligned} a_{2,ij} =& \frac{1}{2}K^{\text{hs}}(1+\chi)\mathcal{C}_{ij}^2\epsilon_{ij}^2\eta_{ij}\Big[x_{0,ij}^{2l_{a,ij}}(I_{1,ij}^S(\eta_{ij}; 2l_{a,ij}) + B_{\text{num},ij}(\eta_{ij}; 2l_{a,ij})) \\ &- 2x_{0,ij}^{l_{a,ij}+l_{r,ij}}(I_{1,ij}^S(\eta_{ij}; l_{a,ij}+l_{r,ij}) + B_{\text{num},ij}(\eta_{ij}; l_{a,ij}+l_{r,ij})) \\ &+ x_{0,ij}^{2l_{r,ij}}(I_{1,ij}^S(\eta_{ij}; 2l_{r,ij}) + B_{\text{num},ij}(\eta_{ij}; 2l_{r,ij}))\Big] \end{aligned} \tag{3.61}$$

3.3.3 Numerical Second Order Perturbation Term for Mixtures Using a Pure Reference

One problem with following the procedure of Lafitte et al. [23], is that the extension of the macroscopic compressibility approximation with a correction factor to mixtures has no physical basis. Thus we have chosen to return to the work of Barker and Henderson. In 1970, they published a paper were they calculated the second order term using equation 2.94 as their basis and not the macroscopic compressibility approximation [41]. In a later paper by Henderson [19] it was further extended to a mixture of square-well particles ($u(r) = \infty, r < \sigma$, $u(r) = \epsilon, \sigma < r < 3\sigma/2$ and $u(r) = 0, r > 3\sigma/2$) and hard-sphere particles. We will in this section explain their work and extend it to a mixture of Lennard-Jones particles.

Starting from the equation 2.94, the first obvious problem is describing the three and four particle distribution functions. Currently there are no exact equations for these, Smith et al. [41] therefore used the superposition approximation [21] for these:

$$g_0(123) = g_0(12)g_0(13)g_0(23) \tag{3.62}$$

$$g_0(1234) = g_0(12)g_0(13)g_0(14)g_0(13)g_0(24)g_0(34) \tag{3.63}$$

For simplicity we have written $g_0(\mathbf{r}_1, \mathbf{r}_2)$ as $g_0(12)$ etc. At low densities this approximation is valid, but at high densities it is poor. Substituting equation 3.62 and 3.63 into equation 2.94 we get

$$
\begin{aligned}
a_2 = &-\frac{\rho}{4}\int g_0(12)w(12)^2\mathrm{d}\mathbf{r}_2 - \frac{\rho^2}{2}\int\int g_0(12)g_0(13)g_0(23)w(12)w(23)\mathrm{d}\mathbf{r}_2\mathrm{d}\mathbf{r}_3 \\
&-\frac{\rho^3}{8}\int\int\int (g_0(12)g_0(13)g_0(14)g_0(23)g_0(24)g_0(34) \\
&-g_0(12)g_0(34))\, w(12)w(34)\mathrm{d}\mathbf{r}_2\mathrm{d}\mathbf{r}_3\mathrm{d}\mathbf{r}_4 \\
&+\frac{k_BT}{8}\left(\frac{\partial\rho}{\partial P}\right)_0\left[\frac{\partial}{\partial\rho}\left(\rho^2\int g_0(12)w(12)\mathrm{d}\mathbf{r}_2\right)\right]^2
\end{aligned}
\tag{3.64}
$$

The next step is to get the integrals on a form where they only use h_0 and wg_0 as functions as they will go towards zero at reasonable distances when integrating over all space (cluster integrals). We do this by substituting all instances of g_0 with $h_0 + 1$, where they are not paired up with w.

$$
\begin{aligned}
a_2 = &-\frac{\rho}{4}\int g_0(12)w(12)^2\mathrm{d}\mathbf{r}_2 \\
&-\frac{\rho^2}{2}\int\int g_0(12)w(12)g_0(23)w(23)(h_0(13)+1)\mathrm{d}\mathbf{r}_2\mathrm{d}\mathbf{r}_3 \\
&-\frac{\rho^3}{8}\int\int\int [g_0(12)w(12)g_0(34)w(34)(h_0(13)+1)(h_0(14)+1) \\
&(h_0(23)+1)(h_0(24)+1) - g_0(12)w(12)g_0(34)w(34)]\,\mathrm{d}\mathbf{r}_2\mathrm{d}\mathbf{r}_3\mathrm{d}\mathbf{r}_4 \\
&+\frac{k_BT}{8}\left(\frac{\partial\rho}{\partial P}\right)_0\left[\frac{\partial}{\partial\rho}\left(\rho^2\int g_0(12)w(12)\mathrm{d}\mathbf{r}_2\right)\right]^2 \\
= &-\frac{\rho}{4}\int g_0(12)w(12)^2\mathrm{d}\mathbf{r}_2 \\
&-\frac{\rho^2}{2}\int\int g_0(12)w(12)g_0(23)w(23)(h_0(13)+1)\mathrm{d}\mathbf{r}_2\mathrm{d}\mathbf{r}_3 \\
&-\frac{\rho^3}{8}\int\int\int g_0(12)w(12)g_0(34)w(34)\,[h_0(13)h_0(14)h_0(23)h_0(24)+ \\
&h_0(13)h_0(14)h_0(23) + h_0(13)h_0(14)h_0(24) + h_0(13)h_0(23)h_0(24)+ \\
&h_0(14)h_0(23)h_0(24) + h_0(13)h_0(14) + h_0(13)h_0(23) + h_0(13)h_0(24)+ \\
&h_0(14)h_0(23) + h_0(14)h_0(24) + h_0(23)h_0(24) + h_0(13) + h_0(14) + h_0(23) \\
&+ h_0(24)]\mathrm{d}\mathbf{r}_2\mathrm{d}\mathbf{r}_3\mathrm{d}\mathbf{r}_4 + \frac{k_BT}{8}\left(\frac{\partial\rho}{\partial P}\right)_0\left[\frac{\partial}{\partial\rho}\left(\rho^2\int g_0(12)w(12)\mathrm{d}\mathbf{r}_2\right)\right]^2
\end{aligned}
\tag{3.65}
$$

Some of the cluster integrals that we have obtained from the second and third integrals are reducible. To illustrate what we mean by a reducible integral it is beneficial to draw these integrals using graph theory, where we let white circles correspond to coordinates held constant under the integration and black circles represent variables of the integration. We let $h_0(r)$ and $w(r)g_0(r)$ be the bonds drawn as:

$$
\begin{aligned}
&\cdots\cdots = w(r)g_0(r) \\
&\text{——} = h_0(r)
\end{aligned}
$$

These can be combined to draw diagrams. Two circles in a diagram are considered connected if there exists a bond between them and a diagram is considered connected if there exist at least one path, using the connected circles, between any pair of circles in the graph. The second integral in equation 3.65 will give us the two following connected diagrams as figure 3.2 shows

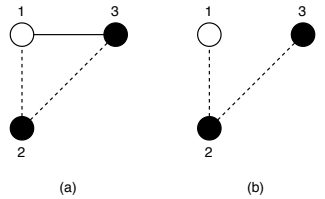

Figure 3.2: A graph illustration of the two connected diagrams from the second integral in equation 3.65, where white circles correspond to coordinates held constant under integration and black circles represents variables of integration. The continuous line represent $h_0(r)$ and the dashed lines represents $w(r)g_0(r)$.

A diagram is considered reducible if it contains an articulation circle and irreducible if it does not. An articulation circle is a circle which if removed, will divide a connected diagram into two or more connected diagrams. We can see from figure 3.2 that (b) is reducible as removing the circle marked 2 will disconnect circle 1 and 3 from each other. The third integral in equation 3.65 will give us the following diagrams as figure 3.3 shows

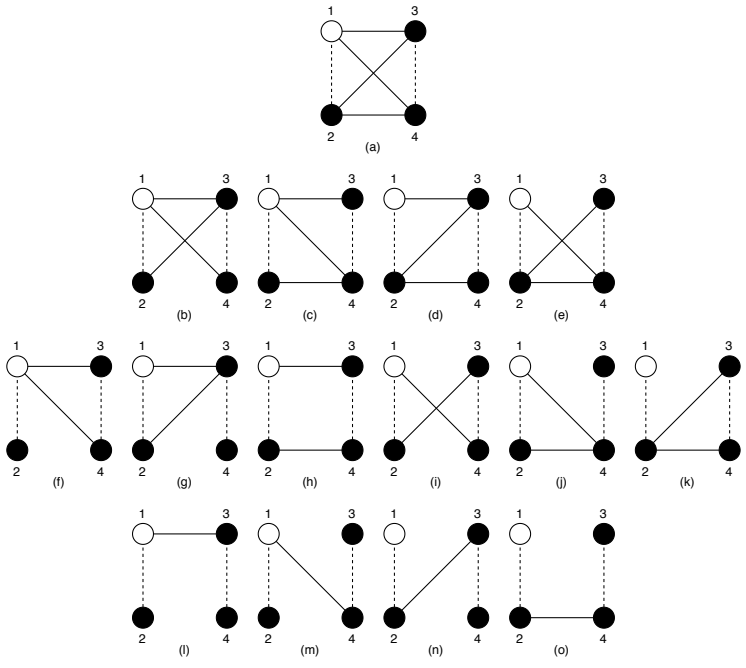

Figure 3.3: A graph illustration of the 15 connected diagrams from the third integral in equation 3.65. White circles correspond to coordinates held constant under integration and black circles represents variables of integration. The continuous lines represents $h_0(r)$ and the dashed lines represents $w(r)g_0(r)$.

We can see from figure 3.3 that (f), (g), (j), (k), (l), (m), (n) and (o) are reducible. According to Smith et al. the last integral in equation 3.64 will only produce reducible cluster integrals when using the substitutions from Baxter [6] and Schofield [34]

$$k_BT\left(\frac{\partial\rho}{\partial P}\right)_0\left(\frac{\partial}{\partial\rho}\right)\left[\rho^2 g_0(12)\right] = 2\rho g_0(12) + \rho^2\int\left[g_0(123) - g_0(12)\right]\mathrm{d}\mathbf{r}_3 \tag{3.66}$$

and

$$k_BT\left(\frac{\partial\rho}{\partial P}\right)_0 = 1 + \rho\int h_0(12)\mathrm{d}\mathbf{r}_2 \tag{3.67}$$

with the superposition approximation from equation 3.63. Some of these reducible cluster integrals cancel out the reducible cluster integrals from the second and third integrals. Unfortunately, due to the superposition approximation, not all the reducible integrals are canceled out. Smith et al. [41] meant that the job of the last integral was to cancel out all the reducible integrals, but due to the superposition approximation this does not happen. Therefore they suggested to omit all the reducible integrals anyway, which we will be doing as well. This give us the following form for the second order perturbation term:

$$\begin{aligned} a_2 = &-\frac{\rho}{4}\int g_0(12)w(12)^2\mathrm{d}\mathbf{r}_2 - \frac{\rho^2}{2}\int\int g_0(12)w(12)g_0(23)w(23)h_0(13)\mathrm{d}\mathbf{r}_2\mathrm{d}\mathbf{r}_3 \\ &-\frac{\rho^3}{8}\int\int\int g_0(12)w(12)g_0(34)w(34)\left[2h_0(13)h_0(24)+\right. \\ &\left.4h_0(13)h_0(14)h_0(24) + h_0(13)h_0(14)h_0(23)h_0(24)\right]\mathrm{d}\mathbf{r}_2\mathrm{d}\mathbf{r}_3\mathrm{d}\mathbf{r}_4 \end{aligned} \tag{3.68}$$

where we have used that the system is isotropic and therefore independent of coordinate labels such that we can add the irreducible integrals that will be equal together. We can rewrite equation 3.68 into the form that Smith et al. presented it as by letting the hard-sphere fluid be our reference system with a hard-sphere diameter d chosen as equation 2.118. We then obtain:

$$a_2 = -\frac{1}{4}\rho J_1 - \frac{1}{2}\rho^2 J_2 - \frac{1}{8}\rho^3(2J_3 + 4J_4 + J_5) \tag{3.69}$$

where

$$J_1 = \int w(12)^2 g_d^{\mathrm{hs}}(12)\mathrm{d}\mathbf{r}_2 \tag{3.70}$$

$$J_2 = \int\int w(12)g_d^{\mathrm{hs}}(12)w(34)g_d^{\mathrm{hs}}(34)h_d^{\mathrm{hs}}(13)\mathrm{d}\mathbf{r}_2\mathrm{d}\mathbf{r}_3 \tag{3.71}$$

$$J_3 = \int\int\int w(12)g_d^{\mathrm{hs}}(12)w(34)g_d^{\mathrm{hs}}(34)h_d^{\mathrm{hs}}(13)h_d^{\mathrm{hs}}(24)\mathrm{d}\mathbf{r}_2\mathrm{d}\mathbf{r}_3\mathrm{d}\mathbf{r}_4 \tag{3.72}$$

$$J_4 = \int\int\int w(12)g_d^{\mathrm{hs}}(12)w(34)g_d^{\mathrm{hs}}(34)h_d^{\mathrm{hs}}(13)h_d^{\mathrm{hs}}(14)h_d^{\mathrm{hs}}(24)\mathrm{d}\mathbf{r}_2\mathrm{d}\mathbf{r}_3\mathrm{d}\mathbf{r}_4 \tag{3.73}$$

$$J_5 = \int\int\int w(12)g_d^{\mathrm{hs}}(12)w(34)g_d^{\mathrm{hs}}(34)h_d^{\mathrm{hs}}(13)h_d^{\mathrm{hs}}(14)h_d^{\mathrm{hs}}(23)h_d^{\mathrm{hs}}(24)\mathrm{d}\mathbf{r}_2\mathrm{d}\mathbf{r}_3\mathrm{d}\mathbf{r}_4 \tag{3.74}$$

In order to calculate these, Smith et al. [41] suggested rewriting these integrals into

$$J_1 = 4\pi\int_0^\infty w(r)^2 g_d^{\mathrm{hs}}(r)r^2\mathrm{d}r \tag{3.75}$$

$$J_2 = 4\pi \int_0^\infty w(r) g_d^{\text{hs}}(r) \gamma(r) r^2 \mathrm{d}r \tag{3.76}$$

$$J_3 = 4\pi \int_0^\infty \gamma(r)^2 r^2 \mathrm{d}r \tag{3.77}$$

$$J_4 = 4\pi \int_0^\infty h_d^{\text{hs}}(r) \gamma(r)^2 r^2 \mathrm{d}r \tag{3.78}$$

where

$$\gamma(x) = \frac{2\pi}{x} \int_0^\infty w(y) g_d^{\text{hs}}(y) y \int_{|x-y|}^{x+y} h_d^{\text{hs}}(z) z \mathrm{d}z \mathrm{d}y \tag{3.79}$$

They also gave an expression for the J_5 integral by expanding the integrand in a series of Legendre polynomials

$$\begin{aligned} J_5 =& 64\pi^3 \sum_l \frac{1}{(2l+1)^2} \int_0^\infty \mathbf{r}_{12}^2 w(\mathbf{r}_{12}) g_d^{\text{hs}}(\mathbf{r}_{12}) \int_0^\infty \mathbf{r}_{13}^2 h_d^{\text{hs}}(\mathbf{r}_{13}) D_l(\mathbf{r}_{12}, \mathbf{r}_{13}) \\ &\cdot \int_0^\infty \mathbf{r}_{14}^2 h_d^{\text{hs}}(\mathbf{r}_{14}) D_l(\mathbf{r}_{12}, \mathbf{r}_{14}) E_l(\mathbf{r}_{13}, \mathbf{r}_{14}) \mathrm{d}\mathbf{r}_{14} \mathrm{d}\mathbf{r}_{13} \mathrm{d}\mathbf{r}_{12} \end{aligned} \tag{3.80}$$

where

$$D_l(\mathbf{r}_{12}, \mathbf{r}_{13}) = \frac{(2l+1)}{2} \int_0^\pi h_d^{\text{hs}}(\mathbf{r}_{23}) \mathcal{P}_l(\cos\theta_{23}) \sin\theta_{23} \mathrm{d}\theta_{23} \tag{3.81}$$

$$E_l(\mathbf{r}_{12}, \mathbf{r}_{13}) = \frac{(2l+1)}{2} \int_0^\pi w(\mathbf{r}_{23}) g_d^{\text{hs}}(\mathbf{r}_{23}) \mathcal{P}_l(\cos\theta_{23}) \sin\theta_{23} \mathrm{d}\theta_{23} \tag{3.82}$$

and

$$\mathbf{r}_{23}^2 = \mathbf{r}_{12}^2 + \mathbf{r}_{13}^2 - 2\mathbf{r}_{12}\mathbf{r}_{13}\cos\theta_{23} \tag{3.83}$$

$\mathcal{P}_l$ is a Legendre polynomial of order l. The next step now is to approximate the radial distribution function $g_d^{\text{hs}}(r)$, as it is needed in equations 3.75 to 3.78 and equation 3.80. For this we have tested two different analytical forms which we will briefly discuss here.

The first one we tested was the one by Wertheim [49] and Throop and Bearman [45] following the implementation by Smith and Henderson [40]. Wertheim solved the equation

$$y(r) = 1 + \rho \int_{r'<d} y(r') \mathrm{d}\mathbf{r}' - \rho \int_{\substack{r'<d \\ |\mathbf{r}-\mathbf{r}'|>d}} y(r') y\left(|\mathbf{r} - \mathbf{r}'|\right) \mathrm{d}\mathbf{r}' \tag{3.84}$$

(has its origin in both the Ornstein-zernike relation and the Percus-Yevick approximation, which are explained briefly in section 7.2 in the appendix) by taking the Laplace transformation of each term. He then solved the transformed terms algebraically which we will not go into detail here. He finally ended up with the following equation to solve

$$g^{\text{py}}(r) = \mathcal{L}^{-1}\{G^{\text{py}}(\tau)\} = \frac{1}{2\pi i r} \int_{\delta - i\infty}^{\delta + i\infty} \frac{\tau L(\tau) e^{\tau r} \mathrm{d}\tau}{12\eta[S(\tau)e^\tau + L(\tau)]} \tag{3.85}$$

where G^{py} is the Laplace transformed g^{py}, τ is the Laplace transform variable and

$$S(\tau) = (1+\eta)^2\tau^3 + 6\eta(1-\eta)\tau^2 + 18\eta^2\tau - 12\eta(1+2\eta) \tag{3.86}$$

$$L(\tau) = 12\eta[(1 + \frac{1}{2}\eta)\tau + (1+2\eta)] \tag{3.87}$$

Wertheim wanted a closed form for any given r, thus he expanded the denominator in powers of $L(\tau)/S(\tau)$ and got the equation on the following form

$$g^{\text{py}}(r) = \sum_{n=1}^{\infty} \frac{(-1)^{n+1}}{24\pi r i} \int_{\delta-i\infty}^{\delta+i\infty} \exp(\tau(r-nd)) \left[\frac{L(\tau)}{S(\tau)}\right]^n \tau \mathrm{d}\tau \tag{3.88}$$

The integral for $r - nd < 0$ would be zero for each of the terms in the sum, as the contour can be closed on the right half plane which has no poles. For $r - nd > 0$ Wertheim closed the contour in the left half plane. All three roots of $S(\tau)$ contributes to this, thus the integrals can be evaluated by the means of the residue theorem at the three roots of $S(\tau)$. In the paper of Smith they have implemented this method up to $r = 5d$, where they after this point has truncated it as 1.

The second version we used by Trokhymchuk et al. [46] have also used equation 3.85 by Wertheim as their foundation. From $d < r < 2d$ they closely followed the work of Wertheim, but through a slightly different take on it by Nezbeda [32] giving the following expression

$$g^{\text{py}}(r) = \frac{\tilde{A}_0}{r} e^{\mu_0[r-\sigma]} + \frac{\tilde{B}_0}{r} \cos(\beta_0[r-\sigma] + \gamma_0) e^{\alpha_0[r-\sigma]} \tag{3.89}$$

while for the remaining range they used the residue theorem on equation 3.85 which give us

$$g^{\text{py}}(r) = \sum_{n=0}^{\infty} g_n^{\text{residue}}(r) \text{for } r \geq d \tag{3.90}$$

where $g_n^{\text{residue}}(r)$ is the residue of $G^{\text{py}}(\tau)$ at the roots of the denominator $L(\tau) + S(\tau)e^{\tau}$. The residue at 0 contributes 1 while the other roots occur as complex-conjugate pairs. Among these there exists a pair $\kappa_0 \pm i\omega_0$ which is closest to the real axis and can determine the asymptotic behaviour of $g^{\text{py}}(r) - 1$ for large r. From this they obtained the expression for the remaining range

$$g^{\text{py}}(r) = 1 + \frac{\tilde{C}_0}{r} \cos(\omega_0 + \delta_0) e^{\kappa_0 r} \tag{3.91}$$

The constants for both of these expressions were found by trying to reflect the physics as much as possible and will not be explained here (we refer the interested reader to their paper for more details [46]).

Henderson [19] extended equation 3.69 to a mixture of square-well and hard-sphere particles. He used a pure hard-sphere fluid as his reference and ended up with the following form for the second order perturbation term

$$\begin{aligned} a_2 = &-\frac{1}{4}\rho \left(\sum_i \sum_j x_i x_j \epsilon_{ij}^2 \right) J_1^* - \frac{1}{2}\rho^2 \left(\sum_i \sum_j \sum_k x_i x_j x_k \epsilon_{ij} \epsilon_{jk} \right) J_2^* \\ &- \frac{1}{8}\rho^3 \left(\sum_i \sum_j \sum_k \sum_l x_i x_j x_k x_l \epsilon_{ij} \epsilon_{kl} \right) \hat{J}_3^* \end{aligned} \tag{3.92}$$

where the asterisk denote that the pair potentials in the integrals is divided by its epsilon value, while $\hat{J}_3$ contains all the remaining integrals. Henderson did not specify or calculate this integral, but found it indirectly from fitting a function F^c to simulation data of the pure fluid second order perturbation term:

$$\begin{aligned} F^c(\rho) =& \hat{k}_1(1 - \exp(-2.75\rho/(\sqrt{2} - \rho)) - (2.75/\sqrt{2})\rho) + \hat{k}_2\rho + \hat{k}_3\rho^2 \\ \approx& a_2 = -\frac{1}{4}\rho J_1 - \frac{1}{2}\rho^2 J_2 - \frac{1}{8}\rho^3 \hat{J}_3 \end{aligned} \tag{3.93}$$

We tested this strategy for a Lennard-Jones fluid by using the python implemented linear least square fitting function (scipy.linalg.lstsq [35]) to obtain $\hat{k}_1$, $\hat{k}_2$ and $\hat{k}_3$. After $F^c(\rho)$ had been obtained he calculated the second order perturbation term for mixtures in the following way

$$\begin{aligned} a_2 = &-\frac{1}{4}\rho\left(\sum_i\sum_j x_i x_j \epsilon_{ij}^2\right) J_1^* - \frac{1}{2}\rho^2\left(\sum_i\sum_j\sum_k x_i x_j x_k \epsilon_{ij}\epsilon_{jk}\right) J_2^* \\ &-\frac{1}{8}\rho^3\left(\sum_i\sum_j\sum_k\sum_l x_i x_j x_k x_l \epsilon_{ij}\epsilon_{kl}\right)\left(-\frac{8}{\epsilon_{11}^2\rho^3}F^c(\rho) - \frac{2}{\rho^2}J_1^* - \frac{4}{\rho}J_2^*\right) \end{aligned} \tag{3.94}$$

The results from using this approach with a Lennard-Jones mixture, were quite poor as can be seen in the discussion section 5.4. We will therefore introduce a new strategy. We will once again assume that the integrals containing the compressibility factor will cancel out all the reducible cluster integrals and we therefore omit all these. Lastly we will be using the Lennard-Jones potential instead of the square-well and hard-sphere potential. We then end up with the following expression:

$$\begin{aligned} a_2 = &-\frac{1}{4}\rho\left(\sum_i\sum_j x_i x_j \epsilon_{ij}^2\right) J_1^* - \frac{1}{2}\rho^2\left(\sum_i\sum_j\sum_k x_i x_j x_k \epsilon_{ij}\epsilon_{jk}\right) J_2^* \\ &-\frac{1}{8}\rho^3\left(\sum_i\sum_j\sum_k\sum_l x_i x_j x_k x_l \epsilon_{ij}\epsilon_{kl}\right)(2J_3^* + 4J_4^* + J_5^*). \end{aligned} \tag{3.95}$$

Given this expression, the only difference in the potential between the different particles is the well depth ϵ. However it can easily be extended to different σ values and even Mie potentials. The next step is to define the hard-sphere diameter. We are using a pure hard-sphere fluid as the reference, thus we will be using the one defined by Leonard et al. [26] (see equation 3.34). We calculated J_1 to J_4 using equation 3.70, 3.71, 3.72 and 3.73 respectively. The inner integral of γ was calculated analytically while the outer integrals were calculated numerically using the Python implemented function scipy.integrate.quad [37]. For the J_5 integral the D_l and E_l terms were first calculated and stored for all the required combinations of $\mathbf{r}_{12}$, $\mathbf{r}_{13}$ and $\mathbf{r}_{14}$ using the Simpsons method with 101 points from 0 to π. The Python implemented scipy.special.legendre [36] was used to obtain the Legendre polynomial values and the Legendre sum was truncated at $l = 11$. After the required D_l and E_l values were calculated, the outer integrals were calculated numerically using a 201 point Simpsons method truncated at $5d$. According to Smith et al. [41] both the truncation of the Legendre sum and the integration range introduce minimal error.

What makes this method especially interesting is that we can calculate each of the six contributions used in the Monte Carlo simulations (this is explained more in detail in section 4.3) and compare them to Monte Carlo data individually. We do this by reformulating equation 3.95 for a binary mixture of particle species 1 and 2 into the following six equations:

$$\begin{aligned} -\frac{1}{2N}[\langle W_{11}W_{11}\rangle_0 - \langle W_{11}\rangle_0\langle W_{11}\rangle_0] = &-\frac{1}{4}\rho x_1^2\epsilon_{11}^2 J_1^* - \frac{1}{2}\rho^2 x_1^3\epsilon_{11}^2 J_2^* \\ &-\frac{1}{8}\rho^3 x_1^4\epsilon_{11}^2(2J_3^* + 4J_4^* + J_5^*) \end{aligned} \tag{3.96}$$

$$-\frac{1}{2N}[\langle W_{22}W_{22}\rangle_0 - \langle W_{22}\rangle_0\langle W_{22}\rangle_0] = -\frac{1}{4}\rho x_2^2\epsilon_{22}^2 J_1^* - \frac{1}{2}\rho^2 x_2^3\epsilon_{22}^2 J_2^* - \frac{1}{8}\rho^3 x_2^4\epsilon_{22}^2(2J_3^* + 4J_4^* + J_5^*) \tag{3.97}$$

$$-\frac{4}{2N}[\langle W_{12}W_{12}\rangle_0 - \langle W_{12}\rangle_0\langle W_{12}\rangle_0] = -\frac{1}{4}\rho x_1 x_2\epsilon_{12}^2 2J_1^* - \frac{1}{2}\rho^2(x_1^2 x_2\epsilon_{12}^2 + x_1 x_2^2\epsilon_{12}^2)J_2^* - \frac{1}{8}\rho^3 4x_1^2 x_2^2\epsilon_{12}^2(2J_3^* + 4J_4^* + J_5^*) \tag{3.98}$$

$$-\frac{2}{2N}[\langle W_{11}W_{22}\rangle_0 - \langle W_{11}\rangle_0\langle W_{22}\rangle_0] = -\frac{1}{8}\rho^3 2x_1^2 x_2^2\epsilon_{11}\epsilon_{22}(2J_3^* + 4J_4^* + J_5^*) \tag{3.99}$$

$$-\frac{4}{2N}[\langle W_{11}W_{12}\rangle_0 - \langle W_{11}\rangle_0\langle W_{12}\rangle_0] = -\frac{1}{2}\rho^2 2x_1^2 x_2\epsilon_{11}\epsilon_{12}J_2^* - \frac{1}{8}\rho^3 4x_1^3 x_2\epsilon_{11}\epsilon_{12}(2J_3^* + 4J_4^* + J_5^*) \tag{3.100}$$

$$-\frac{4}{2N}[\langle W_{12}W_{22}\rangle_0 - \langle W_{12}\rangle_0\langle W_{22}\rangle_0] = -\frac{1}{2}\rho^2 2x_1 x_2^2\epsilon_{22}\epsilon_{12}J_2^* - \frac{1}{8}\rho^3 4x_1 x_2^3\epsilon_{22}\epsilon_{12}(2J_3^* + 4J_4^* + J_5^*) \tag{3.101}$$

3.3.4 Numerical Second Order Perturbation Term for Mixtures Using an Additive Binary Reference

For the equations we have just shown we have used a pure hard-sphere reference fluid. We will now extend them to an additive binary hard-sphere mixture reference fluid, where we will be using equation 3.37 and 3.38 to define the hard-sphere diameters. This will give us the following three binary radial distribution functions $g_{d,11}^{\text{hs}}$, $g_{d,12}^{\text{hs}}$ and $g_{d,22}^{\text{hs}}$. When we take the different radial distribution functions into account we will end up with a much more complicated expression. To simplify the expression we introduce the following four terms

$$J_{1,ij}^* = 4\pi\int_0^\infty w^*(r)^2 g_{d,ij}^{\text{hs}}(r)r^2\mathrm{d}r \tag{3.102}$$

$$J_{2,ijk}^* = 4\pi\int_0^\infty w^*(r)\frac{1}{2}(g_{d,ij}^{\text{hs}}(r)\gamma_{jkik}^*(r) + g_{d,jk}^{\text{hs}}(r)\gamma_{ijik}^*(r))r^2\mathrm{d}r \tag{3.103}$$

$$J_{3,ijkl}^* = 4\pi\int_0^\infty \frac{1}{2}(\gamma_{ijik}^*(r)\gamma_{kljl}^*(r) + \gamma_{ijjl}^*(r)\gamma_{klik}^*(r))r^2\mathrm{d}r \tag{3.104}$$

$$J_{4,ijkl}^* = 4\pi\int_0^\infty h_{d,il}^{\text{hs}}(r)\frac{1}{2}(\gamma_{ijik}^*(r)\gamma_{kljl}^*(r) + \gamma_{ijjl}^*(r)\gamma_{klik}^*(r))r^2\mathrm{d}r \tag{3.105}$$

where

$$\gamma_{ijkl}^*(x) = \frac{2\pi}{x}\int_0^\infty w^*(y)g_{d,ij}^{\text{hs}}(y)y\int_{|x-y|}^{x+y} h_{d,kl}^{\text{hs}}(z)z\mathrm{d}z\mathrm{d}y \tag{3.106}$$

and $w^*(r)$ is the reduced particle interaction potential. We have here approximated the three and four particle radial distribution functions for mixtures by using the superposition approximation with the corresponding radial distribution functions that match the required interactions. For example a three particle superposition approximation for the interaction between one particle of type 1 and two particles of type 2, would be $g_{d,12}^{\text{hs}}(r)g_{d,12}^{\text{hs}}(r)g_{d,22}^{\text{hs}}(r)$. Due to how complicated the J_5^* term is and its contribution being very small, we have chosen to not calculate this term with binary radial distribution

functions and have instead used the J_5^* value as seen from equation 3.80. Using this and the notation we just introduced we can write the second order term as

$$a_2 = -\frac{1}{4}\rho\left(\sum_i\sum_j x_i x_j \epsilon_{ij}^2 J_{1,ij}^*\right) - \frac{1}{2}\rho^2\left(\sum_i\sum_j\sum_k x_i x_j x_k \epsilon_{ij}\epsilon_{jk} J_{2,ijk}^*\right) - \frac{1}{8}\rho^3\left(\sum_i\sum_j\sum_k\sum_l x_i x_j x_k x_l \epsilon_{ij}\epsilon_{kl}(2J_{3,ijkl}^* + 4J_{4,ijkl}^* + J_5^*)\right). \tag{3.107}$$

We now need a way to calculate the binary radial distribution functions $g_{d,11}^{\text{hs}}$, $g_{d,12}^{\text{hs}}$ and $g_{d,22}^{\text{hs}}$. For this we have used the work of Smith et al. [42] who have published their Fortran 77 code. Our procedure for calculating equation 3.107 is as follows. The inner integral in γ_{ijkl}^* was calculated using the Simpsons method with a minimum of 100 points and a maximum of 200 times the integration range number of points when integrating within the range of $r \in \{0, 3\}$. When integrating within the range of $r \in \{3, 7\}$ the Simpsons method using a minimum of 20 points and a maximum of 20 times the integration range number of points was used. We utilized a larger number of integration points in the range between 0 and 3 due to the radial distribution function varying the most in this range (see figure 5.6). All points above $r = 7$ we set to 0. For the outer integral in γ_{ijkl}^* the python implemented scipy.integrate.quad [37] function was used. While for the outermost integral we used a 501 point Simpsons method, truncating at $r = 5$. Our reasoning for using the least accurate integration procedure on the outermost integral was due to computation time as well as the integral accuracy being most affected by the accuracy of the inner integrals. We can once again calculate the six contributions for the Monte Carlo simulation. This time using the following equations:

$$-\frac{1}{2N}[\langle W_{11}W_{11}\rangle_0 - \langle W_{11}\rangle_0\langle W_{11}\rangle_0] = -\frac{1}{4}\rho x_1^2\epsilon_{11}^2 J_{1,11}^* - \frac{1}{2}\rho^2 x_1^3\epsilon_{11}^2 J_{2,111}^* - \frac{1}{8}\rho^3 x_1^4\epsilon_{11}^2(2J_{3,1111}^* + 4J_{4,1111}^* + J_5^*) \tag{3.108}$$

$$-\frac{1}{2N}[\langle W_{22}W_{22}\rangle_0 - \langle W_{22}\rangle_0\langle W_{22}\rangle_0] = -\frac{1}{4}\rho x_2^2\epsilon_{22}^2 J_{1,22}^* - \frac{1}{2}\rho^2 x_2^3\epsilon_{22}^2 J_{2,222}^* - \frac{1}{8}\rho^3 x_2^4\epsilon_{22}^2(2J_{3,2222}^* + 4J_{4,2222}^* + J_5^*) \tag{3.109}$$

$$-\frac{4}{2N}[\langle W_{12}W_{12}\rangle_0 - \langle W_{12}\rangle_0\langle W_{12}\rangle_0] = -\frac{1}{4}\rho x_1 x_2\epsilon_{12}^2 2J_{1,12}^* - \frac{1}{2}\rho^2(x_1^2 x_2\epsilon_{12}^2 J_{2,121}^* + x_1 x_2^2\epsilon_{12}^2 J_{2,212}^*) - \frac{1}{8}\rho^3 x_1^2 x_2^2\epsilon_{12}^2(2(J_{3,1212}^* + J_{3,1221}^* + J_{3,2112}^* + J_{3,2121}^*) + 4(J_{4,1212}^* + J_{4,1221}^* + J_{4,2112}^* + J_{4,2121}^*) + J_5^*) \tag{3.110}$$

$$-\frac{2}{2N}[\langle W_{11}W_{22}\rangle_0 - \langle W_{11}\rangle_0\langle W_{22}\rangle_0] = -\frac{1}{8}\rho^3 x_1^2 x_2^2\epsilon_{11}\epsilon_{22}(2(J_{3,1122}^* + J_{3,2211}^*) + 4(J_{4,1122}^* + J_{4,2211}^*) + J_5^*) \tag{3.111}$$

$$
\begin{aligned}
-\frac{4}{2N}[\langle W_{11}W_{12}\rangle_0 - \langle W_{11}\rangle_0\langle W_{12}\rangle_0] = &-\frac{1}{2}\rho^2 x_1^2 x_2 \epsilon_{11}\epsilon_{12}(J^*_{2,112} + J^*_{2,211}) \\
&-\frac{1}{8}\rho^3 x_1^3 x_2 \epsilon_{11}\epsilon_{12}(2(J^*_{3,1112} + J^*_{3,1121} \\
&+ J^*_{3,1211} + J^*_{3,2111}) + 4(J^*_{4,1112} + J^*_{4,1121} \\
&+ J^*_{4,1211} + J^*_{4,2111}) + J^*_5)
\end{aligned} \tag{3.112}
$$

$$
\begin{aligned}
-\frac{4}{2N}[\langle W_{12}W_{22}\rangle_0 - \langle W_{12}\rangle_0\langle W_{22}\rangle_0] = &-\frac{1}{2}\rho^2 2x_1 x_2^2 \epsilon_{22}\epsilon_{12}(J^*_{2,122} + J^*_{2,221}) \\
&-\frac{1}{8}\rho^3 4x_1 x_2^3 \epsilon_{22}\epsilon_{12}(2(J^*_{3,1222} + J^*_{3,2122} \\
&+ J^*_{3,2212} + J^*_{3,2221}) + 4(J^*_{4,1222} + J^*_{4,2122} \\
&+ J^*_{4,2212} + J^*_{4,2221}) + J^*_5)
\end{aligned} \tag{3.113}
$$

Chapter 4

Numerical Methods and Monte Carlo Simulation

4.1 Numerical Methods

This section will briefly explain the different numerical integration methods used for this thesis.

Consider a function f, that is dependent on x. An approximate integral of precision $d = 2n - 1$ is the Gauss-Legendre Quadrature defined as

$$\int_{-1}^{1} f(x)\mathrm{d}x = \sum_{i=1}^{n} w_i f(x_i) + R_n \tag{4.1}$$

where x_i is the ith root of the Legendre polynomial $\mathcal{P}_n(x)$, w_i is the weight defined as

$$w_i = \frac{2}{(1 - x_i^2)[\mathcal{P}_n'(x_i)]^2} \tag{4.2}$$

and R_n is the residual

$$R_n = \frac{2^{n+1}(n!)^4}{(2n+1)[(2n)!]^3} f^{(2n)}(\xi),\ -1 < \xi < 1 \tag{4.3}$$

For an arbitrary interval $[a, b]$ the approximation can be written as

$$\int_{a}^{b} f(y)\mathrm{d}y \approx \frac{b-a}{2} \sum_{i=1}^{n} w_i f(y_i) \tag{4.4}$$

where y_i is

$$y_i = \left(\frac{b-a}{2}\right) x_i + \left(\frac{b+a}{2}\right) \tag{4.5}$$

[3]. The Gauss-Legendre quadrature is exact for polynomials of degree $2n-1$ or less and can be used for definite integrals [29]. The python function numpy.polynomial.legendre.leggauss has been used to perform these integrations [36].

For integrals where one of the integration limits has been infinite, a Fourier integral has been used to calculate them using the python function scipy.integrate.quad [37]. In

cases where computation time has been an issue the Simpson's rule of integration has been used: For an arbitrary interval $[a, b]$ the approximation can be written using an even number of equal sub-intervals, say $n = 2m$

$$\int_a^b f(x)\mathrm{d}x \approx \frac{1}{3}\frac{(b-a)}{2m}(f(x_0) + 4f(x_1) + 2f(x_2) + 4f(x_3) + \cdots + 2f(x_{2m-2}) + 4f(x_{2m-1}) + f(x_{2m})) \tag{4.6}$$

If the fourth derivative $f^{(4)}$ exists and is continuous on $a \leq x \leq b$ then the residual R will be

$$R = -\frac{b-a}{180}\left(\frac{b-a}{2m}\right)^4 f^{(4)}(\xi) \tag{4.7}$$

where ξ is a suitable unknown value between a and b [22]. The python function scipy.integrate.simps has been used to perform these integrations [38].

4.2 Monte Carlo Methods

As shown in section 2.4, canonical ensemble averages can be used to evaluate the perturbation terms. Say for example that $\langle W_N(\mathbf{r}^N)\rangle_0$ is to be evaluated. The integral is on the following form

$$\langle W_N(\mathbf{r}^N)\rangle_0 = \int W_N(\mathbf{r}^N)\rho_{N,0}^{(N)}\mathrm{d}\mathbf{r}^N \tag{4.8}$$

where

$$\rho_{N,0}^{(N)} = \frac{\exp(-\beta U_{N,0}(\mathbf{r}^N))}{Z_N} = \frac{\exp(-\beta U_{N,0}(\mathbf{r}^N))}{\int \exp(-\beta U_{N,0}(\mathbf{r}^N))\mathrm{d}\mathbf{r}^N} \tag{4.9}$$

For the potential functions that are used in this project, analytical evaluations of these integrals are generally not possible, while numerical methods would quickly require an unrealistic amount of function evaluations. One way to approximate the integral is by the simple Monte Carlo method, which would involve the following steps:

1. Generate an initial configuration by randomly assigning $3N$ Cartesian coordinates to the particles.
2. Calculate $W_N(\mathbf{r}^N)$ and the Boltzmann factor $\exp(-\beta U_{N,0}(\mathbf{r}^N))$ for the configuration.
3. Add the Boltzmann factor to the accumulated sum of Boltzmann factors and the potential to its accumulated sum of potentials and return to the first point.
4. After N_{trial} of iterations the ensemble average can be calculated from:

$$\langle W_N(\mathbf{r}^N)\rangle_0 = \frac{\sum_{i=1}^{N_{\text{trial}}} W_{N,i}(\mathbf{r}^N)\exp(-\beta U_{N,0,i}(\mathbf{r}^N))}{\sum_{i=1}^{N_{\text{trial}}} \exp(-\beta U_{N,0,i}(\mathbf{r}^N))} \tag{4.10}$$

However this is not a feasible approach, as there will be many configurations that have extremely small Boltzmann factors from the high-energy overlap between particles. One way to solve this is by using an importance sampling method. The most commonly used one is from the work of Metropolis in 1954. The Metropolis algorithm generates a Markov chain of states, which satisfies the two following conditions: (1) each trial is from a finite

set of possible outcomes, (2) the outcome of each trial depends only on the trial that immediately preceded it [24]. Two such states m and n are connected by a transition probability Π_{mn}, which is the probability of going from state m to n. Π can be regarded as an $N \times N$ transition matrix for an irreducible Markov chain, where N is the number of possible states. Each row will add to 1

$$\sum_n \Pi_{mn} = 1 \tag{4.11}$$

The probability that the system is in a specific state is represented by a probability vector $\boldsymbol{\rho}$, where each column gives the probability of a state. By saying that $\boldsymbol{\rho}(1)$ represents the initial configuration then the probability of the second state will be given by

$$\boldsymbol{\rho}(2) = \boldsymbol{\rho}(1)\Pi \tag{4.12}$$

while the third will be

$$\boldsymbol{\rho}(3) = \boldsymbol{\rho}(2)\Pi = \boldsymbol{\rho}(1)\Pi^2 \tag{4.13}$$

and so on. The configuration will eventually converge to the limiting distribution

$$\boldsymbol{\rho}_{\text{limit}} = \lim_{\tau \to \infty} \boldsymbol{\rho}(1)\Pi^\tau \tag{4.14}$$

a consequence of this is that the limiting distribution will have to satisfy the eigenvalue equations

$$\boldsymbol{\rho}_{\text{limit}}\Pi = \boldsymbol{\rho}_{\text{limit}} \tag{4.15}$$

$$\sum_m \boldsymbol{\rho}_m \Pi_{mn} = \boldsymbol{\rho}_n \tag{4.16}$$

The problem now is to find the elements of Π so that equation 4.15 and 4.16 are satisfied. A useful trick to solve this is to replace it with the unnecessarily strong condition of microscopic reversibility

$$\boldsymbol{\rho}_m \Pi_{mn} = \boldsymbol{\rho}_n \Pi_{nm} \tag{4.17}$$

By summing over all states of m and by using equation 4.11, one get back the properties of equation 4.15 and 4.16:

$$\sum_m \boldsymbol{\rho}_m \Pi_{mn} = \sum_m \boldsymbol{\rho}_n \Pi_{nm} = \boldsymbol{\rho}_n \sum_m \Pi_{nm} = \boldsymbol{\rho}_n \tag{4.18}$$

Metropolis et al. created such a scheme that would satisfy both equation 4.11 and equation 4.17, known as the asymmetrical solution:

$$\Pi_{mn} = \mathbb{a}_{mn} \qquad \boldsymbol{\rho}_n \geq \boldsymbol{\rho}_m \qquad m \neq n \tag{4.19}$$

$$\Pi_{mn} = \mathbb{a}_{mn}(\boldsymbol{\rho}_n / \boldsymbol{\rho}_m) \qquad \boldsymbol{\rho}_n \leq \boldsymbol{\rho}_m \qquad m \neq n \tag{4.20}$$

The liquid also has to have the possibility of remaining in the same state

$$\Pi_{mm} = 1 - \sum_{n \neq m} \Pi_{mn} \tag{4.21}$$

In this solution $\mathbb{a}$ is a symmetrical stochastic matrix, $\mathbb{a}_{mn} = \mathbb{a}_{nm}$, called the underlying matrix of the Markov chain. This matrix has to be specified in order to implement the Metropolis method. It is done by specifying cubes $\mathcal{R}$ that are centered at each individual particle position $\mathbf{r}_i^m$ with sides of length $2\delta r_{\text{max}}$. Each time a particle is then moved there

will be a large, but finite positions $N_{\mathcal{R}}$ for it to move to with equal probability. Thus $\mathbb{\alpha}_{mn}$ can be simply defined as

$$\mathbb{\alpha}_{mn} = \begin{cases} 1/N_{\mathcal{R}} & \mathbf{r}_i^n \in \mathcal{R} \\ 0 & \mathbf{r}_i^n \notin \mathcal{R} \end{cases} \tag{4.22}$$

Using this choice for $\mathbb{\alpha}$, the Monte Carlo procedure can be described in the following way. First a particle is chosen, this could be done randomly, but in the code used for this project this is performed sequentially, where one cycle is when all the particles has been moved once. The particle is given a uniform random displacement along each of the coordinate directions, with an adjustable maximum displacement of $\delta r_{\max}$. This parameter governs the size of the region as well as the convergence of the Markov chain. The next step is to calculate $\delta U_{N,0,nm} = U_{N,0,n}(\mathbf{r}^N) - U_{N,0,m}(\mathbf{r}^N)$. This does not require a recalculation of all the configurational energy of state m, only the changes from moving the specific particle. So for particle i it would be

$$\delta U_{N,0,nm} = \left(\sum_{j=1}^{N} u_{0,n}(r_{ij}) - \sum_{j=1}^{N} u_{0,m}(r_{ij}) \right) \tag{4.23}$$

The corresponding element of the transition matrix Π, will depend on the initial state m and the final state n. So if $\delta U_{N,0,nm} \leq 0$ is downhill then $\boldsymbol{\rho}_n \geq \boldsymbol{\rho}_m$ and equation 4.19 applies, which means that the new configuration is accepted. If $\delta U_{N,0,nm} > 0$ is uphill then $\boldsymbol{\rho}_n < \boldsymbol{\rho}_m$ and equation 4.20 applies. The move is then accepted with a probability $\boldsymbol{\rho}_n / \boldsymbol{\rho}_m$:

$$\frac{\boldsymbol{\rho}_n}{\boldsymbol{\rho}_m} = \frac{Z_N^{-1} \exp(-\beta U_{N,0,n}(\mathbf{r}^N))}{Z_N^{-1} \exp(-\beta U_{N,0,n}(\mathbf{r}^N))} = \exp\left(-\beta \delta U_{N,0,nm}(\mathbf{r}^N)\right) \tag{4.24}$$

This is done by generating a random number uniformly on (0,1). If the random number is less than $\exp\left(-\beta \delta U_{N,0,nm}(\mathbf{r}^N)\right)$, the move is accepted, otherwise it is rejected. When a move is accepted the potential $W_{N,n}(\mathbf{r}^N)$ is added to the accumulated average potential. The question now, lies in how $\delta r_{\max}$ should be chosen. If chosen to be too small, then a large fraction of moves will be accepted, but the phase space will be explored very slowly. If too large, then nearly all trial moves will be rejected [4]. The code used for this project generally aims for a 0.3-0.5 acceptance rate and will adjust $\delta r_{\max}$ accordingly during simulation to reach this average.

All the simulations performed for this project has been with soft-spheres, which we have defined using equation 2.122, letting $l_r = 12$ and $l_a = 6$ (Lennard-Jones). This may at first seem strange as the Barker and Henderson theory is from a system of hard-spheres, but as section 2.4.2 explains the hard-sphere system is an approximation of the reference soft-sphere system, we therefore believe it will be more accurate to use soft-spheres for the simulations.

4.3 Monte Carlo Settings

We have used the same Metropolis Monte Carlo code as was used in the work of Hammer et al. [16] which has been created by the research group at Sintef Energi AS.

In order to calculate the second order perturbation term from Monte Carlo simulations we used equation 2.68. For a binary mixture with the two particles labeled 1 and 2 the energy can be written as a sum of three contributions

$$W = W_{11} + 2W_{12} + W_{22} \tag{4.25}$$

where the subscript of W_{ij} denotes that the contribution is from the interaction between the particle type i and j. We have omitted the notation showing its dependence of the particle coordinates for simplicity. Using this we can write the following terms as

$$\langle W \rangle_0 = \langle W_{11} \rangle_0 + 2\langle W_{12} \rangle_0 + \langle W_{22} \rangle_0 \tag{4.26}$$

and

$$\begin{aligned}\langle W^2 \rangle_0 - \langle W \rangle_0^2 =& [\langle W_{11} W_{11} \rangle_0 - \langle W_{11} \rangle_0 \langle W_{11} \rangle_0] + 4[\langle W_{12} W_{12} \rangle_0 - \langle W_{12} \rangle_0 \langle W_{12} \rangle_0] \\ &+ [\langle W_{22} W_{22} \rangle_0 - \langle W_{22} \rangle_0 \langle W_{22} \rangle_0] + 2[\langle W_{11} W_{22} \rangle_0 - \langle W_{11} \rangle_0 \langle W_{22} \rangle_0] \\ &+ 4[\langle W_{11} W_{12} \rangle_0 - \langle W_{11} \rangle_0 \langle W_{12} \rangle_0] + 4[\langle W_{12} W_{22} \rangle_0 - \langle W_{12} \rangle_0 \langle W_{22} \rangle_0]\end{aligned} \tag{4.27}$$

where the second equation is used for calculating the second order perturbation term. Each of the contributions are calculated during the Monte Carlo simulation using the mixing rules described in section 3.3 for the interactions between particle type 1 and 2. Each time W is calculated it is calculated using the following equations with the cutoff range (r_c) for the inter-particle potential set to $4\sigma_{11}$:

$$W_{11} = \frac{1}{2} \sum_{i=1}^{N_1} \sum_{j=1}^{N_1} w_{11}(r_{ij}) \tag{4.28}$$

$$W_{12} = \frac{1}{2} \sum_{i=1}^{N_1} \sum_{j=1}^{N_2} w_{12}(r_{ij}) \tag{4.29}$$

$$W_{22} = \frac{1}{2} \sum_{i=1}^{N_2} \sum_{j=1}^{N_2} w_{22}(r_{ij}) \tag{4.30}$$

The energy that was lost due to this cut-off is calculated by assuming that $g_0(r) = 1$ after this point and we end up with the three following long range tail corrections:

$$\frac{W_{11,\text{lrc}}\epsilon_{11}}{N_1} = 2\pi \frac{N_1}{V} \int_{r_c}^{\infty} r^2 w_{11}(r) \mathrm{d}r \tag{4.31}$$

$$\frac{W_{12,\text{lrc}}\epsilon_{11}}{N_1} = 2\pi \frac{N_2}{V} \int_{r_c}^{\infty} r^2 w_{12}(r) \mathrm{d}r \tag{4.32}$$

$$\frac{W_{22,\text{lrc}}\epsilon_{11}}{N_2} = 2\pi \frac{N_2}{V} \int_{r_c}^{\infty} r^2 w_{22}(r) \mathrm{d}r \tag{4.33}$$

The final equation in calculating W at one step is then

$$W = W_{11} + 2W_{12} + W_{22} + W_{11,\text{lrc}} + 2W_{12,\text{lrc}} + W_{22,\text{lrc}} \tag{4.34}$$

The Monte Carlo simulation was performed in a cubic box with periodic boundary condition and every simulation used 500 particles. For the code used in this thesis one MC cycle consists of one trial move per particle. To equilibrate the system, 80 equilibration blocks with $18.750 \cdot 10^3$ MC cycles each were used, while the production phase used 25 blocks with $150 \cdot 10^3$ MC cycles each. The sampling of the configurational attractive energy was calculated every 250 MC move, as this according to Hammer et al. [16] improves the accuracy compared to only sampling every completed MC cycle while still being computationally efficient.

In order to explore the compositional space, we performed MC simulations with the following settings $\epsilon_{22}/\epsilon_{11} \in \{1, 2, 4, 8\}$, $T^* \in \{1, 2, 4, 6, 12\}$, $\rho^* \in \{0.05, 0.1, 0.15, 0.2, 0.25, 0.3, 0.35, 0.4, 0.5, 0.6, 0.7, 0.8, 0.9\}$ and $x_2 \in \{0.25, 0.5, 0.75\}$. Where we have used equation 3.58 and 3.59 for T^* and ρ^* respectively, while using $N_2 \in \{125, 250, 375\}$ to correspond to the mole fractions. In calculating the standard error we first calculate the block average of the property (f) in question

$$\langle f \rangle = \frac{1}{N_{\text{blk}}} \sum_{i=1}^{N_{\text{blk}}} f_i \tag{4.35}$$

where N_{blk} is the number of blocks. Then the standard deviation s^2 is calculated as

$$s_f^2 = \left\langle (f - \langle f \rangle)^2 \right\rangle = \frac{1}{N_{\text{blk}}} \sum_{i=1}^{N_{\text{blk}}} f_i^2 - \langle f \rangle^2 \tag{4.36}$$

With the standard error of the mean $\langle f \rangle$ being

$$s_{\langle f \rangle} = \frac{s_f}{\sqrt{N_{\text{blk}}}} \tag{4.37}$$

Jack knifing is also performed and is the one that is reported when it yields better statistics. It works by first estimating the parameter for each sub-sample omitting the i-th observation

$$\bar{f}_i = \frac{1}{N_{\text{blk}} - 1} \sum_{j=1, j \neq i}^{N_{\text{blk}}} f_i, \, i = 1, ..., N_{\text{blk}} \tag{4.38}$$

Then the standard deviation is calculated as

$$s_{\bar{f}}^2 = \left\langle (\bar{f} - \langle \bar{f} \rangle)^2 \right\rangle = \frac{N_{\text{blk}} - 1}{N_{\text{blk}}} \left(\sum_{i=1}^{N_{\text{blk}}} \bar{f}_i^2 - N_{\text{blk}} \langle \bar{f} \rangle^2 \right) \tag{4.39}$$

Chapter 5

Results and Discussion

This chapter will present the results from the five different implemented models described in this thesis. We will briefly summarize them here.

Lafitte et al.

The work of Lafitte et al. [23] is based on the MCA with a correction factor and the Mie potential. It uses an additive binary reference hard-sphere fluid and is written on an analytical form the following way

$$a_2 = \sum_{i=1}^{n}\sum_{j=1}^{n} x_i x_j a_{2,ij} \tag{5.1}$$

$$\begin{aligned} a_{2,ij} =& \frac{1}{2}K^{\text{hs}}(1+\chi_{ij})\mathcal{C}_{ij}^2\epsilon_{ij}^2\eta_{ij}\Big[x_{0,ij}^{2l_{a,ij}}(I_{1,ij}^S(\eta_{ij};2l_{a,ij})+B_{ij}(\eta_{ij};2l_{a,ij})) \\ &- 2x_{0,ij}^{l_{a,ij}+l_{r,ij}}(I_{1,ij}^S(\eta_{ij};l_{a,ij}+l_{r,ij})+B_{ij}(\eta_{ij};l_{a,ij}+l_{r,ij})) \\ &+x_{0,ij}^{2l_{r,ij}}(I_{1,ij}^S(\eta_{ij};2l_{r,ij})+B_{ij}(\eta_{ij};2l_{r,ij}))\Big] \end{aligned} \tag{5.2}$$

The χ-factor is here dependent on the reduced density and the dimensionless van der Waals energy. See section 3.3.1 for more details on this model.

Westen and Gross

The work of van Westen and Gross [54] is based on the MCA with a correction factor and the Lennard-Jones potential and has been extended to mixtures using an additive binary reference hard-sphere fluid. It is written in a partly analytical form the following way

$$a_2 = \sum_{i=1}^{n}\sum_{j=1}^{n} x_i x_j a_{2,ij} \tag{5.3}$$

$$\begin{aligned} a_{2,ij} =& \frac{1}{2}K^{\text{hs}}(1+\chi)\mathcal{C}_{ij}^2\epsilon_{ij}^2\eta_{ij}\Big[x_{0,ij}^{2l_{a,ij}}(I_{1,ij}^S(\eta_{ij};2l_{a,ij})+B_{\text{num},ij}(\eta_{ij};2l_{a,ij})) \\ &- 2x_{0,ij}^{l_{a,ij}+l_{r,ij}}(I_{1,ij}^S(\eta_{ij};l_{a,ij}+l_{r,ij})+B_{\text{num},ij}(\eta_{ij};l_{a,ij}+l_{r,ij})) \\ &+x_{0,ij}^{2l_{r,ij}}(I_{1,ij}^S(\eta_{ij};2l_{r,ij})+B_{\text{num},ij}(\eta_{ij};2l_{r,ij}))\Big] \end{aligned} \tag{5.4}$$

where $B_{\text{num},ij}$ is calculated numerically. The χ-factor is here dependent on the reduced density and the reduced temperature. See section 3.3.2 for more details on this model.

Henderson

The work of Henderson [19] does not use the MCA and was originally based on a mixture of square-well and hard-sphere potentials, but has here been modified to Lennard-Jones potentials with different well-depths, using a pure reference hard-sphere fluid. It is calculated numerically and uses a correlated term to deal with the higher order distribution functions from the two last integrals. It has the following form:

$$\begin{aligned} a_2 = &-\frac{1}{4}\rho\left(\sum_i\sum_j x_i x_j \epsilon_{ij}^2\right) J_1^* - \frac{1}{2}\rho^2\left(\sum_i\sum_j\sum_k x_i x_j x_k \epsilon_{ij}\epsilon_{jk}\right) J_2^* \\ &-\frac{1}{8}\rho^3\left(\sum_i\sum_j\sum_k\sum_l x_i x_j x_k x_l \epsilon_{ij}\epsilon_{kl}\right)\left(-\frac{8}{\epsilon_{11}^2\rho^3}F^c(\rho) - \frac{2}{\rho^2}J_1^* - \frac{4}{\rho}J_2^*\right) \end{aligned} \tag{5.5}$$

See section 3.3.3 for more details on this model.

Numerical Method Using a Pure Reference

This method does not use the MCA and is based on the Lennard-Jones potential with different well-depths, using a pure reference hard-sphere fluid. It is calculated numerically and is written in the following form:

$$\begin{aligned} a_2 = &-\frac{1}{4}\rho\left(\sum_i\sum_j x_i x_j \epsilon_{ij}^2\right) J_1^* - \frac{1}{2}\rho^2\left(\sum_i\sum_j\sum_k x_i x_j x_k \epsilon_{ij}\epsilon_{jk}\right) J_2^* \\ &-\frac{1}{8}\rho^3\left(\sum_i\sum_j\sum_k\sum_l x_i x_j x_k x_l \epsilon_{ij}\epsilon_{kl}\right)(2J_3^* + 4J_4^* + J_5^*). \end{aligned} \tag{5.6}$$

See section 3.3.3 for more details on this model.

Numerical Method Using an Additive Binary Reference

This method does not use the MCA and is based on the Lennard-Jones potential with different well-depths, using an additive binary reference hard-sphere fluid. It is calculated numerically and is written in the following form:

$$\begin{aligned} a_2 = &-\frac{1}{4}\rho\left(\sum_i\sum_j x_i x_j \epsilon_{ij}^2 J_{1,ij}^*\right) - \frac{1}{2}\rho^2\left(\sum_i\sum_j\sum_k x_i x_j x_k \epsilon_{ij}\epsilon_{jk} J_{2,ijk}^*\right) \\ &-\frac{1}{8}\rho^3\left(\sum_i\sum_j\sum_k\sum_l x_i x_j x_k x_l \epsilon_{ij}\epsilon_{kl}(2J_{3,ijkl}^* + 4J_{4,ijkl}^* + J_5^*)\right). \end{aligned} \tag{5.7}$$

See section 3.3.4 for more details on this model.

The discussion is structured in the following way. First the Monte Carlo simulation data will be presented, followed by a comparison between Lafitte et al. implementation of the second order perturbation term for mixtures with our mixture extension to van Westen and Gross work on the second order perturbation term. After that part we will give our brief thoughts on the three different analytical radial distribution functions used in this thesis. We will then compare the three different numerical implementations for the second order perturbation term for mixtures to Monte Carlo simulation data. The individual Monte Carlo contribution terms will also be investigated and compared to the numerical implementation. A detailed error analysis of the various models will be given and used to create different fitting approaches as well as a better understanding of the problems in modelling mixtures with large difference in well-depth. Lastly some suggestions on the next steps for improving the model will be given.

5.1 Monte Carlo Simulation Data

The Monte Carlo data was obtained by the simulation procedure as explained in sections 4.2 and 4.3. The error of the simulation data was calculated as one standard deviation of the sample mean (see equation 4.36), but had a magnitude of error smaller than the symbol size used to visualize the data, that we have chosen to omit it. This lead us to believe that the simulation data is relatively accurate. The general trend for the data is that a larger epsilon ratio yields a lower second order perturbation term value. The same trend is observed when we increase the fraction of component 2, the reduced density and to a certain degree the reduced temperature. As the amount of data obtained for this project is relatively large, we have chosen to visualize the trend using a principal component analysis (PCA) loadings plot with only one principal component (PC1) on the normalized data [25]. The result can be seen in figure 5.1.

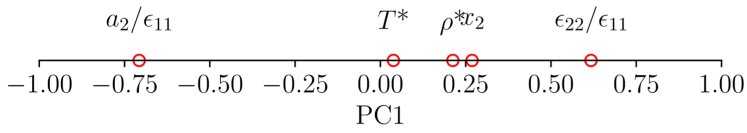

Figure 5.1: The loading's plot with one axis (PC1) based on normalized Monte Carlo data of the second order perturbation term with the variables reduced density (ρ^*), reduced temperature (T^*), epsilon ratio ($\epsilon_{22}/\epsilon_{11}$) and the fraction of component 2 (x_2).

The first component of a PCA is in the direction with the most variance such that it minimizes the average squared distance from a point to the line. As we can see from the figure the second order perturbation term is on the far left on the PC1 line, while all the other variables are on the the right side, showing that they are indeed negatively correlated with the second order term as mentioned earlier. We can also see that the epsilon ratio explains most of the variance for PC1, while the reduced temperature explains the least, suggesting that in general the epsilon ratio has the greatest impact on the second order term while the reduced temperature has the least impact. This is also our observation when we have been analyzing the data.

Another observation we made from the data was that the Monte Carlo data for the epsilon ratio of 8 at the lower reduced temperature and higher reduced density spectrum seemed to be less accurate as it had a tendency to deviate more from the general trend. We therefore performed these simulations again doubling the number of MC steps to see if they would be improved. Another important factor to point out at this range is that we

could potentially be in the metastable region. For pure hard-sphere systems this has been stated to be between $\eta = 0.494$ ($\rho = 0.943$) to $\eta = 0.644$ [31]. However we are dealing with the much less studied mixture of soft-sphere particles described by equation 2.122 and could well be in the metastable region. This region is known to be difficult to perform simulations in and can yield somewhat unreliable data.

5.2 Comparison between Lafitte and van Westen

In the paper of Hammer et al. [16] they showed the many problems of Lafitte et al. [23] (Lafitte) work when it comes to the mixture extension of the second order perturbation term (see section 3.3.1 for details on model). Inspired by Lafitte et al., van Westen and Gross [54] (WG) created a modified version for the second order perturbation term, but only for Lennard-Jones fluids and not Mie fluids. It was also not extend to mixtures. We have extended it to mixtures as shown in section 3.3.2 and will in this part compare it to the work of Lafitte et al..

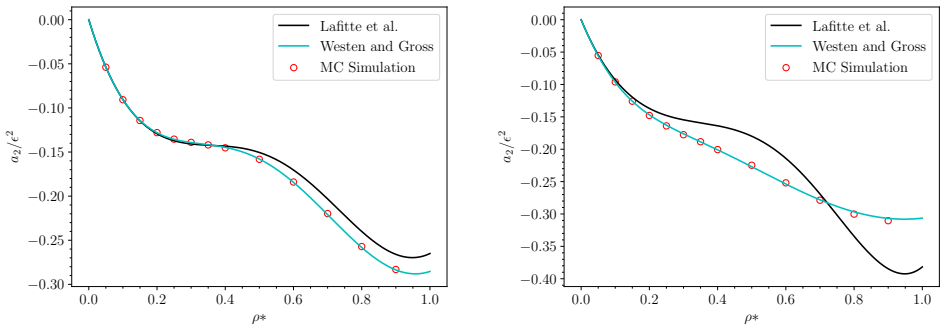

(a) $T^* = 1$ **(b)** $T^* = 12$

Figure 5.2: Comparison of the Lafitte et al. and van Westen and Gross implementation of the second order perturbation term for a pure fluid at the reduced temperature (a) $T^* = 1$ and (b) $T^* = 12$. The Monte Carlo data (MC) performed for this thesis is shown as well to test the accuracy of the models.

Figure 5.2a compares the implementations of the second order perturbation term for a pure Lennard-Jones fluid to Monte Carlo data at the reduced temperature of $T^* = 1$. The figure clearly shows that the implementation of WG predicts better than the work of Lafitte. This is expected as the χ-factor of Lafitte has been correlated to work for a much broader range of potentials than the one by WG and is likely more prone to inaccuracies when only comparing the Lennard-Jones potential. Figure 5.2b compares the implementations of the second order perturbation term for a pure Lennard-Jones fluid to Monte Carlo data at the reduced temperature of $T^* = 12$. At this temperature it appears that the work of Lafitte collapses, while the work of WG still predicts fairly well. This is likely due to how the χ-factor has been correlated. In the work of Lafitte, it is not dependent on the reduced temperature and hence, has only been correlated for the reduced temperature of $T^* = 1$ [23]. The χ-factor of WG however, is dependent on the reduced temperature and has been correlated for a range of reduced temperatures spanning from $T^* = 0.5$ to $T^* = 12$.

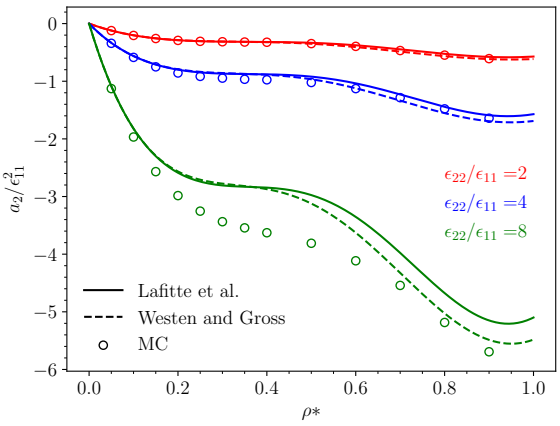

Figure 5.3: Comparison of the Lafitte et al. and van Westen and Gross implementation of the second order perturbation term for a mixture at the reduced temperature $T^* = 1$ and the fraction of component 2 $x_2 = 0.5$ with different epsilon ratios. The MC data from this thesis is shown as well to test the accuracy of the models.

Concluding that the work of WG is better at approximating the second order perturbation term for pure Lennard-Jones fluids than the one by Lafitte, it will be interesting to see how well it performs when extended to mixtures. Figure 5.3 compares their work with Monte Carlo data for a binary mixture with different epsilon ratios at $T^* = 1$ and $x_2 = 0.5$. Unfortunately the figure shows that there is little reason to suggest that the work of WG performs much better than the one by Lafitte. They both seem to predict badly, especially at the high epsilon ratio.

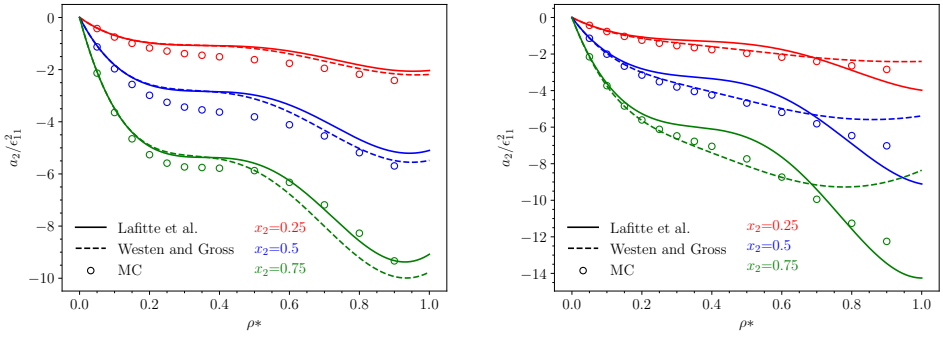

(a) $T^* = 1$ **(b)** $T^* = 12$

Figure 5.4: Comparison of the Lafitte et al. and van Westen and Gross implementation of the second order perturbation term for a mixture at the reduced temperatures (a) $T^* = 1$ and (b) $T^* = 12$ and epsilon ratio $\epsilon_{22}/\epsilon_{11} = 8$ with different component 2 fractions. The MC data from this thesis is shown as well to test the accuracy of the models.

Figure 5.4a compares their work with Monte Carlo data for a binary mixture with different fractions of component 2 at $T^* = 1$ and $\epsilon_{22}/\epsilon_{11} = 8$. This figure clearly shows their inability to accurately predict the second order perturbation term.

Figure 5.4b shows the same, but at the much higher reduced temperature of 12. We can here see that the one by WG seem to predict the general trend in the beginning much better than the one by Lafitte, but fails at the higher reduced density range. For this reason

and the fact that WG predicts pure Lennard-Jones fluid better, we have chosen to only go further with the work by WG for the remaining comparisons.

5.3 Radial Distribution Function Comparisons

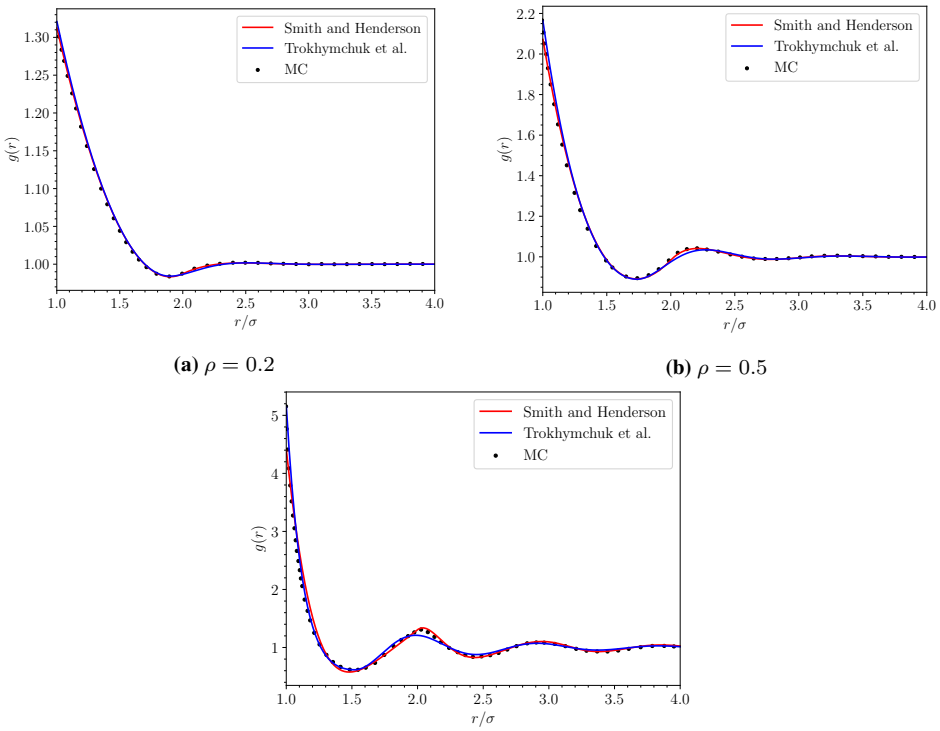

(a) $\rho = 0.2$

(b) $\rho = 0.5$

(c) $\rho = 0.9$

Figure 5.5: A comparison of the radial distribution function implementation for a pure fluid by Smith and Henderson [40] and Trokhymchuk et al. [46] with the MC data extracted from the work of Trokhymchuk et al. [46] at $\sigma = 1$ and the density value 0.2 (a) 0.5 (b) and 0.9 (c).

For the numerical calculations of the second order term, we have used analytical equations for the radial distribution functions (RDF). As the accuracy of these are quite important in order to obtain reasonable numerical values, we have compared the models to Monte Carlo data extracted from the work of Trokhymchuk et al. [46]. The results can be seen in figure 5.5.

We can clearly see that the radial distribution function of Smith and Henderson [40] overall agrees better with the Monte Carlo data, then the one by Trokhymchuk et al. [46] with the exception being at the contact value, where it actually performs worse than the one by Trokhymchuk et al.. This is a well known problem using the Percus-Yevick theory [48]. Despite its issues we will continue testing the work of Trokhymchuk et al. as their relative simple form compared to the one by Smith and Henderson is tempting for future work in obtaining an analytical form.

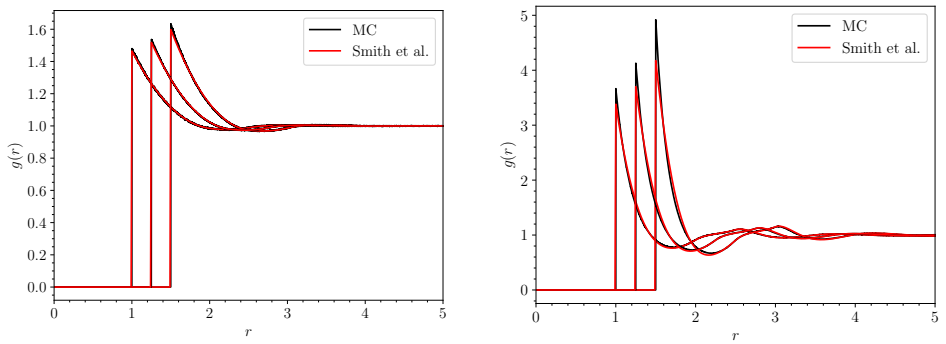

(a) $\rho = 0.3$ **(b)** $\rho = 0.8$

Figure 5.6: A comparison of the radial distribution function implementation by Smith et al. [42] with Monte Carlo (MC) data given by Hammer et al. [16] at $\sigma_{11} = 1$, $\sigma_{22} = 1.5$, $x_2 = 0.5$ and the density value 0.3 (a) and 0.8 (b). The leftmost plot is g_{11}^{hs}, the middle one is g_{12}^{hs} and the rightmost is g_{22}^{hs}.

Figure 5.6 compares the binary radial distribution function by Smith et al. [42] against simulation data. We can see that it is not able to predict the contact value properly, but overall, it seems to estimate the general trend fairly well and will therefore be used for the numerical calculation of the second order perturbation theory, when using an additive hard-sphere mixture reference.

5.4 Comparison of the Numerical Second Order Perturbation Term Using a Pure Hard-Sphere Reference

We will now investigate the performance of the numerical method in calculating the second order perturbation term for mixtures using a pure hard-sphere fluid reference as seen in section 3.3.3. Figure 5.7 compares the numerical second order perturbation term (see equation 3.69) using the radial distribution function of both Smith and Henderson [40] and Trokhymchuk et al. [46] to Monte Carlo data and the work of WG for a pure fluid at the reduced temperatures $T^* = 1$ and $T^* = 12$.

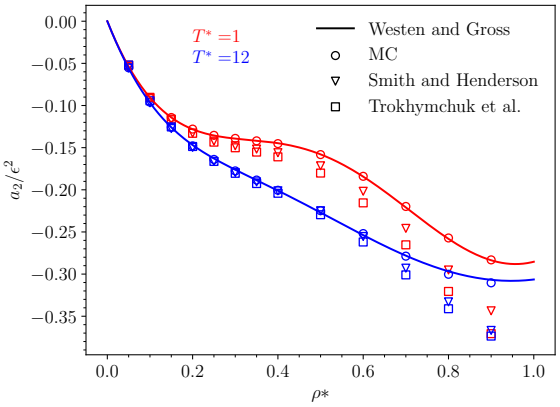

Figure 5.7: Comparison of the van Westen and Gross implementation of the pure second order perturbation term and the numerical second order perturbation term using the radial distribution function by Smith and Henderson and the one by Trokhymchuk et al. at different reduced temperatures. The MC data from this thesis is shown as well to test the accuracy of the models.

We can clearly see that the work of WG is better at predicting the second order perturbation term for a pure fluid than the numerical approach. This is nothing new and has been reported in previous papers [41]. What is more interesting however is the difference in using the two analytical forms for the radial distribution function. We can see that generally the one by Smith and Henderson seem to perform better than the one by Trokhymchuk et al.. To investigate this further we have plotted the ratio of the Monte Carlo data to the numerical second order term in figure 5.8.

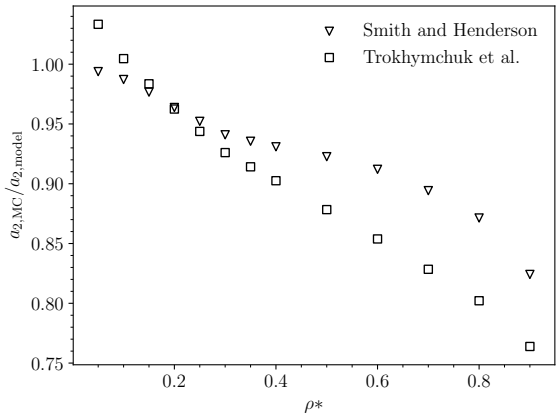

Figure 5.8: Ratio between the Monte Carlo data for the pure second order perturbation term $a_{2,\mathrm{MC}}$ and the numerical second order perturbation term $a_{2,\mathrm{model}}$ at the reduced temperature $T^* = 1$. The figure compares the implementation using the radial distribution function by Smith and Henderson to the implementation using the radial distribution function by Trokhymchuk et al..

We can here see a major problem in using the radial distribution function by Trokhymchuk et al. [46]. It does not appear to converge to one as the reduced density decreases. This is problematic since the Monte Carlo data will be going towards ideal gas here, which a good model should be able to predict. The reason for the failure here of Trokhymchuk

et al. radial distribution function is due to the models reduced density range only being from 0.2-0.9. In the paper they have a few suggestions for fixing this issue by changing the function at this range, but to avoid any potential function discontinuity that this could lead to, we have instead chosen to only look at the one by Smith and Henderson for further comparisons, which seem to converge to one as the reduced density decreases.

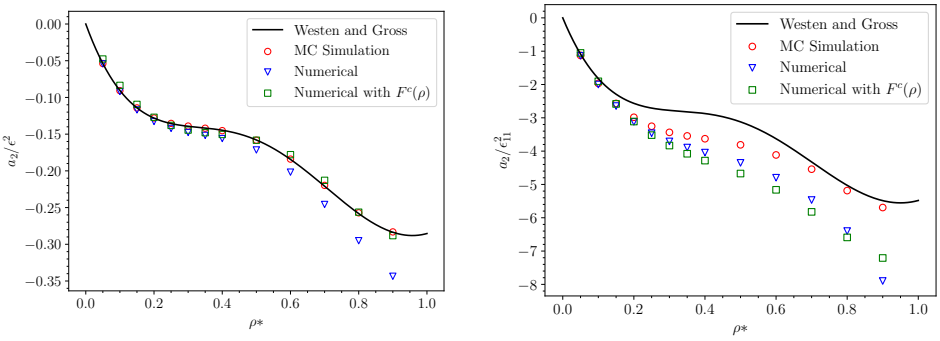

(a) Pure fluid ($\epsilon_{22}/\epsilon_{11} = 1$)

(b) $\epsilon_{22}/\epsilon_{11} = 8$

Figure 5.9: Comparison between the van Westen and Gross implementation of the second order perturbation term, the numerical second order perturbation term following the work of Henderson [19] (using $F^c(\rho)$) and the numerical second order term as we proposed it in equation 3.95. The MC data from this thesis is shown as well to test the accuracy of the models. The reduced temperature is at $T^* = 1$ and (a) shows the models for a pure fluid while (b) shows the model for a mixture with $x_2 = 0.5$ and $\epsilon_{22}/\epsilon_{11} = 8$.

In figure 5.9 we compare the method created by Henderson [19] which originally was made for a mixture of square-well and hard-sphere particles, but has now been extended to a mixture of Lennard-Jones particles (see equation 3.94 in section 3.3.3 and table 7.1 for the constants), to the numerical method using a pure hard-sphere reference fluid as seen in equation 3.95 in section 3.3.3. We can see that it predicts the pure fluid considerably better, but still not better than the model by van Westen and Gross [54]. For a mixture with epsilon ratio of 8 it deviates more than all the other models. According to Henderson [19], the model gave reasonable results for the mixture of square-well and hard-sphere particles. This comes as no surprise, as the perturbation terms will only be dependent on the density and the component fraction, while for the Lennard-Jones mixture they will also be dependent on the temperature as it does not have a hard-core. Secondly the use of a pure component reference system is correct for the case of the mixture of hard-sphere and square-well particles, while for the Lennard-Jones mixture, this is not true. Combining these observations we can see that the J^* integrals (see equation 3.70 to 3.74) will only be dependent on the density, thus making the $F^c(\rho)$ function the same independent of the temperature, component fraction and the epsilon value of the square-well particles. This however does not hold true for the mixture of Lennard-Jones particles and is the reason we did not continue following the approach of Henderson.

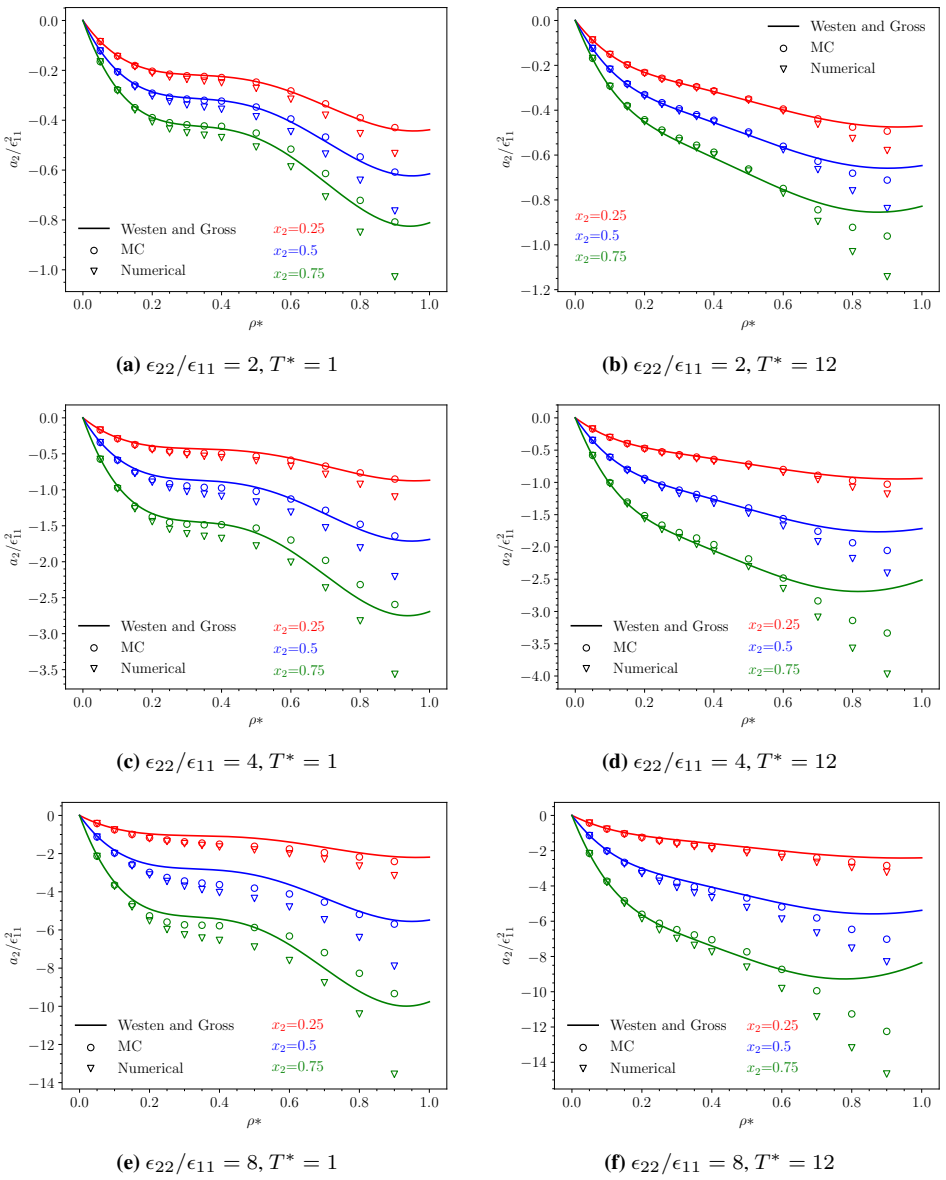

(a) $\epsilon_{22}/\epsilon_{11} = 2, T^* = 1$

(b) $\epsilon_{22}/\epsilon_{11} = 2, T^* = 12$

(c) $\epsilon_{22}/\epsilon_{11} = 4, T^* = 1$

(d) $\epsilon_{22}/\epsilon_{11} = 4, T^* = 12$

(e) $\epsilon_{22}/\epsilon_{11} = 8, T^* = 1$

(f) $\epsilon_{22}/\epsilon_{11} = 8, T^* = 12$

Figure 5.10: Comparison of the van Westen and Gross implementation of the second order perturbation term and the numerical second order perturbation term using the radial distribution function by Smith and Henderson at different reduced temperatures, fractions of component 2 and epsilon ratios. The MC data from this thesis is shown as well to test the accuracy of the models.

Figure 5.10 compares the numerical second order term for mixtures using a pure hard-sphere fluid as the reference (see equation 3.95) and the radial distribution function of Smith and Henderson against Monte Carlo data and the mixture extension of WG. We can see that at the reduced temperature of 1, they both struggle somewhat in predicting the Monte Carlo data especially at the higher reduced density range. However interestingly the numerical method seem to be following the trend of the data to a higher degree than WG, but overestimates the rate in which it decreases, thus it consistently has lower

values than the simulation data, while the extension of WG, both overestimates and underestimates the value. At the reduced temperature of 12, we can clearly see that both models predict better. This is not surprising for the numerical approach as it is based on the superposition approximation, which will be more accurate at higher temperatures as the particles, as we can see from equation 4.24 used in Monte Carlo simulation with soft-spheres, will have a higher probability of overlap and therefore be less structured. In other words the three and four body interactions will be more independent of each other. Physically this is explained by the greater kinetic energy that the particles will have making overlap easier and therefore lead to a more chaotic and less structured system. It is unclear why it improved the WG method. It could be due to the trend being less affected by it being a mixture and thus making the fitted χ-factor of WG more valid. Another interesting observation is how they seem to predict less well as the epsilon ratio increases. This could be due to how an increased well-depth for one of the particle types will counter the increase in temperature when it comes to the probability of overlap as we can see from equation 4.24 and 3.41. This leads again to more structure. Lastly we notice the total neglect of the downward trend at the higher reduced density values of the WG method. It seem to be increasing instead. This does not happen with the numerical method.

5.5 Error Analysis

In this part of the discussion, we will be looking closer at the numerical second order perturbation term and try to analyze what is causing the error as well as suggest some ways to correct it.

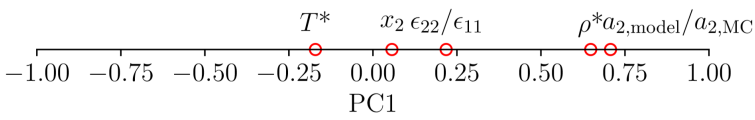

Figure 5.11: The loading's plot with one axis (PC1) based on normalized ratios between the numerical method ($a_{2,\mathrm{model}}$) using a pure hard-sphere reference and Monte Carlo data of the second order perturbation term with the variables reduced density (ρ^*), reduced temperature (T^*), epsilon ratio ($\epsilon_{22}/\epsilon_{11}$) and the fraction of component 2 (x_2).

Figure 5.11 shows a PCA loadings plot with one principal component (PC1) on the ratio of the numerical second order perturbation term using a pure hard-sphere reference divided by the MC data. We have used the entire data set that we have simulated and have normalized the ratios before performing PCA. We can clearly see from this plot that the main contributor to variance in the error is the reduced density followed by the reduced temperature and the epsilon ratio. We can also see that the fraction of component two contributes little to the variance of the PC1. This further confirms our observations from the previous figures that the main error occurs at the higher reduced density range.

To understand where the error may come from, it may be enriching to go through the major approximations we used in order to obtain the equation for the second order perturbation term (equation 3.95). The first approximation is that we are using the superposition approximation to estimate the higher order distribution functions, the second is that we assume the radial distribution functions for the 1-1, 1-2 and 2-2 interactions to be the same by using the pure hard-sphere fluid as our reference system, the last approximation is that we assume the integrals containing the compressibility factor will cancel out all

the reducible cluster integrals. The first approximation we will be looking into is the pure hard-sphere reference approximation. We will test this one by checking whether equation 3.107 in section 3.3.4 which is based on an additive binary reference performs any better.

5.5.1 Additive Reference Versus Pure Reference

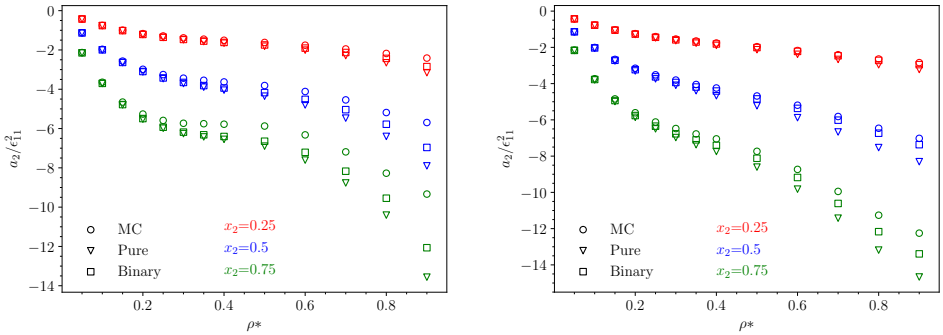

(a) $T^* = 1$ **(b)** $T^* = 12$

Figure 5.12: Comparison between the numerical second order perturbation term when using a pure hard-sphere fluid as reference and the numerical second order perturbation term when using a binary hard-sphere mixture as a reference, with epsilon ratio of 8, at different reduced temperatures and fractions of component 2. The MC data from this thesis is shown as well to test the accuracy of the models.

As we can see from the figure 5.12, using an additive binary hard-sphere reference fluid through the binary hard-sphere code by Smith et al., yields only a very slight improvement on the second order perturbation term. This lead us to believe that the major issue is the superposition approximation. As we saw in figure 5.10, the numerical second order approximation has difficulty in accurately predicting the second order perturbation term, even for pure fluids. However the major benefit in using this method is that we can divide it into six parts and compare each of those to the six contributions from the Monte Carlo data (see equation 4.27). This will hopefully give us some more insight in how well the superposition approximation and the assumption that the integrals containing the compressibility factor should cancel all the reducible cluster integrals are.

5.5.2 Comparison of the Six Interaction Terms

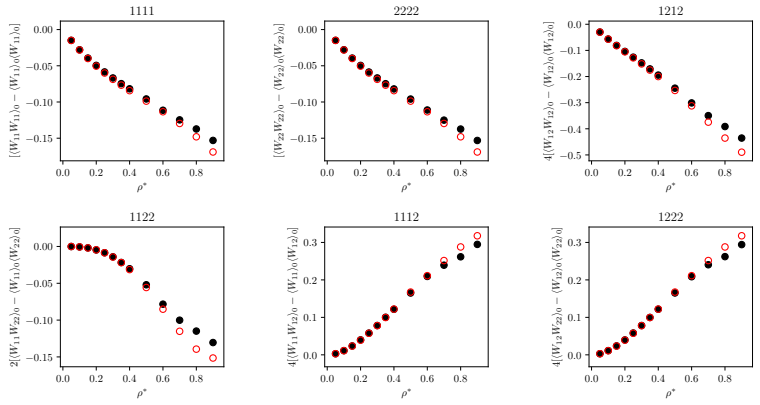

Figure 5.13: Comparison between MC data (black circles) and the numerical method (red transparent circles) for each of the terms as seen in equations 3.96 to 3.101. The reduced temperature is at $T^* = 1$, the epsilon ratio is at $\epsilon_{22}/\epsilon_{11} = 1$ and the component fraction is at $x_2 = 0.5$.

Figure 5.13 compares all six of the Monte Carlo contributions to their respective equation approximations as given in equations 3.96 to 3.101. We have for these figures used a pure fluid ($\epsilon_{22}/\epsilon_{11} = 1$), but have randomly assigned a number of particles to be particle 2 such that the fraction of particle 2 equals x_2. This is in order to get a better understanding of its problems in predicting a pure fluid. We can see that they predict reasonably well up to around the reduced density value of 0.5. After this point they seem to diverge more from the simulation data, but still in general follow the same trend.

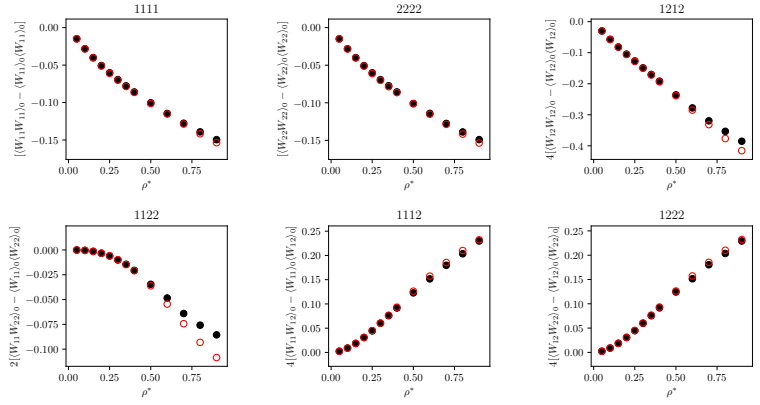

Figure 5.14: Comparison between MC data (black circles) and the numerical method (red transparent circles) for each of the terms as seen in equations 3.96 to 3.101. The reduced temperature is at $T^* = 12$, the epsilon ratio is at $\epsilon_{22}/\epsilon_{11} = 1$ and the component fraction is at $x_2 = 0.5$.

Figure 5.14 shows that at the higher temperature ($T^* = 12$), the numerical method predicts the data better, which comes as no surprise as this was something we observed earlier on in the discussion. We also notice that the numerical method seems to struggle the most in predicting the $-\frac{2}{2N}[\langle W_{11}W_{22}\rangle_0 - \langle W_{11}\rangle_0\langle W_{22}\rangle_0]$ term, which we will for simplicity denote as the 1122 term. This may be due to it being purely calculated by the four parti-

cle distribution function with the reducible cluster integrals cancelled (see equation 3.99), thus it will be heavily affected by the superposition approximation.

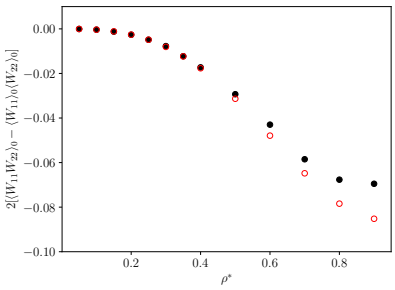

(a) $x_2 = 0.25$

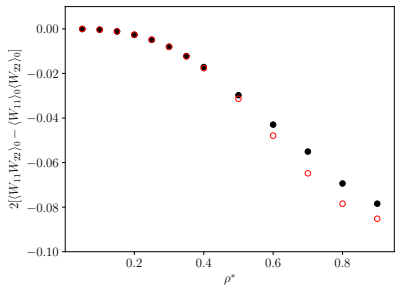

(b) $x_2 = 0.75$

Figure 5.15: Comparison between MC data (black circles) and the numerical method (red transparent circles) for the term $-\frac{2}{2N}[\langle W_{11}W_{22}\rangle_0 - \langle W_{11}\rangle_0\langle W_{22}\rangle_0]$ as seen in equations 3.99. The reduced temperature is at $T^* = 1$, the epsilon ratio is at $\epsilon_{22}/\epsilon_{11} = 1$ and the component fraction is at $x_2 = 0.25$ (a) and $x_2 = 0.75$ (b).

From figure 5.15 we can observe a worrying result. It appears that the simulation results for the 1122 term give different results for $x_2 = 0.25$ and $x_2 = 0.75$, which is not what we would expect for a pure fluid, where particle 1 and 2 are the same ($\epsilon_{22}/\epsilon_{11} = 1$). It should in theory yield the same result and be independent of whether the fraction of particle 1 is 0.25 or 0.75. To investigate this further we repeated the simulations for the reduced density values of 0.7-0.9 doubling the number of Monte Carlo steps. The results are shown in figure 5.16.

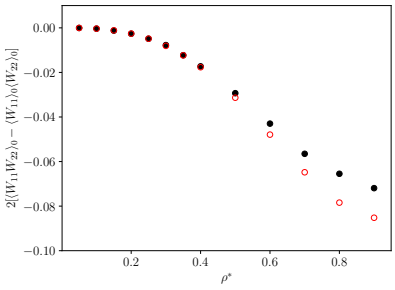

(a) $x_2 = 0.25$

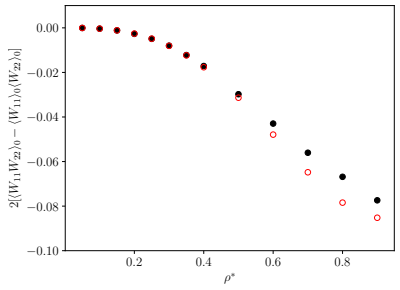

(b) $x_2 = 0.75$

Figure 5.16: Comparison between MC data, when using 25 000 equilibrium steps and 300 000 steps per block at the reduced densities ρ^* =0.7-0.9 (black circles) and the numerical method (red transparent circles) for the term $-\frac{2}{2N}[\langle W_{11}W_{22}\rangle_0 - \langle W_{11}\rangle_0\langle W_{22}\rangle_0]$ as seen in equation 3.99. The reduced temperature is at $T^* = 1$, the epsilon ratio is at $\epsilon_{22}/\epsilon_{11} = 1$ and the component fraction is at $x_2 = 0.25$ (a) and at $x_2 = 0.75$ (b).

We still observe the same tendency in figure 5.16 as in the previous figure 5.15 and currently have no explanation for this phenomena.

In figure 5.17 we compare the old simulation data against the new simulation data and the numerical model.

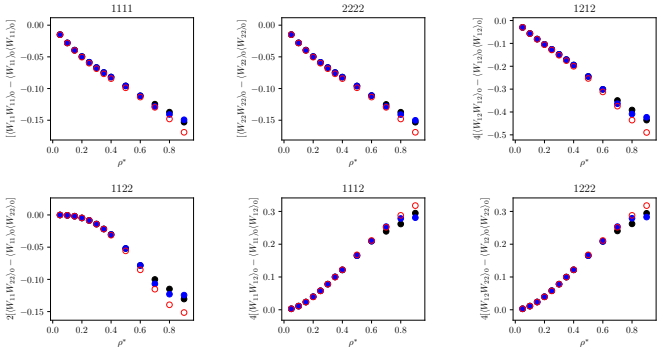

(a) $T^* = 1$

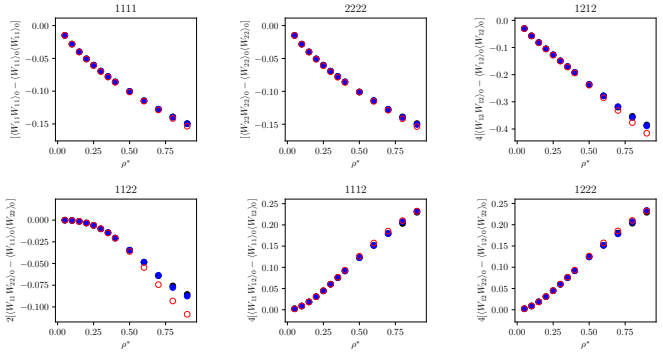

(b) $T^* = 12$

Figure 5.17: Comparison between MC data (black circles) with the default 18 750 equilibrium steps and 150 000 steps per block and the MC data (blue circles) with 25 000 equilibrium steps and 300 000 steps per block for the reduced density range 0.7-0.9. The numerical method (red transparent circles) is also shown here as seen in equations 3.96 to 3.101. The reduced temperature is at (a) $T^* = 1$ and (b) $T^* = 12$, the epsilon ratio is at $\epsilon_{22}/\epsilon_{11} = 1$ and the component fraction is at $x_2 = 0.5$.

We can see from figure 5.17 that there is an observable difference in the two simulation data, questioning the reliability of the simulation data at the higher reduced densities. For the higher reduced temperature ($T^* = 12$) they agree more. In the remaining part of the discussion, the old simulation data will be used. However in future work it may be beneficial to perform simulations with a greater number of Monte Carlo steps at the higher reduced density range.

We will now investigate whether using an additive binary hard-sphere reference fluid will improve the prediction of the six interaction terms from the Monte Carlo simulations.

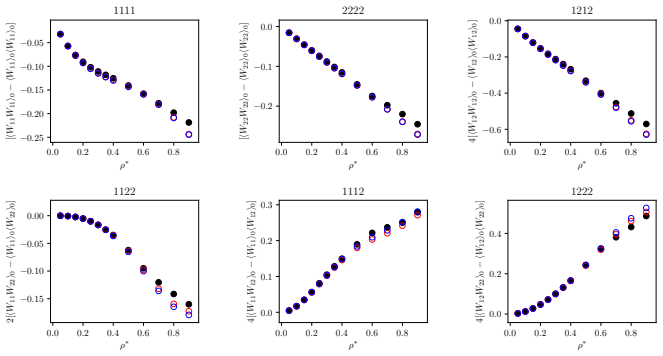

(a) $x_2 = 0.25$

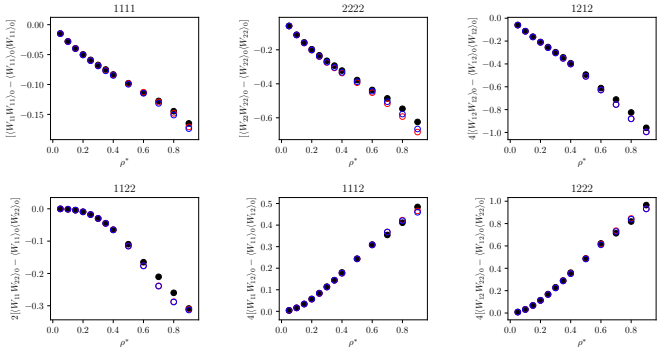

(b) $x_2 = 0.5$

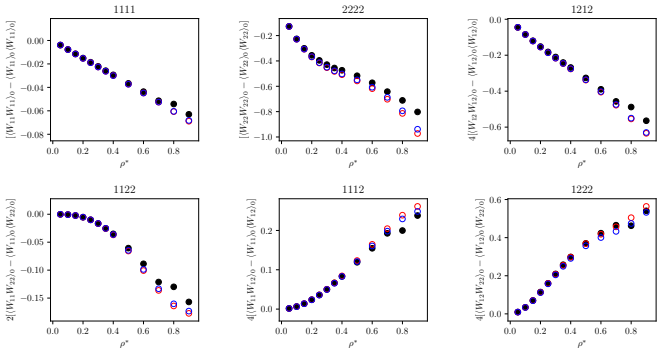

(c) $x_2 = 0.75$

Figure 5.18: Comparison between MC data (black circles), the numerical method using a pure reference (red transparent circles) and the numerical method using an additive binary reference (blue transparent circles) for each of the terms as seen in equations 3.96 to 3.101 and equations 3.108 to 3.113. The reduced temperature is at $T^* = 1$, the epsilon ratio is at $\epsilon_{22}/\epsilon_{11} = 2$ and the component fraction is at (a) $x_2 = 0.25$, (b) $x_2 = 0.5$ and (c) $x_2 = 0.75$.

Figure 5.18 compares all six of the Monte Carlo contributions to their respective equation approximations as given in equations 3.96 to 3.101 for the pure reference and as given in equations 3.108 to 3.113 for the additive reference with $\epsilon_{22}/\epsilon_{11} = 2$ and $T^* = 1$. We can see from the figures that the three contributions $-\frac{1}{2N}[\langle W_{11}W_{11}\rangle_0 - \langle W_{11}\rangle_0\langle W_{11}\rangle_0]$, $-\frac{1}{2N}[\langle W_{22}W_{22}\rangle_0 - \langle W_{22}\rangle_0\langle W_{22}\rangle_0]$ and $-\frac{4}{2N}[\langle W_{12}W_{12}\rangle_0 - \langle W_{12}\rangle_0\langle W_{12}\rangle_0]$ which we will refer to as the 1111, 2222 and 1212 terms respectively for simplicity, seem to perform slightly better when the additive binary reference is used. The reason for this could be that there is a slight difference in the radial distribution functions, as the hard-sphere diameter for component 1 is $d_{11} = 0.973$ and $d_{22} = 0.984$ for component 2, thus the single reference radial distribution function fails in representing the "pure" interactions. Another interesting observation is how the 1111 term seem to have a less linear shape, but rather a more curved one, when $x_2 = 0.25$ (see figure 5.18a). We also see the same happen with the 2222 term when $x_2 = 0.75$ (see figure 5.18c). The numerical method seem to struggle predicting these trends by overestimating them independent of the reference system used in calculating these.

We can also see a similar tendency for the cross interaction terms $-\frac{4}{2N}[\langle W_{11}W_{12}\rangle_0 - \langle W_{11}\rangle_0\langle W_{12}\rangle_0]$ and $-\frac{4}{2N}[\langle W_{12}W_{22}\rangle_0 - \langle W_{12}\rangle_0\langle W_{22}\rangle_0]$ which we will refer to as the 1112 and 1222 terms respectively for simplicity. In this case it seems like the 1112 term experiences some sort of bend around $\rho^* \approx 0.6$ when $x_2 = 0.25$, which the numerical method has a hard time explaining (see figure 5.18a). A similar bend occurs in the 1222 term when $x_2 = 0.75$ (see figure 5.18c), which the numerical method also seem to struggle in predicting.

Lastly we have the 1122 term, which interestingly, the numerical method using a pure reference seem to predict better than the numerical method using a binary reference, at $x_2 = 0.25$, but worse at $x_2 = 0.75$, while being almost indistinguishable at $x_2 = 0.5$. We believe that this has to do with the way the pure reference hard-sphere diameter is calculated (see equation 3.34). We expect the numerical method using an additive binary hard-sphere reference to more accurately represent the system. Therefore we think that using the single component hard-sphere radial distribution function, with the hard-sphere diameter as seen in equation 3.34, has the unfortunate property of exaggerating the contribution of component 1 for the diameter at $x_2 = 0.25$, and exaggerating the contribution of component 2 for the diameter at $x_2 = 0.75$. We believe it is only coincidental that the pure reference predicts the 1122 term better at $x_2 = 0.25$ (see figure 5.18a). As mentioned previously, the 1122 term is purely calculated from the four particle distribution function with the irreducible cluster integrals cancelled, which still lead us to believe that the main error for this term is from the superposition approximation.

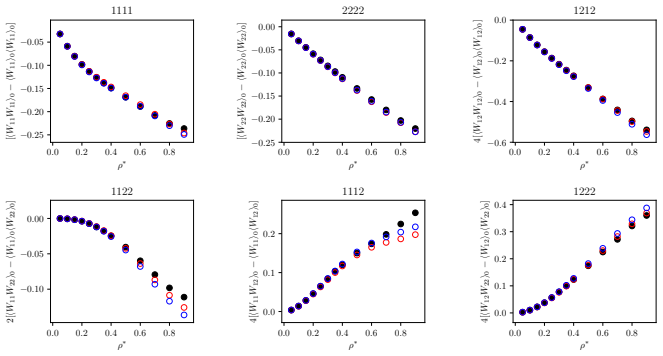

(a) $x_2 = 0.25$

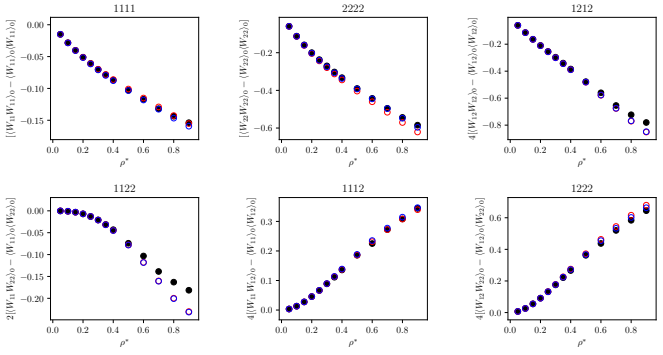

(b) $x_2 = 0.5$

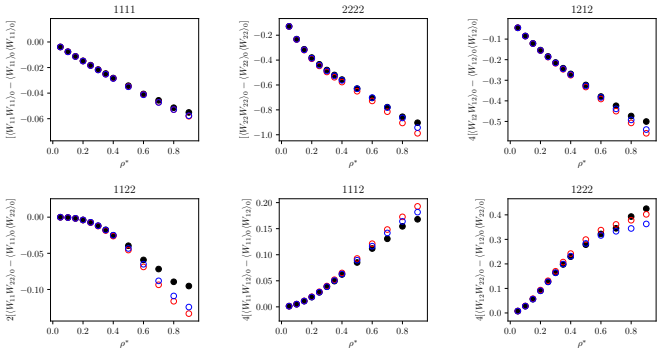

(c) $x_2 = 0.75$

Figure 5.19: Comparison between MC data (black circles), the numerical method using a pure reference (red transparent circles) and the numerical method using an additive binary reference (blue transparent circles) for each of the terms as seen in equations 3.96 to 3.101 and equations 3.108 to 3.113. The reduced temperature is at $T^* = 12$, the epsilon ratio is at $\epsilon_{22}/\epsilon_{11} = 2$ and the component fraction is at (a) $x_2 = 0.25$, (b) $x_2 = 0.5$ and (c) $x_2 = 0.75$.

Figure 5.19 compares all six of the Monte Carlo contributions to their respective equation approximations as given in equations 3.96 to 3.101 for the pure reference and as given in equations 3.108 to 3.113 for the additive reference with $\epsilon_{22}/\epsilon_{11} = 2$ and $T^* = 12$. We can see from the figure that there is a larger difference between the binary and the pure reference in predicting the 1111, 2222 and 1212 terms, where the binary reference generally performs better. The reason for this could be that the difference between the radial distribution functions are greater when the reduced temperature is at the higher spectrum. This becomes apparent if we look at the hard-sphere diameters. For component 1 it is $d_{11} = 0.891$ and for component 2 it is $d_{22} = 0.920$, thus it has a hard-sphere ratio of $d_{22}/d_{11} = 1.033$, which is greater than the hard-sphere ratio of $d_{22}/d_{11} = 1.011$ at $T^* = 1$. The problem with the 1112 and 1222 terms as discussed previously also seem to be worse at this temperature. We can also see the same problematic trend in predicting the 1122 term as we observed when $T^* = 1$.

Since we have used a different and less accurate approach in calculating the integrals for the additive binary reference system compared to the pure reference system, we have compared the pure J_1, J_2, J_3 and J_4 integrals using the two different integration approaches in table 5.1 to test its accuracy.

Table 5.1: A comparison of the various J integrals as seen in equations 3.70 to 3.73. We show the results of the integrals when they have been calculated for a pure fluid using the python implemented quad function, combined with the analytical form for the inner integral (denoted as Quad integration). We also show the other integration method, were we used a combination of the Simpsons method and the quad function without an analytical form for the inner integral (denoted as Simpsons integration).

T^*	ρ^*	J	Quad integration	Simpsons integration
1	0.05	J_1	5.276555112004786	5.276586796093443
		J_2	-9.939632898767748	-9.938262267332528
		J_3	29.397135819160578	29.394667776295154
		J_4	-4.492568853770168	-4.565941672813765
	0.9	J_1	7.176044111870223	7.176203707218072
		J_2	-6.1307740525137735	-6.135635188960642
		J_3	9.746206304423024	9.72620447866978
		J_4	-1.9872267992887147	-2.040599222630942
12	0.05	J_1	5.20077408228156	5.200804706024412
		J_2	-7.977720268505207	-7.979628949504402
		J_3	18.588399547162798	18.611505244181863
		J_4	-1.7564894764212216	-1.814120191300096
	0.9	J_1	5.758339875350886	5.758418694632738
		J_2	-4.436725738186285	-4.440228854624521
		J_3	4.794968662017447	4.815815720708088
		J_4	-0.060060352867348336	-0.09764420832030662

We can see from table 5.1 that the two integration methods yield fairly similar results and we therefore conclude that any problems with the addditive binary reference system is not due to the method of integration. In the next two figures we will be looking at the case when $\epsilon_{22}/\epsilon_{11} = 8$, in other words when the difference between component 1 and 2 is even more profound.

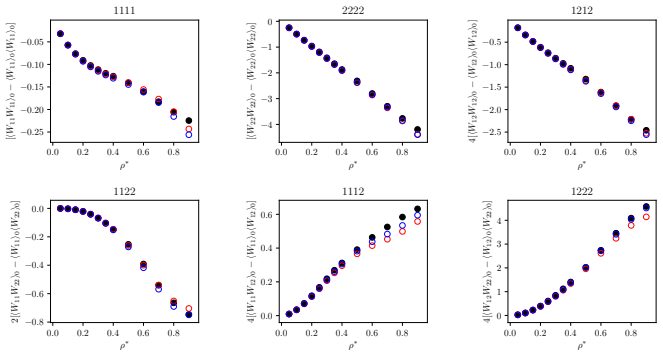

(a) $x_2 = 0.25$

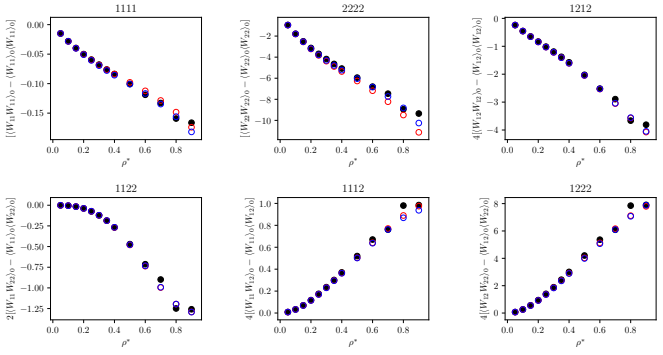

(b) $x_2 = 0.5$

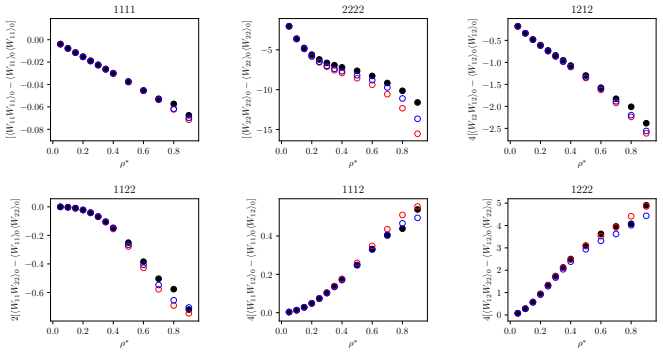

(c) $x_2 = 0.75$

Figure 5.20: Comparison between MC data (black circles), the numerical method using a pure reference (red transparent circles) and the numerical method using an additive binary reference (blue transparent circles) for each of the terms as seen in equations 3.96 to 3.101 and equations 3.108 to 3.113. The reduced temperature is at $T^* = 1$, the epsilon ratio is at $\epsilon_{22}/\epsilon_{11} = 8$ and the component fraction is at (a) $x_2 = 0.25$, (b) $x_2 = 0.5$ and (c) $x_2 = 0.75$.

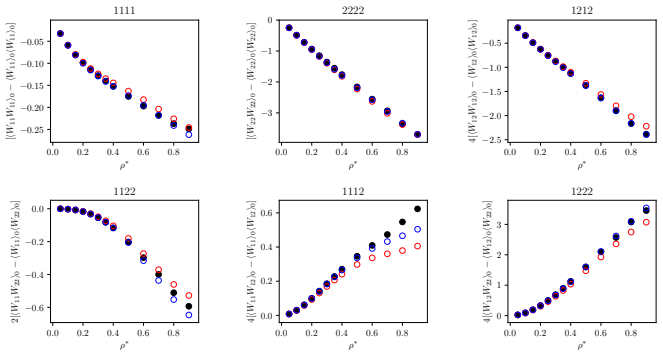

(a) $x_2 = 0.25$

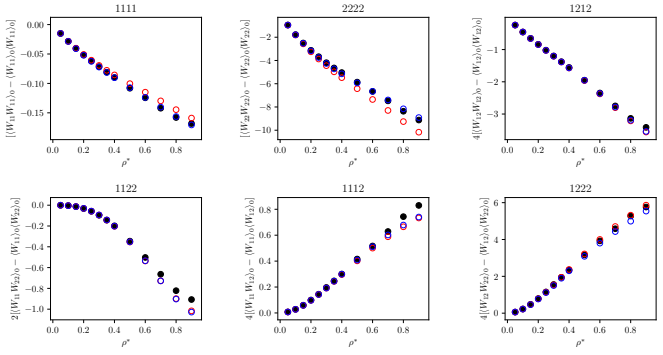

(b) $x_2 = 0.5$

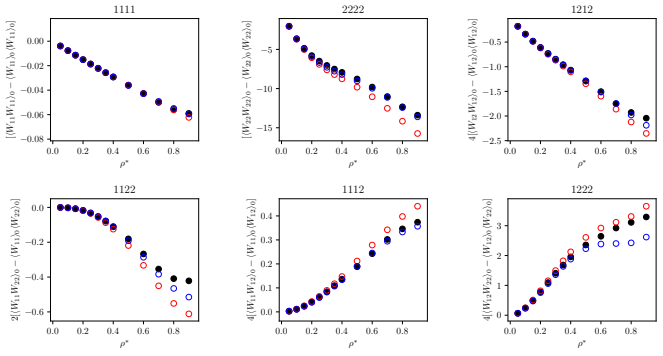

(c) $x_2 = 0.75$

Figure 5.21: Comparison between MC data (black circles), the numerical method using a pure reference (red transparent circles) and the numerical method using an additive binary reference (blue transparent circles) for each of the terms as seen in equations 3.96 to 3.101 and equations 3.108 to 3.113. The reduced temperature is at $T^* = 12$, the epsilon ratio is at $\epsilon_{22}/\epsilon_{11} = 8$ and the component fraction is at (a) $x_2 = 0.25$, (b) $x_2 = 0.5$ and (c) $x_2 = 0.75$.

Figures 5.20 and 5.21 compare all six of the Monte Carlo contributions to their respective equation approximations as given in equations 3.96 to 3.101 for the pure reference and as given in equations 3.108 to 3.113 for the additive reference with $\epsilon_{22}/\epsilon_{11} = 8$ and the reduced temperature $T^* = 1$ and $T^* = 12$, respectively. We can see from the figures that the 1111, 2222 and 1212 terms are generally predicted better, when the additive bi-

nary reference is used. The difference between the two is much more profound when the epsilon ratio is at the much higher ratio $\epsilon_{22}/\epsilon_{11} = 8$, especially at the reduced temperature $T^* = 12$. In this range the hard-sphere ratio is $d_{22}/d_{11} = 1.082$, which is larger than the hard-sphere ratio of $d_{22}/d_{11} = 1.033$, the ratio it had when $\epsilon_{22}/\epsilon_{11} = 2$ and $T^* = 12$. The same problem in predicting the non-linear trend of the 1111 term when $x_2 = 0.25$ (see figures 5.20a and 5.21a) and the 2222 term when $x_2 = 0.75$ (see figures 5.20c and 5.21c), is observed as well. The additive binary reference seems to predict the 1112 term notably better than the pure reference when $x_2 = 0.75$ (see figures 5.20c and 5.21c), but fails considerably at $x_2 = 0.25$ (see figures 5.20a and 5.21a). While the 1222 term is well predicted by the additive binary reference at $x_2 = 0.25$ (see figures 5.20a and 5.21a), but fails at $x_2 = 0.75$ (see figures 5.20c and 5.21c). The failure is especially severe at the reduced temperature $T^* = 12$. This could potentially be due to the way we calculate the 1222 term, when using the binary reference as seen in equation 3.113. It consists of an approximation of the three and four particle distribution functions for a binary mixture, which we have estimated with the superposition approximation, using the binary radial distribution functions that correspond with the interactions in question (see section 3.3.4). This is not necessarily the best way of approximating them and should probably be investigated further in future work.

For the 1122 term, we once again see the same trend for the pure reference method, where at $x_2 = 0.75$ it predicts lower values than the additive binary reference and at $x_2 = 0.25$ it predicts higher values. However this time the higher values at $x_2 = 0.25$ is not more accurate, but rather so high that they are greater than the MC data values. This further supports our hypothesis that the additive binary reference is the more accurate approach and that the pure reference, due to the way it is calculated, exaggerates the contribution of the particle that has the highest fraction of the mixture. We also observe that at $x_2 = 0.5$ (see figures 5.20b and 5.21b), the pure and additive binary references are nearly indistinguishable for the 1122 term.

5.5.3 Correlation Procedures

As using a binary reference system only seems to partly improve the second order perturbation term for mixtures, we have decided to investigate methods in correlating the terms, in hope of improving the model. One way we could do this is through correcting each of the six terms such that they match the Monte Carlo contributions. We did this by first correcting the 1122 term which is approximated by equation 3.99. We chose this term as our basis as it only relies on the sum $2J_3^* + 4J_4^* + J_5^*$, thus we have a direct way to fit the four particle distribution term with the reducible cluster integrals omitted, to Monte Carlo data. We used the pure Monte Carlo data as our basis ($\epsilon_{22}/\epsilon_{11} = 1$) and divided the 1122 term MC contribution by $-\frac{1}{8}\rho^3 4x_1^2x_2^2\epsilon_{12}^2$, which is the value in front of $2J_3^* + 4J_4^* + J_5^*$ in equation 3.99. Then we divided this new found value by $2J_3^* + 4J_4^* + J_5^*$. We did this for each of the three fractions $x_2 = 0.25$, $x_2 = 0.5$ and $x_2 = 0.75$, and took the average of them. Then we repeated this for each reduced density from 0.4-0.9 and each reduced temperature value and finally fitted it to the following function:

$$(1 + \hat{k}_1 T^*)\exp(\hat{k}_2 \rho^*) \tag{5.8}$$

using the python implemented function scipy.optimize.curve_fit [39] (the constants can be found in the appendix in table 7.2). The form it has was chosen to ensure that it will be 1 for the lower reduced density values as these values seem to already be estimated well. We also added the reduced temperature as a variable, as we did see a slight temperature dependence in the error. The fitted function was multiplied to the $2J_3^* + 4J_4^* + J_5^*$ term

and the result can be seen in figure 5.22.

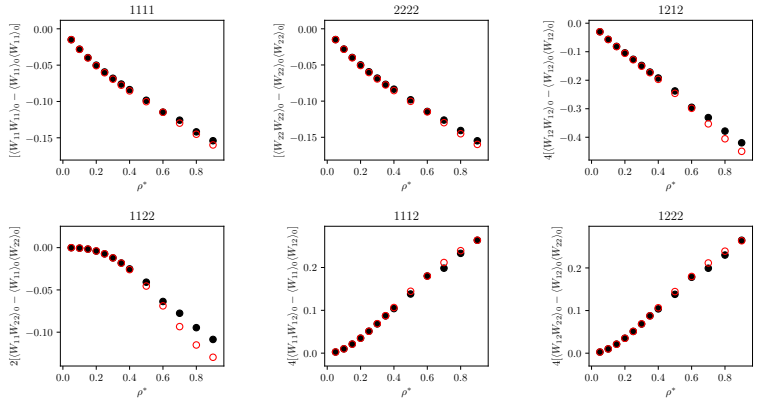

(a) Without correction on $(2J_3^* + 4J_4^* + J_5^*)$

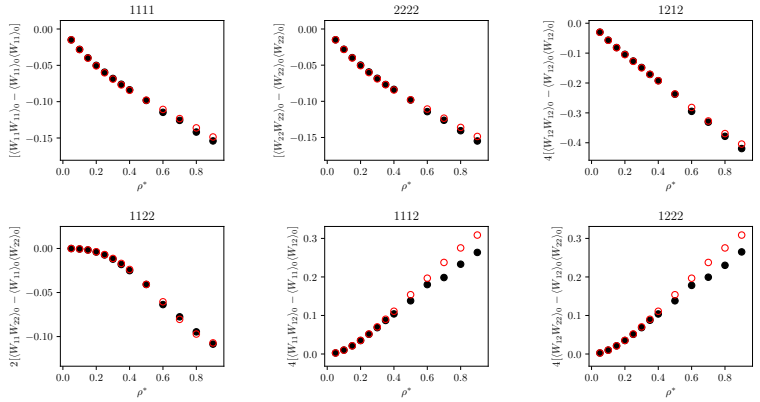

(b) With correction on $(2J_3^* + 4J_4^* + J_5^*)$

Figure 5.22: Comparison between MC data (black circles) and the numerical method (red transparent circles) for each of the terms as seen in equations 3.96 to 3.101. The reduced temperature is at $T^* = 4$, the epsilon ratio is at $\epsilon_{22}/\epsilon_{11} = 1$ and the component fraction is at $x_2 = 0.5$. (a) is without the correction (see equation 5.8) on $(2J_3^* + 4J_4^* + J_5^*)$ and (b) is with the correction.

We can see from figure 5.22 that the approximation of the 1122 term is much better, but we also notice that the approximations of the 1112 and 1222 terms are much worse now, leading us to believe that the error in the J_2^* term, which these two rely on in addition to the $2J_3^* + 4J_4^* + J_5^*$ term was cancelled out by the error in $2J_3^* + 4J_4^* + J_5^*$. We therefore fitted the J_2^* term following the same procedure, but using equation 3.100 and 3.101 as the basis. They were fitted to the same type of equation as equation 5.8 (the constants can be found in the appendix in table 7.3). The result can be seen in figure 5.23.

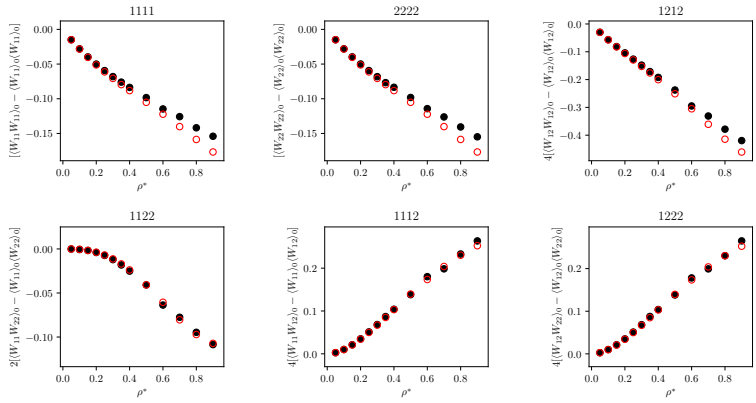

Figure 5.23: Comparison between Monte Carlo data (black circles) and the numerical method (red transparent circles) for each of the terms as seen in equations 3.96 to 3.101. The reduced temperature is at $T^* = 4$, the epsilon ratio is at $\epsilon_{22}/\epsilon_{11} = 1$ and the component fraction is at $x_2 = 0.5$. Here the $(2J_3^* + 4J_4^* + J_5^*)$ and J_3^* terms are corrected (see equation 5.8).

We can see from figure 5.23 that the 1122, 1112 and 1222 terms are now well approximated, while the 1111, 2222 and the 1212 terms are now worse. We could naively try to also fit the J_1^* term, which these three contributions all rely on, however we know from previous papers [23, 41] that the equation for J_1^* (3.70) is well understood and therefore should not need any further fitting. The source of inaccuracy could lie in how we fitted the previous terms, thus we performed the same exercise, but instead used Monte Carlo data to estimate J_2^* and $(2J_3^* + 4J_4^* + J_5^*)$ directly. The result can be seen in figure 5.24.

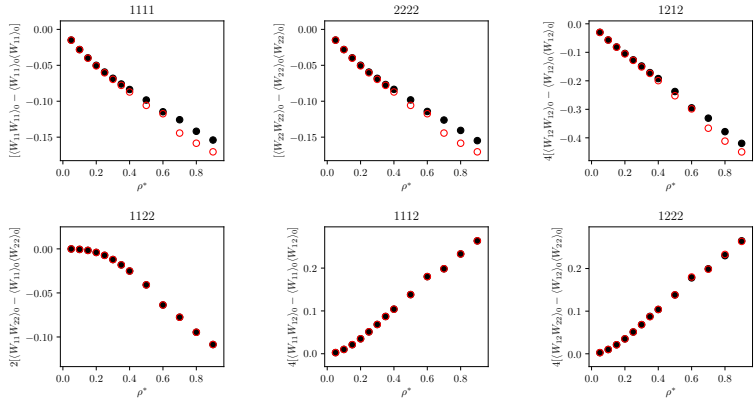

Figure 5.24: Comparison between MC data (black circles) and an estimated version using J_2^* and $(2J_3^* + 4J_4^* + J_5^*)$ estimated from MC data (red transparent circles) for each of the terms as seen in equations 3.96 to 3.101. The reduced temperature is at $T^* = 4$, the epsilon ratio is at $\epsilon_{22}/\epsilon_{11} = 1$ and the component fraction is at $x_2 = 0.5$.

As we can see from figure 5.24, the same problem emerges. This lead us to believe that the problem lies in how we handle the last term in equation 3.64 and that we may not be able to just use this term to simply cancel out all the reducible cluster integrals. This will need some further investigation in the future.

As the term wise correlation did not seem to give the desired outcome, we have simply tried to correlate the entire expression, as it seem to underestimate in a similar fashion over

the entire range we are investigating. We have based it on the calculations using the pure hard-sphere reference, instead of the additive binary hard-sphere reference. The additive binary reference did generally predict better, but as the improvement was minor and since the calculation procedure for the additive binary reference was quite computationally exhaustive, we have decided to perform the correlation using the pure reference, to see if it is possible to still obtain a reasonable approximation from the simpler method. Figure 5.25 shows the ratio between the Monte Carlo data and the numerical approximation at various fractions, epsilon ratios and reduced temperatures.

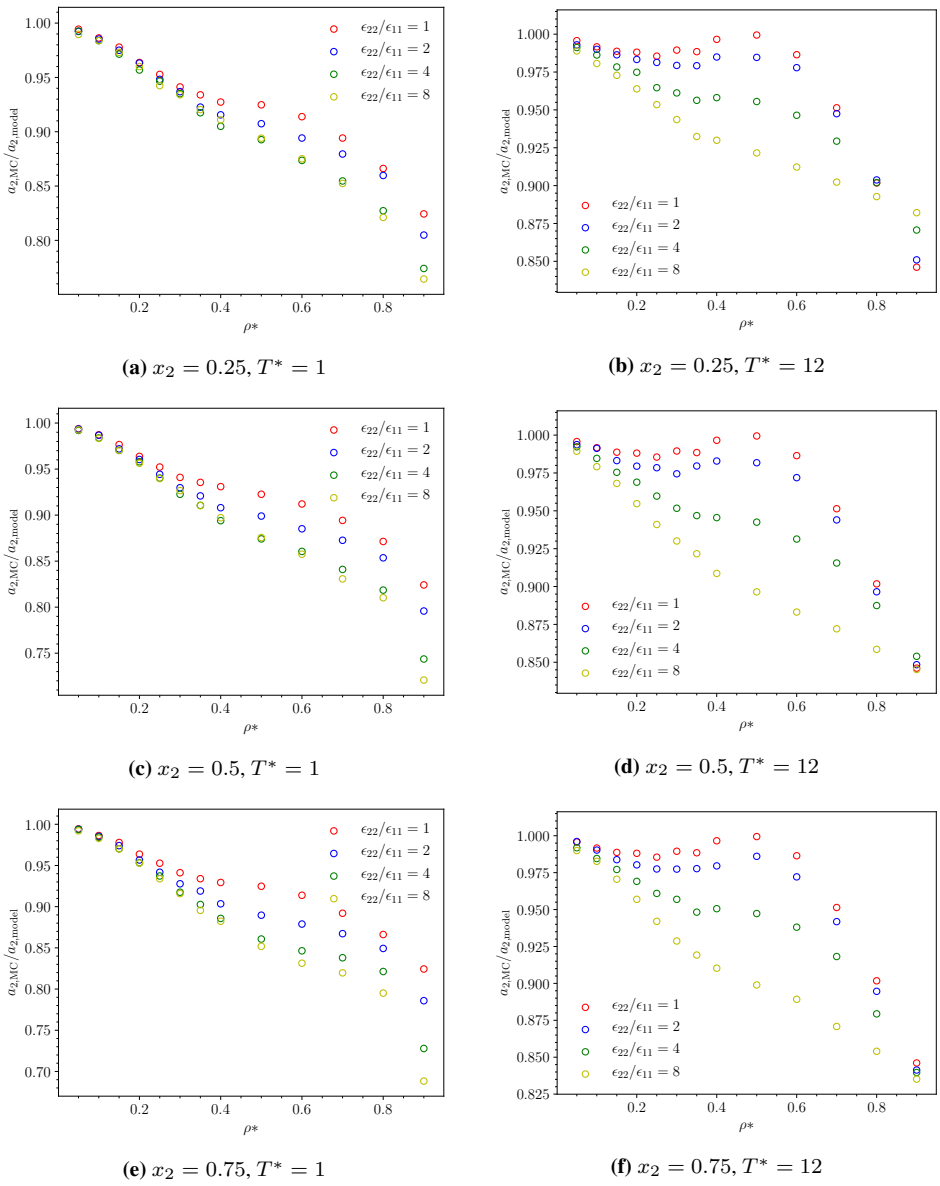

(a) $x_2 = 0.25, T^* = 1$

(b) $x_2 = 0.25, T^* = 12$

(c) $x_2 = 0.5, T^* = 1$

(d) $x_2 = 0.5, T^* = 12$

(e) $x_2 = 0.75, T^* = 1$

(f) $x_2 = 0.75, T^* = 12$

Figure 5.25: Ratio between the MC data for the second order perturbation term $a_{2,\mathrm{MC}}$ and the numerical second order perturbation term $a_{2,\mathrm{model}}$ using a pure hard-sphere reference at different reduced temperatures, fractions of component 2 and epsilon ratios.

We can see from figure 5.25 that the ratio trend is not particular simple. We will however still give correlation a try as it may still yield reasonable results. For the correlation, we took the logarithm of the average of the ratio values across the various epsilon ratios and component 2 fractions for each combination of reduced temperature and reduced density from $0.5 - 0.9$, and correlated it to the logarithm of the function

$$\exp((1 + \hat{k}_1 T^*)\hat{k}_2 \rho^*) \tag{5.9}$$

using the python implemented function scipy.optimize.curve_fit [39] (the constants can be found in the appendix in table 7.4). The form was chosen to ensure that the function goes toward 1 for the lower reduced density, as the numerical method seem to estimate the value in this region pretty well. The result from multiplying the function with the numerical second order perturbation term for mixtures using a pure reference can be seen in figure 5.26.

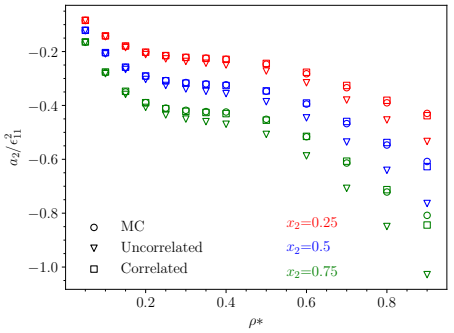

(a) $\epsilon_{22}/\epsilon_{11} = 2, T^* = 1$

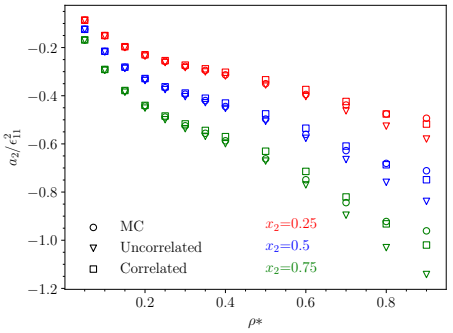

(b) $\epsilon_{22}/\epsilon_{11} = 2, T^* = 12$

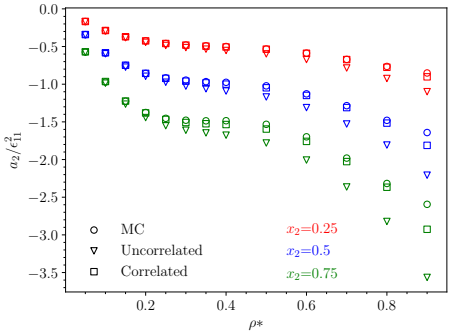

(c) $\epsilon_{22}/\epsilon_{11} = 4, T^* = 1$

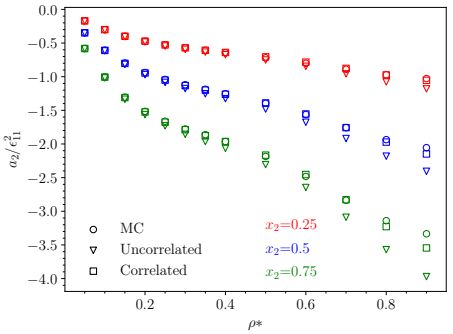

(d) $\epsilon_{22}/\epsilon_{11} = 4, T^* = 12$

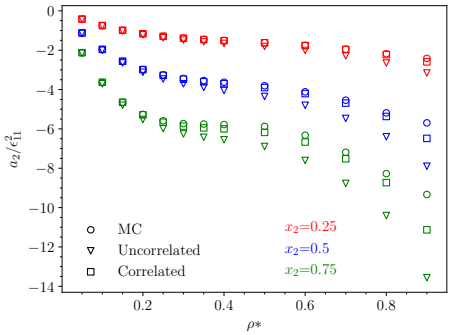

(e) $\epsilon_{22}/\epsilon_{11} = 8, T^* = 1$

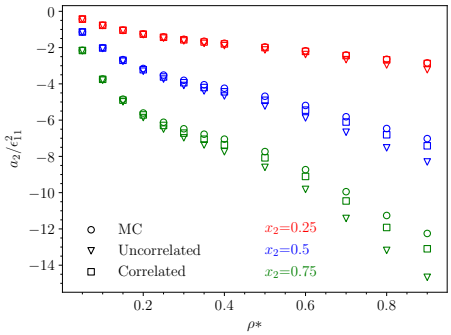

(f) $\epsilon_{22}/\epsilon_{11} = 8, T^* = 12$

Figure 5.26: Comparison of the numerical second order perturbation term using the radial distribution function by Smith and Henderson without a correlation function (uncorrelated) and with a correlation function (correlated) at different reduced temperatures, fractions of component 2 and epsilon ratios. The MC data from this thesis is shown as well to test the accuracy of the models.

We can see that it predicts reasonable well, but it still does not have a satisfactory accuracy. This is as expected, as there seem to be a dependence on the epsilon ratio for the three and four particle distribution functions, which the superposition approximation and our simple fitting model are not able to account for. We could have correlated a function with an epsilon ratio dependence, but this is not a very satisfactory solution as this opens the possibility for having to do the same with the sigma ratio as well as other Mie fluid parameters. It does also not give any good answer to what the underlying problem is and it makes the numerical method pretty much futile, as we could then just extend the χ-factor from the WG method to take mixture parameters into account, as this method is much less computationally demanding.

5.6 The Next Steps for Improving the Model

We can see from the discussion that it is no easy task to improve the second order perturbation term for mixtures. The extension of the WG method for mixtures did seem to perform slightly better than the work of Lafitte et al., especially at the higher temperatures, but it is not entirely satisfactory. To our knowledge, no one has yet properly derived the MCA with a χ-factor based on a thorough understanding of how the particles in the neighbouring shells are correlated with each other, when we have a mixture. This may be the key in understanding how to improve the approach for mixtures. It could also possibly be that the only way to improve the MCA for mixtures is through correlation. Which would be unfortunate as this would not yield any better understanding of the mechanics behind mixtures.

The numerical approach we have shown, seem to be the better option if a physical understanding of the problem is to be obtained, however it also has its fair amount of challenges such as the problems in getting it onto an analytical form, which as it is today seem to be a near impossible task. This will be very important if it is to be used in an industrial situation where computational efficiency is required [55]. Another current problem with this method is its dependence on the three and four particle distribution functions, which we have shown can not be satisfactorily approximated using the superposition approximation. A better understanding of these functions will be vital if this method is ever to be successful.

Chapter 6

Conclusion

In this thesis, we have investigated the challenges in predicting the Barker and Henderson second order perturbation term for mixtures and suggested some strategies for future improvements. We performed Monte Carlo simulations for all the combinations of the following parameter settings: $\epsilon_{22}/\epsilon_{11} \in \{1, 2, 4, 8\}$, $T^* \in \{1, 2, 4, 6, 12\}$, $\rho^* \in \{0.05, 0.1, 0.15, 0.2, 0.25\ , 0.3, 0.35, 0.4, 0.5, 0.6, 0.7, 0.8, 0.9\}$ and $x_2 \in \{0.25, 0.5, 0.75\}$. The data has shown to be somewhat unreliable at the higher reduced density range. Inspired by the work of Lafitte et al. [23] for mixtures we have extended the work of van Westen and Gross [54] for mixtures and compared it to the model by Lafitte et al. and Monte Carlo data. The extension predicted significantly better than the work of Lafitte et al. at the higher reduced temperature range, but only slightly better at the lower reduced temperature range.

We also extended and modified the work of Henderson [19] for Lennard-Jones mixtures with different well-depths using both a pure hard-sphere reference and an additive binary hard-sphere reference. The pure hard-sphere reference seem to predict the general trend fairly well, but overestimates the downward slope at the higher reduced density range. This is less severe at the higher reduced temperature range. The additive binary hard-sphere reference seem to slightly improve the agreement with the simulation data. We have also for the first time to our knowledge performed an extensive study on each of the six contributions to the Monte Carlo data: the 1111 term $\left(-\frac{1}{2N}[\langle W_{11}W_{11}\rangle_0 - \langle W_{11}\rangle_0\langle W_{11}\rangle_0]\right)$, the 1212 term $\left(-\frac{4}{2N}[\langle W_{12}W_{12}\rangle_0 - \langle W_{12}\rangle_0\langle W_{12}\rangle_0]\right)$, the 2222 term $\left(-\frac{1}{2N}[\langle W_{22}W_{22}\rangle_0 - \langle W_{22}\rangle_0\langle W_{22}\rangle_0]\right)$, the 1122 term $\left(-\frac{2}{2N}[\langle W_{11}W_{22}\rangle_0 - \langle W_{11}\rangle_0\langle W_{22}\rangle_0]\right)$, the 1112 term $\left(-\frac{4}{2N}[\langle W_{11}W_{12}\rangle_0 - \langle W_{11}\rangle_0\langle W_{12}\rangle_0]\right)$ and the 1222 term $\left(-\frac{4}{2N}[\langle W_{12}W_{22}\rangle_0 - \langle W_{12}\rangle_0\langle W_{22}\rangle_0]\right)$, and compared them to the approximate equations from the numerical method, in calculating the second order perturbation term. Our findings can be summarized as:

- The numerical method is generally able to predict the six terms reasonably well up to $\rho^* = 0.5$.
- The 1111, 1212 and 2222 terms were generally better approximated using an additive binary reference than a pure reference. The difference was especially noticeable at the higher reduced temperature and epsilon ratio range.
- At $T^* = 1$, the 1111 term deviate more from a linear behavior at $x_2 = 0.25$, while the 2222 term deviate more from a linear behavior at $x_2 = 0.75$, which the

numerical method seem to struggle in accurately explaining.

- The 1112 term is well-predicted by the additive binary reference at $x_2 = 0.75$, but fails considerably at $x_2 = 0.25$ and vice versa for the 1222 term. This is even more exaggerated at the higher reduced temperature.
- The numerical method generally struggles in predicting the 1122 term, but using an additive binary reference seem to yield more consistent results.

A strategy in fitting each of the numerical integrals to the six terms calculated by Monte Carlo, revealed a problem with the numerical method, which is believed to come from the way the reducible cluster integrals are omitted. This will need further investigation. A strategy in correlating the entire expression seemed to predict significantly better, however this did not give any better understanding of the current problem.

For the numerical method presented in this project to be reliable in the future, a better understanding of the 3- and 4-particle distribution functions will be needed as the major current issues with this strategy is believed to stem from the superposition approximation. We will also need some way to extend it to an analytical form, for it to be reliable in industrial work, either this or we could return to the work of Lafitte et al. [23], where some major improvements to the MCA and the χ-factor will be needed.

Chapter 7

Further Work

There are several parts in this projects that would benefit from a more extensive investigation. As seen in the discussion (see section 5) the Monte Carlo data is not entirely reliable at the higher reduced density and the lower reduced temperature range. Redoing these points by doubling or even quadrupling the number of MC steps, could perhaps resolve this problem. A bootstrapping procedure would probably also be wise, as this would make it easier for error estimation, since the outcome space of the data will be predicted.

The models by Lafitte et al. and van Westen and Gross, which are both based on the MCA with a correction factor, may perform better if a proper and extensive extension for the MCA and the χ-factor to mixtures was generalized. The best option here, would likely be to obtain a proper understanding on how the particles in the neighbouring shells are correlated with each other. In the paper by Gil-Villegas et al. [13], they used the local compressibility approximation (LCA), instead of the MCA and extended it for mixtures. This could also be worthwhile exploring.

Probably our biggest suggestion for further work on this project is the approximations of the 3- and 4-particle distribution functions, as we have seen that the superposition approximation is not able to properly predict these. There are several interesting approximations on this that has been suggested, such as the ladder approximation by Blawzdziewicz et al. [7] which showed promising results when used for perturbation onto a square-well potential [8]. There are also many other approximations, which are based on improving the superposition approximation. These have been covered extensively in the excellent paper by Grouba et al. [15].

We have in this thesis been mostly focusing on Lennard-Jones fluid mixtures with difference in well-depths. An investigation in how well the numerical approach will perform for various Mie fluid mixtures or in mixtures with different sigmas could be interesting.

An investigation on some of the thermodynamic properties that can be obtained from the Helmholtz free energy, could give more insight in the problems we currently have for the numerical method in calculating the second order perturbation term for mixtures. Maybe an approach in a similar fashion as van Westen and Gross did, by adding the perturbation terms one by one could yield interesting results.

Lastly a proper investigation on how some of the other perturbation theories would perform when extended to mixtures such as the WCA theory [17], could be interesting. According to van Westen and Gross [54], the WCA diameter is supposed to perform better as it is not only temperature dependent, but also density dependent.

Bibliography

[1] Aasen, A., Hammer, M., Ervik, Å., Müller, E.A., Wilhelmsen, Ø., 2019. Equation of state and force fields for feynman–hibbs-corrected mie fluids. i. application to pure helium, neon, hydrogen, and deuteriums. The Journal of Chemical Physics 151, 064508.

[2] Aasen, A., Hammer, M., Müller, E.A., Wilhelmsen, Ø., 2020. Equation of state and force fields for feynman–hibbs-corrected mie fluids. ii. application to mixtures of helium, neon, hydrogen, and deuterium. The Journal of Chemical Physics 152, 074507.

[3] Abramowitz, M., Stegun, I.A., 1972. Handbook of Mathematical Functions With Formulas, Graphs, and Mathematical Tables. United States Department of Commerce, National Bureau of Standards (NBS).

[4] Allen, M.P., Tildesley, D.J., 2017. Computer Simulation of Liquids. Oxford.

[5] Barker, J., Henderson, D., 1967. Perturbation theory and equation of state for fluids. ii. a successful theory of liquids. The Journal of chemical Physics 47, 4714–4721.

[6] Baxter, R.J., 1964. Direct correlation functions and their derivatives with respect to particle density. The Journal of Chemical Physics 41, 553–558.

[7] Blawzdziewicz, J., Cichocki, B., Szamel, G., 1989. Ladder approximation for three- and four particle correlation functions. The Journal of Chemical Physics 91, 7467–7476.

[8] Blawzdziewicz, J., Stell, G., 1990. Ladder approximation for three- and four-particle correlation functions: Application to thermodynamic perturbation theory. Physical Review A 42, 5917–5927.

[9] Boublík, T., 1970. Hard-sphere equation of state. The Journal of Chemical Physics 53, 471–472.

[10] Carnahan, N.F., Starling, K.E., 1969. Equation of state for nonattracting rigid spheres. The Journal of chemical Physics 51, 635–636.

[11] Chapman, W.G., Gubbins, K.E., Jackson, G., Radosz, M., 1989. Saft: Equation-of-state solution model for associating fluids. Fluid Phase Equilibria 52, 31–38.

[12] Eyring, H., Henderson, D., Jost, W., 1971. Physical Chemistry An Advanced Treatsie. volume 8A. Academic Press.

[13] Gil-Villegas, A., Galindo, A., Whitehead, P.J., Mills, S.J., Jackson, G., 1997. Statistical associating fluid theory for chain molecules with attractive potentials of variable range. The Journal of chemical Physics 106, 4168–4186.

[14] Gross, J., Sadowski, G., 2001. Perturbed-chain saft: An equation of state based on a perturbation theory for chain molecules. Industrial & Engineering Chemistry Research 40, 1244–1260.

[15] Grouba, V.D., Zorin, A.V., Sevastianov, L.A., 2004. The superposition approximation: A critical review. International Journal of Modern Physics B 18, 1–44.

[16] Hammer, M., Aasen, A., Ervik, Å., Wilhelmsen, Ø., 2020. Choice of reference, influence of non-additivity, and present challenges in thermodynamic perturbation theory for mixtures. The Journal of Chemical Physics 152, 134106.

[17] Hans C. Andersen, J.D.W., Chandler, D., 1971. Relationship between the hard-sphere fluid and fluids with realistic repulsive forces. Physical Review A 4, 1597–1607.

[18] Hansen, J.P., McDonald, I.R., 2013. Theory of Simple Liquids : With Applications to Soft Matter. Elsevier Science & Technology.

[19] Henderson, D., 1974. Perturbation theory for a mixture of hard spheres and square-well molecules. The Journal of Chemical Physics 61, 926–931.

[20] Jones, J.E., 1924. On the determination of molecular fields. —ii. from the equation of state of a gas. Royal Society 106, 463–477.

[21] Kirkwood, J.G., 1935. Statistical mechanics of fluid mixtures. The Journal of Chemical Physics 3, 300–313.

[22] Kreyszig, E., 2011. Advanced Engineering Mathematics. volume 10. John Wiley & Sons.

[23] Lafitte, T., Apostolakou, A., Avendaño, C., Galindo, A., Adjiman, C.S., Müller, E.A., Jackson, G., 2013. Accurate statistical associating fluid theory for chain molecules formed from mie segments. The Journal of chemical Physics 139, 154504.

[24] Leach, A.R., 2001. Molecular Modelling Principles and Applications. Pearson.

[25] scikit learn, 2019. sklearn.decomposition.PCA. `https://scikit-learn.org/stable/modules/generated/sklearn.decomposition.PCA.html`. [Online; accessed 04-June-2020].

[26] Leonard, P.J., Henderson, D., Barker, J.A., 1970. Perturbation theory and liquid mixtures. Transactions of the Faraday Society 66, 2439–2452.

[27] Malijevský, A., Labík, S., 1986. The bridge function for hard spheres. Molecular Physics 60, 663–669.

[28] Mansoori, G.A., Carnahan, N.F., Starling, K.E., Jr, T.W.L., 1971. Equilibrium thermodynamic properties of the mixture of hard spheres. The Journal of Chemical Physics 54, 1523–1525.

[29] Mathews, J.H., Fink, K.K., 2004. Numerical methods using MATLAB. Pearson.

[30] Mie, G., 1903. Zur kinetischen theorie der einatomigen körper. Annalen der Physik 316, 657–697.

[31] Mulero, A., 2008. Theory and Simulation of Hard-Sphere Fluids and Related Systems. Springer.

[32] Nezbeda, I., 1974. Analytic solution of percus-yevick equation for fluid of hard spheres. Czechoslovak Journal of Physics B 24, 55–62.

[33] Perrot, P., 1998. A to Z of Thermodynamics. Oxford University Press.

[34] Schofield, P., 1965. Wavelength-dependent fluctuations in classical fluids: I. the long wavelength limit. Proceedings of the Physical Society 88, 149–170.

[35] Scipy, 2019a. numpy.linalg.lstsq. `https://docs.scipy.org/doc/numpy/reference/generated/numpy.linalg.lstsq.html`. [Online; accessed 03-December-2019].

[36] Scipy, 2019b. numpy.polynomial.legendre.leggauss. `https://docs.scipy.org/doc/numpy/reference/generated/numpy.polynomial.legendre.leggauss.html`. [Online; accessed 08-December-2019].

[37] Scipy, 2019c. scipy.integrate.quad. `https://docs.scipy.org/doc/scipy/reference/generated/scipy.integrate.quad.html`. [Online; accessed 03-December-2019].

[38] Scipy, 2019d. scipy.integrate.simps. `https://docs.scipy.org/doc/scipy/reference/generated/scipy.integrate.simps.html`. [Online; accessed 04-June-2020].

[39] Scipy, 2019e. scipy.optimize.curve_fit. `https://docs.scipy.org/doc/scipy/reference/generated/scipy.optimize.curve_fit.html`. [Online; accessed 04-June-2020].

[40] Smith, W.R., Henderson, D., 1970. Analytical representation of the percus-yevick hard-sphere radial distribution function. Molecular Physics 19, 411–415.

[41] Smith, W.R., Henderson, D., Barker, J.A., 1970. Approximate evaluation of the second-order term in the perturbation theory of fluids. The Journal of Chemical Physics 53, 508–515.

[42] Smith, W.R., Henderson, D.J., Leonard, P.J., Barker, J.A., Grundke, E.W., 2008. Fortran codes for the correlation functions of hard sphere fluids. Molecular Physics 106, 3–7.

[43] de Souza, L.E., Ben-Amotz, D., 1993. Optimized perturbed hard sphere expressions for the structure and thermodynamics of lennard-jones fluids. Molecular Physics 78, 137–149.

[44] Sutherland, W., 1893. Lii. the viscosity of gases and molecular force. Philosophical Magazine 36, 507–531.

[45] Throop, G.J., Bearman, R.J., 1965. Numerical solutions of the percus—yevick equation for the hard-sphere potential. The Journal of Chemical Physics 42, 2408–2411.

[46] Trokhymchuk, A., Nezbeda, I., Jirsák, J., Henderson, D., 2005. Hard-sphere radial distribution function again. The Journal of Chemical Physics 123, 024501.

[47] Tsonopoulos, C., Prausnitz, J.M., 1969. Equations of state a review for engineering applications. Cryogenics 9, 315–327.

[48] Verlet, L., Weis, J.J., 1972. Equilibrium theory of simple liquids. Physical Review A 5, 939–952.

[49] Wertheim, M.S., 1963. Exact solution of the percus-yevick integral equation for hard spheres. Physical Review Letters 10, 321–323.

[50] Wertheim, M.S., 1984a. Fluids with highly directional attractive forces. i. statistical thermodynamics. Journal of Statistical Physics 35, 19–34.

[51] Wertheim, M.S., 1984b. Fluids with highly directional attractive forces. ii. thermodynamic perturbation theory and integral equations. Journal of Statistical Physics 35, 35–47.

[52] Wertheim, M.S., 1986a. Fluids with highly directional attractive forces. iii. multiple attraction sites. Journal of Statistical Physics 42, 459–476.

[53] Wertheim, M.S., 1986b. Fluids with highly directional attractive forces. iv. equilibrium polymerization. Journal of Statistical Physics 42, 477–492.

[54] van Westen, T., Gross, J., 2017. A critical evaluation of perturbation theories by monte carlo simulation of the first four perturbation terms in a helmholtz energy expansion for the lennard-jones fluid. The Journal of chemical Physics 147, 014503.

[55] Wilhelmsen, Ø., Aasen, A., Skaugen, G., Aursand, P., Austegard, A., Aursand, E., Gjennestad, M.A., Lund, H., Linga, G., Hammer, M., 2017. Thermodynamic modeling with equations of state: Present challenges with established methods. Industrial and Engineering Chemistry Research 56, 3503–3515.

[56] Yuhua Song, E.A.M., Strait, R.M., 1989. Why does the carnahan-starling equation work so well? The Journal of chemical Physics 93, 6916–6919.

[57] Zhang, B.J., 1999. Calculating thermodynamic properties from perturbation theory: I. an analytic representation of square-well potential hard-sphere perturbation theory. Fluid Phase Equilibria 154, 1–10.

[58] Zwanzig, R.W., 1954. High-temperature equation of state by a perturbation method. i. nonpolar gases. The Journal of chemical Physics 22, 1420–1426.

[59] Zwillinger, D., Moll, V., 2014. Table of Integrals, Series, and Products. Academic Press.

Appendix

7.1 Table of Correlation Constants

Table 7.1: The constants obtained for the correlated function F^c (see equation 3.93).

Constant	Correlated Value
$\hat{k}_1$	4.32485439
$\hat{k}_2$	-1.08075001
$\hat{k}_3$	4.89332707

Table 7.2: The constants obtained for the correlation (see equation 5.8) used to correct the $(2J_3^* + 4J_4^* + J_5^*)$ term.

Constant	Correlated Value
$\hat{k}_1$	-0.00145076
$\hat{k}_2$	-0.20523767

Table 7.3: The constants obtained for the correlation (see equation 5.8) used to correct the J_2^* term.

Constant	Correlated Value
$\hat{k}_1$	0.00016559
$\hat{k}_2$	-0.12706174

Table 7.4: The constants obtained for the correlation (see equation 5.9) used to correct the entire numerical second order perturbation term using a pure hard-sphere reference.

Constant	Correlated Value
$\hat{k}_1$	0.03728314
$\hat{k}_2$	-0.22793082

7.2 Ornstein-Zernike and Percus-Yevick

In this section, we will describe a method for developing an expression for the radial distribution function, specifically through the Ornstein-Zernike equation.

In order to develop a method for creating an expression for the radial distribution function it will be convenient to start with the case of inhomogeneous fluids. To do this

we return to the Hamiltonian as shown in equation 2.1 which included a term representing the interaction of the particles with an external spatially varying field (Φ_N). The effect of including this term is to break up the translational symmetry. Using this hamiltonian we rewrite the grand partition function, which is still related to the grand potential by $\Xi = \exp(-\beta\Omega)$, into

$$\Xi = \sum_{N=0}^{\infty} \frac{1}{N!} \int \exp(-\beta V_N) \left(\prod_{i=1}^{N} \exp[-\beta\phi(\mathbf{r}_i)] \right) \mathrm{d}\mathbf{r}^N \tag{7.1}$$

where ϕ is related to Φ in the following way

$$\Phi_N(\mathbf{r}^N) = \sum_{i=1}^{N} \phi(\mathbf{r}_i) = \int \rho(\mathbf{r})\phi(\mathbf{r})\mathrm{d}\mathbf{r} \tag{7.2}$$

The definition of the particle densities is changed to

$$\rho^{(n)}(\mathbf{r}^n) = \frac{1}{\Xi} \sum_{N=n}^{\infty} \frac{1}{(N-n)!} \int \exp(-\beta V_N) \left(\prod_{i=1}^{N} \exp[-\beta\phi(\mathbf{r}_i)] \right) \mathrm{d}\mathbf{r}^{(N-n)}. \tag{7.3}$$

We recast the grand partition function into

$$\Xi = \sum_{N=0}^{\infty} \frac{1}{N!} \int \cdots \int \exp(-\beta V_N) \left(\prod_{i=1}^{N} \frac{1}{\Lambda^3} \exp[\beta\psi(\mathbf{r}_i)] \right) \mathrm{d}\mathbf{r}_1 \cdots \mathbf{r}_N \tag{7.4}$$

where

$$\psi(\mathbf{r}) = \mu - \phi(\mathbf{r}) \tag{7.5}$$

This quantity is the intrinsic chemical potential, the quantity to μ not explicitly dependent on $\phi(\mathbf{r})$. If we say that the definition of $\phi(\mathbf{r})$ includes the confining potential (the interaction between the particles and the confining wall), then the volume V can be replaced by $\phi(\mathbf{r})$. Using equation 2.25 the infinitesimal change in equilibrium state is

$$\delta\mathcal{U} = T\delta\mathcal{S} + \int \rho^{(1)}(\mathbf{r})\delta\phi(\mathbf{r})\mathrm{d}\mathbf{r} + \mu\delta N \tag{7.6}$$

It then follows from the definition of Helmholtz free energy that the change in A in an infinitesimal process is

$$\delta A = -\mathcal{S}\delta T + \int \rho^{(1)}(\mathbf{r})\delta\phi(\mathbf{r})\mathrm{d}\mathbf{r} + \mu\delta N \tag{7.7}$$

We define the intrinsic Helmholtz free energy $\mathcal{A}$ as

$$\mathcal{A} = A - \int \rho^{(1)}(\mathbf{r})\delta\phi(\mathbf{r})\mathrm{d}\mathbf{r} \tag{7.8}$$

with

$$\begin{aligned} \delta\mathcal{A} &= -\mathcal{S}\delta T - \int \delta\rho^{(1)}(\mathbf{r})\phi(\mathbf{r})\mathrm{d}\mathbf{r} + \mu\delta N \\ &= -\mathcal{S}\delta T - \int \delta\rho^{(1)}(\mathbf{r})\psi(\mathbf{r})\mathrm{d}\mathbf{r} \end{aligned} \tag{7.9}$$

since $\mu\delta N = \int \delta\rho^{(1)}(\mathbf{r})\mu \mathrm{d}\mathbf{r}$. From the definition of functional derivatives we see that

$$\frac{\delta\mathcal{A}}{\delta\rho^{(1)}(\mathbf{r})} = \psi(\mathbf{r}). \tag{7.10}$$

The last thing to notice is that the intrinsic Helmholtz free energy can also be divided into two parts

$$\mathcal{A} = \mathcal{A}^{\text{id}} + \mathcal{A}^{\text{res}} \tag{7.11}$$

where

$$\mathcal{A}^{\text{id}} = k_B T \int \rho^{(1)}(\mathbf{r})(\ln[\Lambda^3\rho^{(1)}(\mathbf{r})] - 1)\mathrm{d}\mathbf{r}. \tag{7.12}$$

We now introduce the direct correlation functions $c^{(n)}(\mathbf{r}^n)$. The single particle correlation function is defined as

$$c^{(1)}(\mathbf{r}) = -\beta\frac{\delta\mathcal{A}^{\text{res}}}{\delta\rho^{(1)}(\mathbf{r})} \tag{7.13}$$

while the pair function is defined as

$$c^{(2)}(\mathbf{r},\mathbf{r}') = \frac{\delta c^{(1)}(\mathbf{r})}{\delta\rho^{(1)}(\mathbf{r}')} = -\beta\frac{\delta^2\mathcal{A}^{\text{res}}}{\delta\rho^{(1)}(\mathbf{r})\delta\rho^{(1)}(\mathbf{r}')} \tag{7.14}$$

Combining equation 7.10, 7.12 and 7.13 we get the following relation

$$\beta\psi(\mathbf{r}) = \beta\frac{\delta\mathcal{A}^{\text{res}}}{\delta\rho^{(1)}(\mathbf{r})} = \ln[\Lambda^3\rho^{(1)}(\mathbf{r})] - c^{(1)}(\mathbf{r}). \tag{7.15}$$

By inserting $\psi = \mu - \phi$ and $z = \exp(\beta\mu)/\Lambda^3$ we get

$$\rho^{(1)}(\mathbf{r}) = z\exp[-\beta\phi(\mathbf{r}) + c^{(1)}(\mathbf{r})]. \tag{7.16}$$

For the case of a uniform fluid where $\phi = 0$ we can reformulate the equation into

$$-k_B T c^{(1)} = \mu - k_B T\ln[\Lambda^3\rho] = \mu^{\text{res}}. \tag{7.17}$$

Another way to formulate the definition of $c^{(2)}$ is the well known Ornstein-Zernike relation:

$$h^{(2)}(\mathbf{r},\mathbf{r}') = c^{(2)}(\mathbf{r},\mathbf{r}') + \int c^{(2)}(\mathbf{r},\mathbf{r}'')\rho^{(1)}(\mathbf{r}'')h^{(2)}(\mathbf{r}'',\mathbf{r}')\mathrm{d}\mathbf{r}'' \tag{7.18}$$

where $h^{(2)}(\mathbf{r},\mathbf{r}') = g^{(2)}(\mathbf{r},\mathbf{r}') - 1$. By solving the equation recursively we get

$$\begin{aligned} h^{(2)}(\mathbf{r}_1,\mathbf{r}_2) =& c^{(2)}(\mathbf{r}_1,\mathbf{r}_2) + \int c^{(2)}(\mathbf{r}_1,\mathbf{r}_3)\rho^{(1)}(\mathbf{r}_3)c^{(2)}(\mathbf{r}_3,\mathbf{r}_2)\mathrm{d}\mathbf{r}_3 \\ &+ \int\int c^{(2)}(\mathbf{r}_1,\mathbf{r}_3)\rho^{(1)}(\mathbf{r}_3)c^{(2)}(\mathbf{r}_3,\mathbf{r}_4)\rho^{(1)}(\mathbf{r}_4)c^{(2)}(\mathbf{r}_4,\mathbf{r}_2)\mathrm{d}\mathbf{r}_3\mathrm{d}\mathbf{r}_4 + \cdots \end{aligned} \tag{7.19}$$

We can see from this equation that the total correlation between particles 1 and 2 ($h^{(2)}(\mathbf{r}_1,\mathbf{r}_2)$) is due to the direct correlation between particle 1 and 2 as well as the indirect correlation propagated through increasingly large numbers of intermediate particles. If the fluid is both uniform and isotropic, we can write the Ornstein-Zernike relation as

$$h(r) = c(r) + \rho\int c(|\mathbf{r}-\mathbf{r}'|)h(r')\mathrm{d}\mathbf{r}' \tag{7.20}$$

One need to solve for both $h(r)$ and $c(r)$ in order to solve the Ornstein-Zernike equation. This requires an additional relation known as a closure relation. The most successfully and commonly used one is probably the Percus-Yevick approximation which we will derive in a slightly different way from the original paper. The idea is to expand the single-particle correlation function of an inhomogeneous fluid about that of a uniform reference system in powers of $\Delta\rho^{(1)}$. We use Percus idea of switching on the interaction $\phi(\mathbf{r})$ with a particle fixed at the origin $\mathbf{r}_0 = 0$. We let the total potential energy of the remaining particles in the external field due to particle 0, be on the form of equation 7.2 with

$$\phi(\mathbf{r}_i) = u(\mathbf{r}_0, \mathbf{r}_i). \tag{7.21}$$

It can be shown that the single particle density in presence of an external field $\rho_\phi^{(1)}$ is related to the two particle density without a field

$$\rho_\phi^{(1)}(\mathbf{r}_1) = \frac{\rho^{(2)}(\mathbf{r}_0, \mathbf{r}_1)}{\rho} \tag{7.22}$$

or reformulated to

$$\rho_\phi^{(1)}(\mathbf{r}_1) = \rho g(\mathbf{r}_0, \mathbf{r}_1). \tag{7.23}$$

The effect of switching on the interaction with the particle 0, is to change the potential from 0 to $\Delta\phi = u(\mathbf{r}_0, \mathbf{r}_1)$ which gives a change in the single-particle density

$$\Delta\rho^{(1)}(\mathbf{r}_1) = \rho g(\mathbf{r}_0, \mathbf{r}_1) - \rho = \rho h(\mathbf{r}_0, \mathbf{r}_1) \tag{7.24}$$

Using this we will expand $\exp[c^{(1)}(\mathbf{r})]$ in powers of $\Delta\rho^{(1)}(\mathbf{r})$ to first order as

$$\exp[c^{(1)}(\mathbf{r})] \approx \exp[c_0^{(1)}] + \int \Delta\rho^{(1)}(\mathbf{r}') \left.\frac{\exp[c^{(1)}(\mathbf{r})]}{\delta\rho^{(1)}(\mathbf{r}')}\right|_{\phi=0} \mathrm{d}\mathbf{r}' \tag{7.25}$$

Using equation 7.14 and 7.17 this can be written as

$$\exp[c^{(1)}(\mathbf{r})] \approx \exp(-\beta\mu_0^{\text{res}}) \left(1 + \int \Delta\rho^{(1)}(\mathbf{r}') c_0^{(2)}(\mathbf{r}, \mathbf{r}') \mathrm{d}\mathbf{r}'\right) \tag{7.26}$$

For a uniform fluid and using equation 7.24 we can rewrite it into

$$\exp[c^{(1)}(\mathbf{r})] \approx \exp(-\beta\mu_0^{\text{res}}) \left(1 + \rho \int c(|\mathbf{r} - \mathbf{r}'|) h(\mathbf{r}') \mathrm{d}\mathbf{r}'\right) \tag{7.27}$$

Using equation 7.16, 7.17, 7.21 and the Ornstein-Zernike relation we get an expression for the pair distribution function

$$\begin{aligned} g(\mathbf{r}) =& \exp[-\beta u(\mathbf{r})] \left(1 + \rho \int c(|\mathbf{r} - \mathbf{r}'|) h(\mathbf{r}') \mathrm{d}\mathbf{r}'\right) \\ =& \exp[-\beta u(\mathbf{r})][1 + h(\mathbf{r}) - c(\mathbf{r})] \end{aligned} \tag{7.28}$$

This is the Percus-Yevick (PY) approximation and can be written as

$$c(\mathbf{r}) \approx (1 - \exp[\beta u(\mathbf{r})]) g(\mathbf{r}) \tag{7.29}$$

Using the cavity distribution function $y(r)$ and the Mayer function $f_{\text{M}}(r) = \exp[-\beta u(r)] - 1 = e(r) - 1$ the PY approximation can be written in its familiar form

$$c(r) = y(r) f_{\text{M}}(r) \tag{7.30}$$

The PY approximation is especially good when used on hard-spheres with diameter d. In this case it becomes

$$c(r) = \begin{cases} -y(r) & r < d \\ 0 & r > d \end{cases} \tag{7.31}$$

It is even further restricted by the fact that

$$g(r) = 0, r < d \tag{7.32}$$

Using these two relations the Ornstein-Zernike relation can be rewritten into

$$y(r) = 1 + \rho \int_{r'<d} y(r')\mathrm{d}\mathbf{r}' - \rho \int_{\substack{r'<d \\ |\mathbf{r}-\mathbf{r}'|>d}} y(r')y\left(|\mathbf{r}-\mathbf{r}'|\right)\mathrm{d}\mathbf{r}' \tag{7.33}$$

[18].